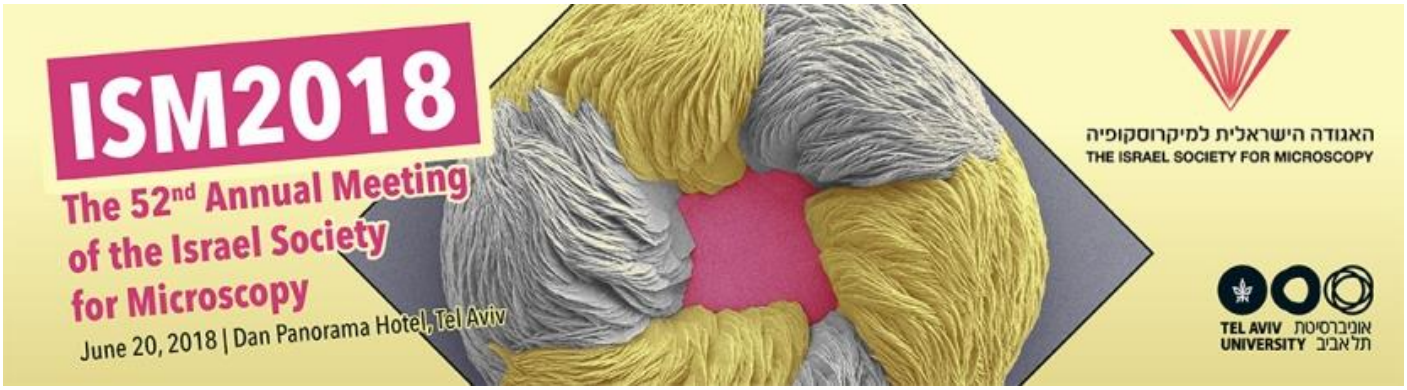


# ABSTRACTS

## LECTURES & POSTERS

PLENARY LECTURE 1

*Invited Plenary Lecture*

## 3D-OPTICAL NANOMETRY FOR AND WITH BIOMOLECULAR MOTOR SYSTEMS

**Stefan Diez**

*B CUBE - Center for Molecular Bioengineering, Technische Universität Dresden, Dresden, Germany*

Our lab is interested in the development and the application of novel optical techniques to investigate molecular transport in cell biology and nanotechnology. Building on our experience in single-molecule imaging and in the in vitro reconstruction of subcellular mechano-systems we study cooperative effects in motor transport and cell motility. Moreover we aim to apply biomolecular motor systems in synthetic, engineered environments for the generation, manipulation and detection of nanostructures. Towards this end, the talk will focus on how fluorescent microtubules themselves (with and without attached quantum dots) can be used as probes to measure optical near fields. In contrast to many alternative methods, microtubules possess the advantages that they can be applied in a highly parallel manner and that they do not alter the fields to be measured.

---

PLENARY LECTURE 2

*Invited Plenary Lecture*

## IMAGING AND CONTROLLING THE GROWTH OF NANOSTRUCTURES IN THE TRANSMISSION ELECTRON MICROSCOPE

**Frances M. Ross**

*IBM, T. J. Watson Research Center, Yorktown Heights, New York, USA*

Building functional nanostructures with atomic level precision requires a detailed understanding of materials growth, and in particular the physics of self-assembly at the nanoscale. Experiments in which a self-assembly process takes place *in situ* in the transmission electron microscope allow continuous observations of individual nanostructures, and even measurements of their properties, while they grow and change. The resulting movies and measurements help to quantify the mechanisms that control nanostructure formation and can also reveal unexpected reaction pathways. I will describe experimental techniques to probe processes taking place in both vapour and liquid phase. I will illustrate with examples including nanocrystal epitaxy on graphene and electrochemical deposition of metals. I will discuss how new types of nanostructure can be designed using the self-assembly phenomena revealed *in situ* and consider some possible applications. Finally I will provide a perspective on the exciting recent advances in transmission electron microscopy that will impact *in situ* growth experiments in the future.

---

## SINGLE PARTICLE cryo-EM OF BIOLOGICAL MACROMOLECULES

**Nadav Elad**
*Electron Microscopy Unit, Weizmann Institute of Science, Rehovot, Israel*

Single particle cryo-electron microscopy (cryo-EM) involves the 3D visualization of biological macromolecules in solution. Substantial improvements in the technique now enable to determine macromolecular structures to atomic resolution, attracting great interest in the structural biology field. These breakthroughs have awarded the 2017 Nobel Prize in Chemistry to Jacques Dubochet, Joachim Frank and Richard Henderson, who played a major role in the development of the method over the past 5 decades.

In order to resolve the structure of a macromolecule, it is first purified from the cellular environment and imaged at cryogenic temperatures using a transmission electron microscope (TEM). The resulting images, formed from the interaction of the electrons with the sample, are 2D projections of the macromolecule. Then, many 2D projections of the same macromolecule viewed from different orientations are combined *in silico* to form a 3D reconstruction. The reconstruction provides detailed information on the macromolecule and can be used for different purposes such as understanding protein function, interactions and dynamics, and for drug design.

Several technological advances have contributed to the improvement in map resolution, including advances in imaging quality and throughput, direct detection, new algorithms and computation power. Notably, although the improvement in map resolution has been major driving force, cryo-EM experiments entail additional elaborate information about the investigated macromolecule, such as the existence of multiple populations in the solution, oligomeric states and conformational heterogeneity. In my talk, I will introduce the theory and practice of single particle cryo-EM, and explain how recent ideas and technology have revolutionized the field.

---

SPECIAL SESSION ON CryoEM - 2017 NOBEL PRIZE FOR CHEMISTRY

## CRYO ELECTRON MICROSCOPY - A BRIDGE BETWEEN STRUCTURE AND FUNCTION

**Gabriel A. Frank**
*Department of Life Sciences and NIBN, Ben-Gurion University of the Negev, Beer-Sheva, Israel*

The field of cryo electron microscopy (cryo-EM) has seen dramatic advances in the past several years, with a rapidly growing number of near atomic resolution structures being published. This ‘resolution-revolution’ is a result of breakthroughs in detectors’ technology and computational methods. The highest resolution structures achieved by cryo-EM are of ridged single conformation proteins. However, the most important contribution of cryo-EM to our understanding of the molecular architecture of life, is its ability to determine structures in conformationally heterogeneous samples. While sorting out several conformations in a sample is already common in cryo-EM experiments, the ability to relate the different conformations to biochemical states and reaction coordinates is still under development. This talk will review how structures are determined in cryo-EM experiments and the ongoing computational and experimental directions for quantitative analysis of conformationally heterogeneous systems.

---

*Invited Lecture*

## MECHANICAL COMMUNICATION IN CARDIAC CELL BEATING

**Shelly Tzlil**
*Mechanical Engineering, Technion, Haifa, Israel*

Cell-cell communication enables cells to coordinate their activity and is essential for growth, development and function. Intercellular communication is discussed almost exclusively as having a chemical or an electrical origin, however; recent experiments demonstrate that cells can communicate mechanically by responding to mechanical deformations generated by their neighbors. However, the characteristics of mechanical communication, its role and its ability to regulate biochemical processes within the cell are still largely unknown.

In this talk, I will describe the use of imaging techniques to explore mechanical communication in cardiac cell beating and in the sensory organ of the fly.

We have recently shown that an isolated cardiac cell can be trained to beat at a given frequency by mechanically stimulating the underlying substrate using a 'mechanical cell'. The 'mechanical cell' consists of an oscillatory probe that mimics the mechanical aspect of a cell by generating substrate deformations identical to the ones induced by a neighboring beating cell. We further showed that the probe-induced beating rate is maintained by the cell for over an hour after mechanical stimulation had stopped, implying that long-term modifications occur within the cell. Continuing on this work, we study the dynamics of mechanically-coupled beating cardiomyocytes. We measure the mechanical interaction between neighboring cells and show that beat-to-beat variability strongly depends on the strength of mechanical coupling. A stochastic 'mechanical cell' is used to study the threshold for noise reduction and its dependence on mechanical coupling.

---



## FORCES ACTING AT THE INTERFACE OF T-CELLS AND APCS AND DRIVE T CELL ACTIVATION

**Yair Razvag**[1], Yair Neve-Oz[1], Meital Reches[2], Eilon Sherman[1]
[1]*Physics, The Hebrew University of Jerusalem, Jerusalem, Israel*
[2]*Chemistry, The Hebrew University of Jerusalem, Jerusalem, Israel*

In recent years, major breakthroughs in understanding and controlling the adaptive immune system have led to a new emergent personalized medicine field, the immunotherapy. Generally, a person immune system is exploited in the treatment against a disease, mostly many kinds of cancer, either by amplifying or by supressing an immune response.

Due to their central role in mounting an immune response, T-cells are promising candidates for immunotherapy treatments. T cells probe the surface of antigen presenting cells (APCs) for cognate foreign antigens in order to initiate an adequate immune response. This unique system requires the detection of a very weak signal (very rare foreign peptide - antigen) in the presence of considerable noise (abundant self peptides). In spite of its importance, much remains to be learned about the physical mechanisms that lead to T cell activation. Current models of mechanisms of T cell activation include dynamic molecular aggregation, conformational changes (mechanical effects) and kinetic segregation of inactivating molecules from sites of activation. Experimental evidence exist for each mechanism and thus imply that all mechanisms are involved simultaneously in the complex process of T cell activation.

The goals of this research work is to (1) quantify dynamic molecular patterning during cell activation, focusing on the role of protein tyrosine phosphatases in T cell activation, and (2) to resolve and quantify the effects of mechanical and
topographical properties over synapse creation and T cell activation.

For that purpose, we used live-cell multi-color single-molecule-localization microscopy (SMLM) to identify and study the dynamic separation between T cell antigen receptor (TCR) and CD45 glycoprotein

phosphatases in early forming cell contacts under TCR-activating and non-activating conditions. Atomic-Force Microscopy (AFM) and SMLM identified these
contacts with engaged microvilli and enabled to characterize their morphology, rigidity, and dynamics. We found the dynamic separation is with a complex nature as the TCR is both activated and de-activated by the CD45. Thus, although seperated by activation, the CD45 remains in the area of the signaling complex.
Furthermore, we utilize AFM measurements on living cells to study the relation, if any, between morphology and rigidity, in particular in T cells. We found there is a strong correlation between the two as the topography peaks, i.e, the microvili pretrusions, are with higher values of rigidity. We hypothesized that it might be the driven force in tight adhesion contacts at the immune synapse (IS).
Moreover, we developed a physical model and simulations that accurately captured the dynamic TCR-CD45 separation and the rigidity-topography relation under the experimental conditions.
Altogether, we expect that our findings and understanding the nature of the physical interactions that take place at the IS will shed light on the critical process of T cell activation. By so we pave the way for new novelty immunotherapy
treatments.

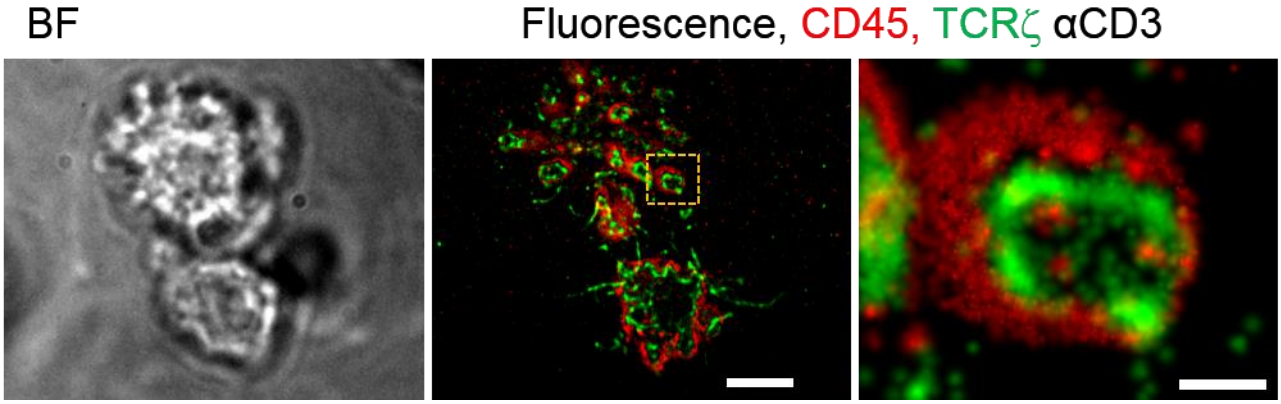


References:

Yair Razvag, Yair Neve-Oz, Julia Sajman, Meital Reches and Eilon Sherman
Nanoscale kinetic segregation of the T cell antigen receptor and CD45 in engaged microvilli facilitates early T cell activation. Nature Communications 2018 9:732

Yair Razvag, Yair Neve-Oz, Eilon Sherman and Meital Reches
Morphology rigidity correlation regulates T cell activation
Submitted for publication

---

Parallel Sessions I: LIFE SCIENCES

## MINIMALLY INVASIVE MICRO-ENDOSCOPY FOR BIOMEDICAL IMAGING IN HIGHLY SCATTERING MEDIA

**Omer Wagner**[1,4], Aditya Pandya[3], Yoav Chemla[2,4], Hadar Pinhas[1,4], Irina Schelkanova[3], Asaf Shahmoon[1], Yossi Mandel[2,4], Alexandre Douplik[3], Zeev Zalevsky[1,4]
[1]*Faculty of Engineering, Bar Ilan University, Ramat Gan, Israel*
[2]*Faculty of Life Sciences, School of Optometry and Visual Science, Bar Ilan University, Ramat Gan, Israel*
[3]*Physics Department, Ryerson University, Toronto, Canada*
[4]*Institute for Nanotechnology and Advanced Materials (BINA), Bar Ilan University, Ramat Gan, Israel*

Minimally invasive micro-endoscopes have been developed as a strategy to get high spatial resolution while one can both insert the device deeply into the target area and implant it for a long time for monitoring

purposes. This overcomes limitations of real non-invasive approaches with spatial limited resolution such as magnetic resonance imaging (MRI), computed tomography (CT), high and low frequency ultrasound (US). Furthermore, it also bypasses the limitations of high spatial resolution techniques, such as multiple photon fluorescence or confocal fluorescence that are applicable only at shallow interrogation depths and lack the ability to conduct long time observations. Combining capabilities to image through scattering medium enhances the technique capabilities and makes less harm to the imaged organ. Importantly, this could be of high value for retinal imaging, where delicate elements such as choroidal blood vessels are needed to be imaged beyond different cell layers.

Here we present a high spatial resolution setup based on a lensless, minimally invasive single mode fiber [1]. Our method allows for imaging to be done at a certain working distance above the surface, without interference to the imaged object. Fast overlapping scans enlarge the region of interest and enable dramatic signal to noise enhancement. The overlapping scans also allow employing of post-processing super-resolution algorithms. Having 5000 inner cores, each is 835 nm in diameter with 2.3 μm pitch between nearest cores, this setup can both image with high resolution and perform data collection for long time periods. This yields continuous knowledge on micron sized cells and organ sections. In-vitro imaging results of weak ARPE cells signals and rat retina are presented. Imaging beyond a scattering tissue is demonstrated using Hemoglobin filled microchannel made of Polydimethylsiloxane (PDMS) covered by intralipid in different widths.

Our experimental setup is schematically described in Fig. 1. White light emitting diode illuminated the sample from two positions - from below the sample for transmission mode, and from above it for reflectance mode. The scanning end of the optical microendoscope was located above the sample. A V-groove holder, axially positioned, held this end and translated using 3-axis motorized stage. The external end of the optical microendoscope was positioned and aligned within the focal plane of 20X objective, which in turn was coupled with a CMOS camera.

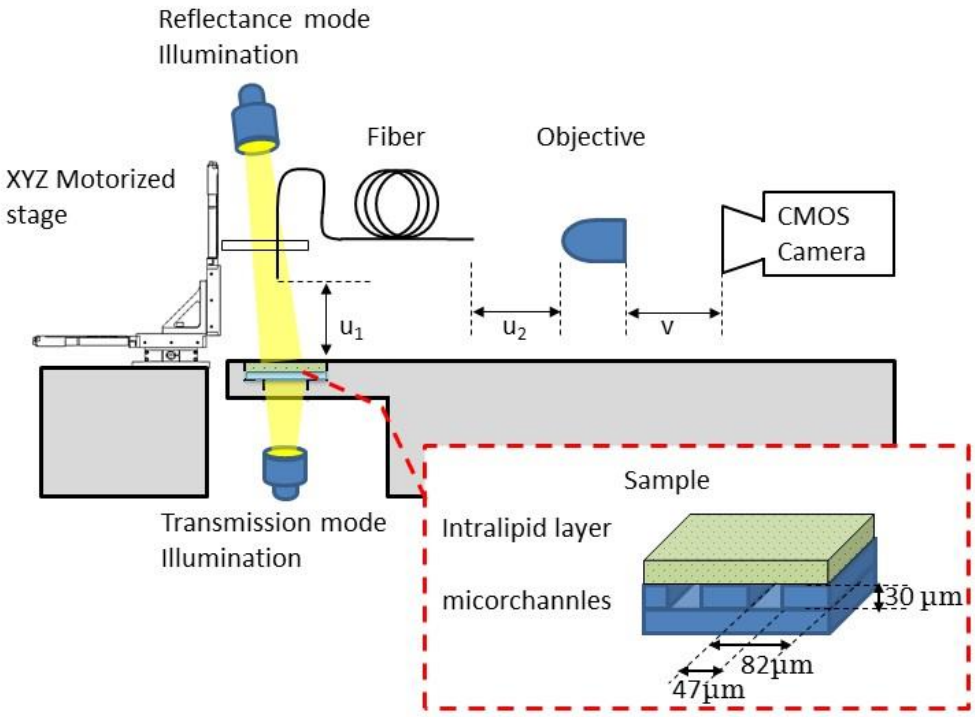


Fig. 2 shows the resulting imaging for the hemoglobin filled capillaries. Each rectangle shows the results of imaging with different width of the intralipid scattering medium. For each width, the whole scanned area is shown on the left, a zoomed image is shown in the middle and the intensity distribution along the red line in

the zoomed image is shown on the right. Imaging without any layer (a-c), yielded 47.3 µm line width with a contrast value of 0.45. Adding a 240 µm thick diffusive layer, 47 µm line width with a contrast value of 0.31 was measured (d-f). Increasing the thickness to 320 and 360 µm the line broadened in 3 microns and the contrast dropped to 0.27 and 0.2 respectively.

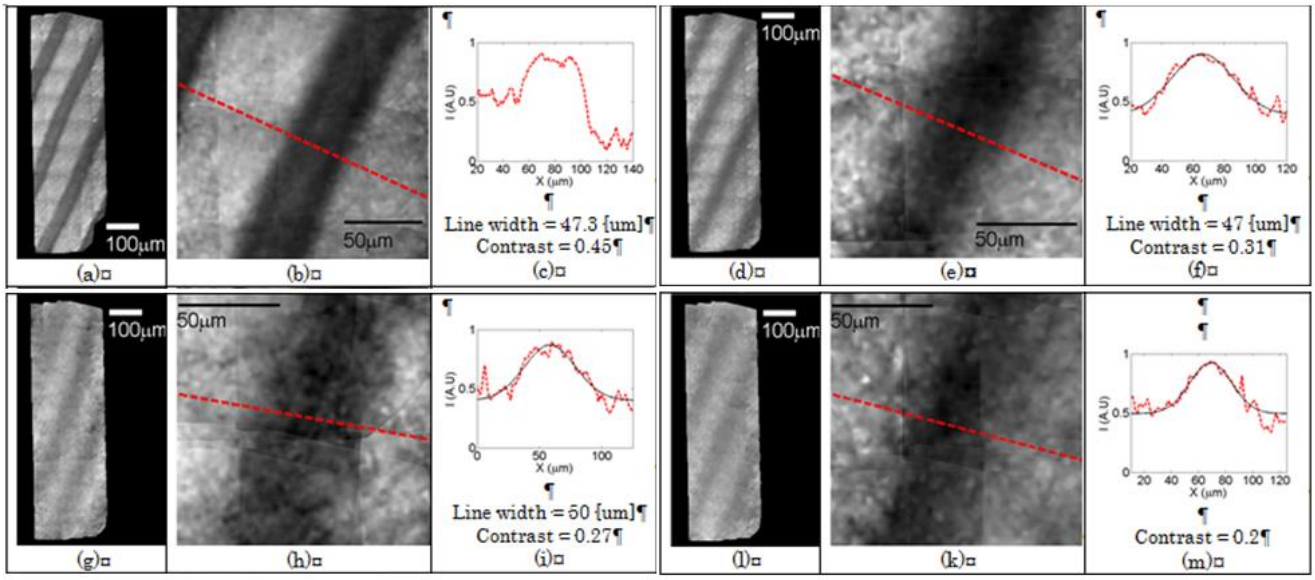


Fig. 3 shows the resulting imaging for non-labeled ARPE cells. Taking acquisitions with 20 µm translations allowed image stitching and applying super resolving (SR) algorithms leading to a single cells images. The red dashed rectangle area in the figure (a) is zoomed. The intensities of a raw image (b) are highly fluctuating and noisy. In each image the cores intensities are extracted and flat-corrected (c). Note the narrow fiber sampling to estimate the sampling density in comparison with the cells. The ARPE cells can clearly be distinguished after image stitching and SR algorithms (d). Their morphology could further be examined with the higher resolution.

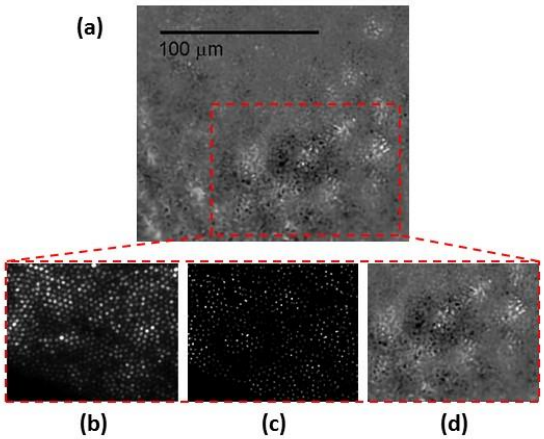


Fig. 4 shows 5 µm thick sliced rat retina imaging. On the left of (a) slice is shown using a phase microscope with a X4 magnification, the slice was then marked using a grid target and imaged again (b). A location marked by a yellow dashed rectangle was chosen, imaged with X20 magnification, and then scanned using our fiber. In the phase contrast image (b) the different retinal layers can be identified and numbered by the labels under the dashed red arrows. A distinct choroidal blood vessel (marked by an asterisk) is clearly seen. The fiber scan image, scanned with 10 µm translations at the same square area found using the grid target, is shown in (c). The scan succeeded to resolve the 10µm width choroidal blood vessel (marked by an asterisk).

The asterisk and Numbers 1-8 label: Choroidal blood vessel (*), Inner nuclear layer(1), Outer Plexiform layer(2), Outer nuclear layer(3), Outer segments(4), RPE – pigmented epithelium(5), Choroid(6), Sclera(7) and Conjunctiva(8).

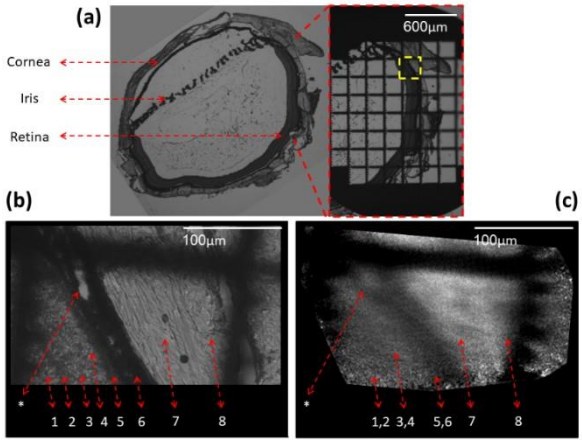


---

Parallel Sessions I: LIFE SCIENCES

## B CELL CLONAL SELECTION IN RESPONSE TO ORAL VACCINATION

**Adi Biram**[1], Anneli Strömberg[2], Eitan Winter[3], Liat Stoler-Barak[1], Yoseph Addadi[4], Gur Yaari[3], Mats Bemark[2], Ziv Shulman[1]

[1]*Immunology, Weizmann Institute of Science, Rehovot, Israel*

[2]*Department of Microbiology and Immunology, Institute of Biomedicine, University of Gothenburg, Gothenburg, Sweden*

[3]*Faculty of Engineering, Bar Ilan University, Ramat Gan, Israel*

[4]*Department of Life Science Core facilities, Weizmann Institute of Science, Rehovot, Israel*

The intestinal immune system is constitutively exposed to dietary and microbiome-derived antigens. Maintenance of host defense requires a balance between immune effector responses and tolerance under homeostatic conditions which is mainly achieved through production of antibodies in intestinal tissues (1). Effective antibody immune responses and establishment of long-lasting protection from invading pathogens depend on an increase in antibody affinity over time. This process, known as antibody affinity maturation, takes place in germinal centers (GC) where B cells undergo diversification by somatic hypermutation (SHM) and affinity-based clonal selection (2, 3). Mucosal-derived antigens are delivered into microanatomical structures within the PP known as subepithelial domes (SED) where B cells and antigen presenting cells reside (4). Following antigen uptake in the SED, antigen specific B cells migrate into the GC for further clonal expansion and diversification (5). Since the SED has a dome-like shape, it is unfeasible to capture its full structure neither by conventional immunohistochemistry nor by two photon laser scanning microscopy (TPLSM) methods. We combined whole organ imaging by light sheet fluorescence microscopy (LSFM) with an oral immunization model that allows us to examine the mechanism of B cell clonal selection in PPs. We find that B cells are subjected to stringent clonal selection by T cells during SED departure, resulting in increased clonal dominance in GCs revealed by single cell immunoglobulin sequencing. Opposed to GCs, SED B cell clones are highly diversified, indicating that clonal selection takes place during SED departure. Our results demonstrate that the threshold for GC entry following oral immunization in PPs is different from the responses elicited by conventional vaccines in draining lymph nodes. These findings have wide implications for design of oral vaccination strategies.

References

- Reboldi A, Cyster JG (2016) Peyer's patches: Organizing B-cell responses at the intestinal frontier. *Immunol Rev* 271(1):230–245.
- Victora GD, Nussenzweig MC (2012) Germinal Centers. *Annu Rev Immunol* 30(1):429–457.

- EISEN HN, SISKIND GW (1964) VARIATIONS IN AFFINITIES OF ANTIBODIES DURING THE IMMUNE RESPONSE. *Biochemistry* 3:996–1008.
- Reboldi A, et al. (2016) IgA production requires B cell interaction with subepithelial dendritic cells in Peyer's patches. *Science (80- )* 352(6287):aaf4822.
- Bergqvist P, et al. (2012) Re-utilization of germinal centers in multiple Peyer's patches results in highly synchronized, oligoclonal, and affinity-matured gut IgA responses. *Mucosal Immunol* 6(1):122–135.


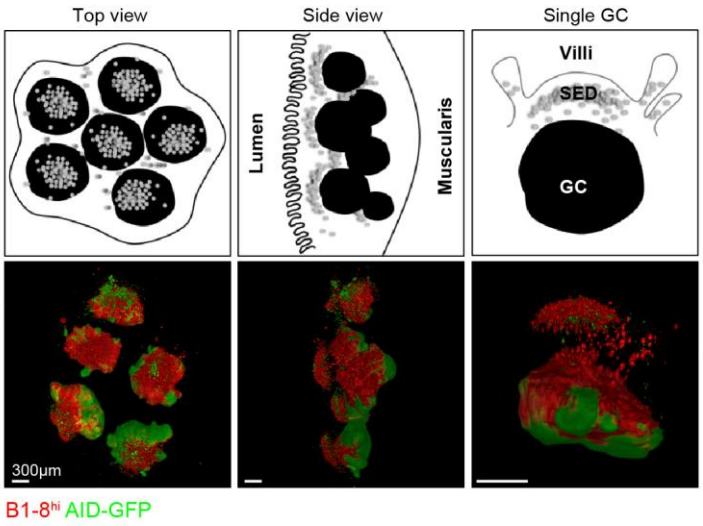


Figure 1- **Antigen specific B cell responses in the Peyer's patch.** A schematic representation of tissue position illustrate PP orientation in the images below (upper panel). Antigen-specific B cells (DsRed B1-8$^{hi}$, red) were adoptively transferred into AID reporter mice (AID-GFP, green) where endogenous AID-expressing cells serve as landmarks for the SED and GC compartments and imaged by LSFM (lower panel ). Transferred B cells colonize the SEDs, expand and infiltrate preformed GCs marked by AID-GFP.

---

Parallel Sessions I: LIFE SCIENCES

*Invited Lecture*

## EVALUATING THE DEVELOPMENTAL POTENTIAL OF OOCYTES AND PREIMPLANTATION EMBRYOS BASED ON MECHANICAL AND MACHINE LEARNING TOOLS


**Amnon Buxboim**[1,2,3], Yoav Kan-Tor[1], Oren Wintner[3], Roy Friedman[2], Adi Zseskin[3], Ity Erlich[1], Tamar Amitai[1], Arye Berger[2], Danny Kitsberg[2], Dorit Kalo[9], Iris Har-Vardi[4,5], Yuval Or[6], Zeev Shoham[6], Miriam Almagor[6], Onit Sapir[7], Arieh Horowitz[8], Zvi Roth[9], Matan Gavish[1], Assaf Ben-Meir[8]

[1]*School of Computer Science and Engineering, The Hebrew University of Jerusalem, Jerusalem, Israel*

[2]*Cell and Developmental Biology, The Hebrew University of Jerusalem, Jerusalem, Israel*

[3]*Alexander Grass Center for Bioengineering, The Hebrew University of Jerusalem, Jerusalem, Israel*

[4]*Fertility and IVF Lab, Soroka Medical Center, Be'er Sheva, Israel*

[5]*Health Sciences, Ben-Gurion University of the Negev, Be'er Sheva, Israel*

[6]*Fertility and IVF Unit, Kaplan Medical Center, Rehovot, Israel*

[7]*Beilinson Women's Hospital, Rabin Medical Center, Petah Tikva, Israel*

[8]*Obstetrics and Gynecology, Hadassah Medical Center, Jerusalem, Israel*
[9]*Animal Sciences, The Hebrew University of Jerusalem, Rehovot, Israel*

Early assessment of the developmental potential of preimplantation embryos to implant and generate a live birth is important for obtaining insights into the critical developmental cues and for advancing in vitro fertilization (IVF) based assisted reproductive technologies (ART). To address this unmet need, we combine advanced machine learning methods and in situ mechanical characterization of oocytes and embryos. We established an expansive database that consists of 70,000 preimplantation human embryos, which includes 3D video recordings, morphokinetic annotations, maternal information, clinical protocols, and transfer, implantation and live birth rates for each embryo. Based on this database, we trained convolutional neural networks (CNN's) and deep learning classifiers. Our classification algorithms perform automated morphokinetic annotation and predict embryo blastulation and implantation rates at early stages of development with exceptional accuracy. In parallel, we designed a culture-plate based device for performing non-invasive measurements of the viscoelastic properties of the embryos. We define mechanical parameters that differentiate between low-competence and high-competence embryos. Taken together, we present automated, non-invasive, standardized and accurate tools for early evaluation of embryonic competence and highlight physical and dynamic parameters that correlate with embryonic functions.

---

## Parallel Sessions II: LIFE SCIENCES

*Margulis Prize Lecture*

# DEEP-STORM: SUPER RESOLUTION SINGLE MOLECULE MICROSCOPY BY DEEP LEARNING

**Elias Nehme**[1,2], Lucien Weiss[2], Tomer Michaeli[1], Yoav Shechtman[2]
[1]*Department of Electrical Engineering, Technion, Israel Institue of Technology, Haifa, Israel*
[2]*Department of Biomedical Engineering, Technion, Israel Institue of Technology, Haifa, Israel*

In conventional microscopy, the spatial resolution is bounded by Abbe's diffraction limit, corresponding to ~half the optical wavelength. Super resolution methods, e.g. stimulated emission depletion (STED) [1], structured illumination microscopy (SIM) [2], and localization microscopy (PALM/STORM) [3-5] have revolutionized biological imaging in the last decade, enabling the observation of cellular structures at the nanoscale. Localization microscopy relies on acquiring a sequence of diffraction-limited images, each containing point-spread functions (PSFs) produced by a sparse set of emitting fluorophores. Next, the emitters are localized with high precision. By combining the recovered emitter positions from each frame, a super-resolved image is produced with resolution typically an order of magnitude better than the diffraction limit (down to tens of nanometers).

In localization microscopy, regions with high densities of overlapping emitters pose an algorithmic challenge. This emitter-sparsity constraint leads to a long acquisition time (seconds to minutes), which limits the ability to capture fast dynamics of sub-wavelength processes within live cells. To overcome this limitation, various algorithms have been developed to handle overlapping PSFs to enable higher sample density. While successful localization of densely-spaced emitters has been demonstrated, all existing methods suffer from two fundamental drawbacks: data-processing time and sample-dependent parameter tuning. Even accelerated sparse-recovery methods such as CEL0 [6], still involve a time-consuming iterative procedure, and scale poorly with the recovered grid size. In addition, current methods rely on parameters that balance different tradeoffs in the recovery process. These need to be tuned carefully through trial and error to obtain satisfactory results; ergo, requiring user expertise and tweaking time.

Recently, we demonstrated precise, fast, parameter-free, super resolution image reconstruction by harnessing Deep-Learning [7]. Convolutional neural networks have shown impressive results in a variety of image processing and computer-vision tasks, such as single-image resolution enhancement, and segmentation. By employing a fully convolutional neural network, we reconstructed super-resolution images from very dense fields of overlapping emitters (up to 6 emitters per ). Our method, dubbed Deep-STORM, does not explicitly

localize emitters. Instead, it creates a super-resolved image from the raw data directly. The net produces images with reconstruction resolution comparable or better than existing methods; furthermore, the method is extremely fast, and our software can leverage GPU computation for further enhanced speed. Moreover, Deep-STORM is parameter free, requiring no expertise from the user, and is easily implemented for any single-molecule dataset. Importantly, Deep-STORM is general and does not rely on any prior knowledge of the structure in the sample, making the method applicable to any single-molecule dataset.

We tested Deep-STORM on experimental and simulated super-resolution data, and benchmarked against the recently developed high-performance multi-emitter fitting algorithm CEL0 [6], and against the fastest multi-emitter fitting algorithm to our knowledge (FALCON [8]).

First, we reconstructed a simulated microtubule dataset available on the EPFL SMLM challenge website [9]. We quantified the quality of the results using the standard normalized mean square error: . Deep-STORM showed improved NMSE of 37% compared to 69% for CEL0 and 61% for FALCON. Second, we tested the result of Deep-STORM on experimental data obtained from Sage et al. [8], training solely on simulated data with similar experimental conditions - namely, SNR and emitter density. Deep-STORM resolves nearby lines and fine structures, and produces more continuous shapes compared to the output of CEL0 (Fig. 1) and FALCON (see SI of [7]).

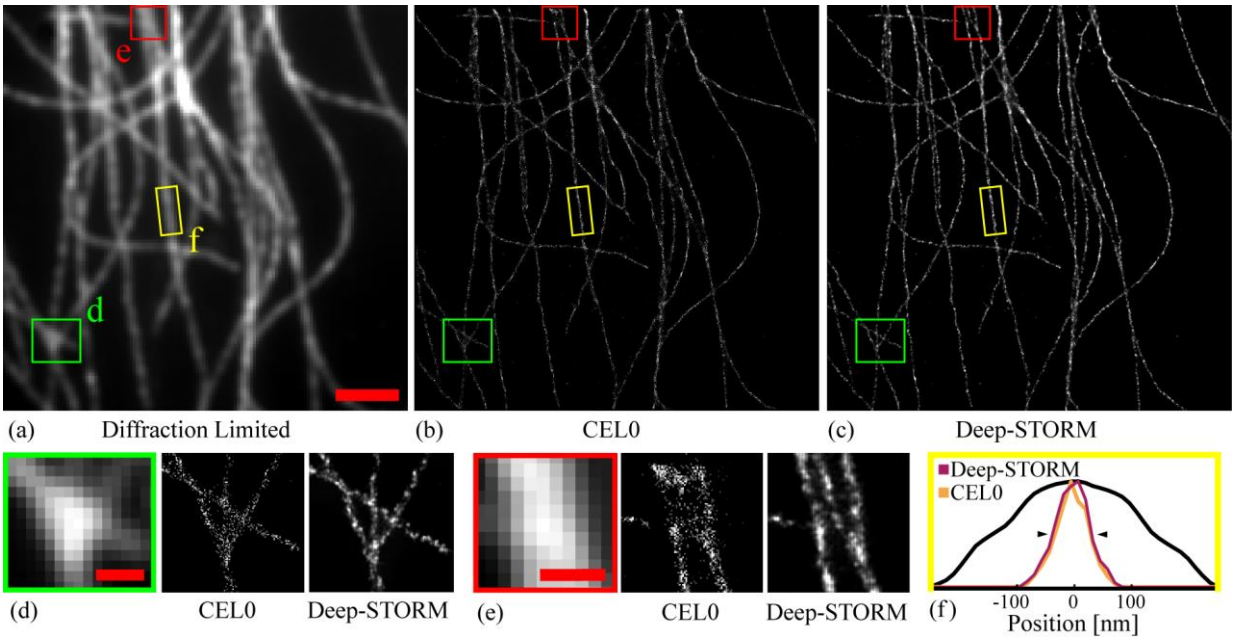


**Figure 1.** Experimentally measured microtubules. (a) Sum of the acquisition stack. Scale bar is 2 mm. (b) Reconstruction by the CEL0 method. (c) Reconstruction by Deep-STORM. (d)-(e) Magnified views of two selected regions. Scale bars are 0.5 mm. (f) The width projection of the highlighted yellow region. The attained FWHM (black triangles) for CEL0 was 61 nm and 67 nm for Deep-STORM. The black line shows the diffraction-limited projection.

Deep-STORM not only yields image reconstruction results that are comparable to or better than leading algorithms, but also does so ~1-3 orders of magnitude faster. Table 1 compares the run time of Deep-STORM vs. CEL0 and FALCON on both simulated and experimental microtubule datasets. Deep-STORM exhibits significantly superior runtime, especially when introducing GPU acceleration, equivalent to localizing ~20000 emitters per second, compared to ~1500 emitters per second by the fastest existing multi-emitter fitting method to our knowledge (FALCON [8]).

**Table 1.** Runtime comparison.

| Dataset | Grid size | CEL0 CPU [s] | FALCON CPU / GPU [s] | Deep-STORM CPU/GPU [s] |
|---|---|---|---|---|
| Sim. | 512 X 512 | 18677 | 1465/122 | 123/4 |
| Exp. | 1024 X 1024 | 175200 | 10177/434 | 715/27 |

Ultimately, the key ingredient in training neural networks is the training set. The best training set should include the aberrations in the experimental imaging system; however, very large data sets are typically used to train a deep neural network, and obtaining massive amounts of experimental images is not straightforward. However, we found that a reasonable number of experimental images (100) is sufficient to train a high-quality net. We trained and tested Deep-STORM on a sample containing randomly scattered fluorescent quantum dots to evaluate the performance on experimental data with a variety of SNR conditions encountered in single-molecule data sets, and at high density. Comparing to reconstruction of the same images using a net trained on simulated data, we found that the experimentally-trained net outperforms the simulated net, detecting 96% compared to 88% of the emitters, with a reduced false positive rate of 1.6% compared to 8.7%. This test demonstrates that while simulated data can serve as excellent training data - experimentally obtained images are even better. Additionally, a high-quality reconstruction net can be trained using a small number of experimentally measured images.

To conclude, Deep-STORM combines state-of-the-art resolution enhancement, unprecedented speed, and high flexibility (parameter-free operation). This combination produces a technique potentially capable of video-rate analysis of super-resolution localization-microscopy data that requires no expertise from the end user, overcoming some of the most significant limitations of existing localization methods.

References:

[1] S. W. Hell and J. Wichmann, “Breaking the diffraction resolution limit by stimulated emission: stimulated-emission depletion fluorescence microscopy,” Opt. Lett., vol. 19, pp. 780–782, Jun 1994.

[2] M. Gustafsson, “Surpassing the lateral resolution limit by a factor of two using structured illumination microscopy.” J. microscopy 198, 82–7 (2000).

[3] E. Betzig, et al., “Imaging intracellular fluorescent proteins at nanometer resolution,” Science (2006).

[4] S. T. Hess, T. P. Girirajan, and M. D. Mason, “Ultra-high resolution imaging by fluorescence photoactivation localization microscopy,” Biophys. J. 91, 4258 – 4272 (2006).

[5] M. J. Rust, M. Bates, and X. Zhuang, “Sub-diffraction-limit imaging by stochastic optical reconstruction microscopy (STORM),” Nat. Methods 3, 793–795 (2006).

[6] S. Gazagnes, E. Soubies, and L. Blanc-Féraud, “High density molecule localization for super-resolution microscopy using CEL0 based sparse approximation,” ISBI 2017-IEEE Int. Symp. on Biomed. Imaging p. 4 (2017).

[7] E. Nehme, et al., “Deep-STORM: Super resolution single molecule microscopy by deep learning“, **arXiv:**1801.09631. Accepted to Optica (2018).

[8] J. Min, et al., “FALCON: fast and unbiased reconstruction of high-density superresolution microscopy data,” Sci. Reports 4, 4577 (2015).

[9] D. Sage, et al., “Quantitative evaluation of software packages for single-molecule localization microscopy,” Nat. Methods 12, 717–724 (2015).

---

*Invited Lecture*

## CHARACTERIZING MRNA EXPORT AT HIGH RESOLUTION IN INDIVIDUAL NUCLEAR PORES IN SINGLE CELLS

**Yaron Shav-Tal**
*The Goodman Faculty of Life Sciences, Bar-Ilan University, Ramat Gan, Israel*

The export of mRNA from the cell nucleus is one of the pillars of the gene expression pathway in eukaryotes. We set out to characterize interactions involved in the various stages of mRNA transition through individual nuclear pores. Using different types of mRNA export blocks together with single-molecule mRNA tracking in living human cells we could detect the regions of the NPC at which the mRNAs were stuck. Our results suggest that the initial mRNA binding to the NPC does not require NXF1/Tap, whereas mRNA passage through NPC and release into the cytoplasm does. In accordance, super-resolution microscopy showed that NXF1/Tap is consistently occupying positions within the cytoplasmic side of the NPC. Measurements performed within individual nuclear pores using super-resolution STED microscopy, showed the positioning of NXF1/Tap in individual pores during regular and export blockage conditions. We then could further pinpoint these interactions with specific nucleoporins using a FLIM-FRET approach for measuring protein-protein interactions inside single NPCs. Altogether, these approaches have allowed the detection and measurements in intact cells, of specific interactions taking place between NXF1/Tap and mRNAs, and between NXF1/Tap and proteins within the NPCs. We have found that specific interactions at the cytoplasmic side of the NPC are crucial for the release of the mRNA to the cytoplasm, and have identified positions within the NPC that are mechanistically fundamental for the directional flow of mRNA and NXF1/Tap from the nucleus into the cytoplasm.

---



## SPONTANEOUS BUCKLING OF CONTRACTILE POROELASTIC ACTOMYOSIN SHEETS

**Ron Brand**, Anne Bernheim, Vitali Yeruhimowitz, Yaron Ideses
*Chemical Engineering, Ben-Gurion University of the Negev, Beer Sheva, Israel*

A central property of developing plant and animal tissues is their ability to form a diversity of folded patterns and to adopt curved shapes through mechanical instabilities that break the planar symmetry of growing epithelia[1,2–4]. The folding of growing epithelia can result from external mechanical constraints that restrict in-plane expansion[5]. Morphological changes can also occur in unconstrained sheets[6], where the emergence of wrinkles is associated with excess growth of the margins relative to the center of the sheet. This mechanism explains the shape of leaves and flowers[6–8]. In contrast to the shaping of growing tissues, the deformation of animal embryos during gastrulation often proceeds largely in absence of tissue growth and relies on active contractility[9–11]. In most cases, the mechanisms which are responsible for tissue folding are usually studied in cell epithelia (layer(s) of cells). In that case, shape deformations have been observed, when a contractile epithelium was subjected to anisotropic contraction [13] as well as in the case when it was coupled to an elastic substrate. [10] This presents a major difficulty for studying the intrinsic effect of actomyosin contractility on tissue folding *in vivo* where the external deformations and substrate cannot be controlled.

In recent work, we show that suspended, contractile actomyosin gel sheets can provide a good model system for studying contraction-induced folding. [12] We show that contractile acto-myosin gel sheets behave as a poroelastic material, where a flow of fluid is generated during contraction. We also observed that the acto-myosin sheet can spontaneously buckle and that the buckling instability resulted from system self-organization and the spontaneous emergence of density gradients driven by the active contractility. These new findings demonstrate that buckling can be spontaneously generated by myosin activity and does not require mechanical coupling to the environment or *pre-imposed* gradients in the material properties of the

sheet. The latter effect has been shown to be responsible for buckling in synthetic systems prepared with inhomogeneous crosslinkers densities or elastic moduli [14].

We fabricated symmetric, circular thin suspended contractile elastic acto-myosin sheets of controllable extent and elastic properties [12] by polymerizing actin in the presence of the strong passive cross-linker fascin and clusters of myosin II motors that act as active crosslinkers. Contractile elastic gels formed only if actin polymerization occurred in the presence of the motors and passive cross-linkers. [15–17] The polymerization process was performed in chambers with a high aspect ratio. Specifically, the sheets had initial radii (lateral extension) of about 1/2 and an initial thickness of typically a hundred (vertical extension). This corresponds to an aspect ratio, . The actomyosin gels spontaneously contracted through the activity of myosin motors with no need for external stimuli, save for the presence of ATP in solution. Contraction occurred only above a myosin concentration threshold [16]. For lower concentrations, the mechanical stresses generated by the motors were apparently too weak to overcome the gel's elasticity, whereas for higher motor concentrations the gel ruptured. [16,17]

The anisotropy in the gel extensions decoupled the contraction processes in the vertical and lateral directions. Namely, contraction started in the vertical direction and only when vertical contraction was essentially terminated, did the contraction begin along the lateral direction, thereby generating 2d actomyosin gel sheets of finite thickness. We found that during lateral contraction, the sheet thickness remained essentially constant. The actomyosin gels thus correspond to materials with an effective Poisson ratio ; as discussed below, this is due to the flow of water out of the material as it contracts which is the signature of poroelasticity [10,12] of combined fluid flow and gel deformation as opposed to gel elasticity alone. At advanced stages of planar contraction, the sheet spontaneously started to buckle. The buckling instability resulted from system self-organization and was due to the spontaneous emergence of density gradients (highest at the gel edge and lowest in the center) driven by the active contractility that persisted in steady state. Buckling occured when contraction of the gel periphery could not follow the contraction in the gel bulk. This is reminiscent of surfaces under the constraint of a fixed perimeter that is longer than the perimeter of a circle of the same surface area. The emerging folds were directed perpendicular to the boundary and had a roughly sinusoidal shape (Figure 1). The characteristic wavelength of the folded pattern was proportional to the sheet thickness, e.g., for a sheet thickness of with a corresponding wavelength of . Note that the macroscopic buckling phenomenon shown here occurs on a much larger length scale compared to the mesh size of the gel ( at the end of the contraction process) and does not result from the buckling of individual filaments observed in dilute actomyosin networks in the presence of weak cross-linkers such as α-actinin. [18-20)

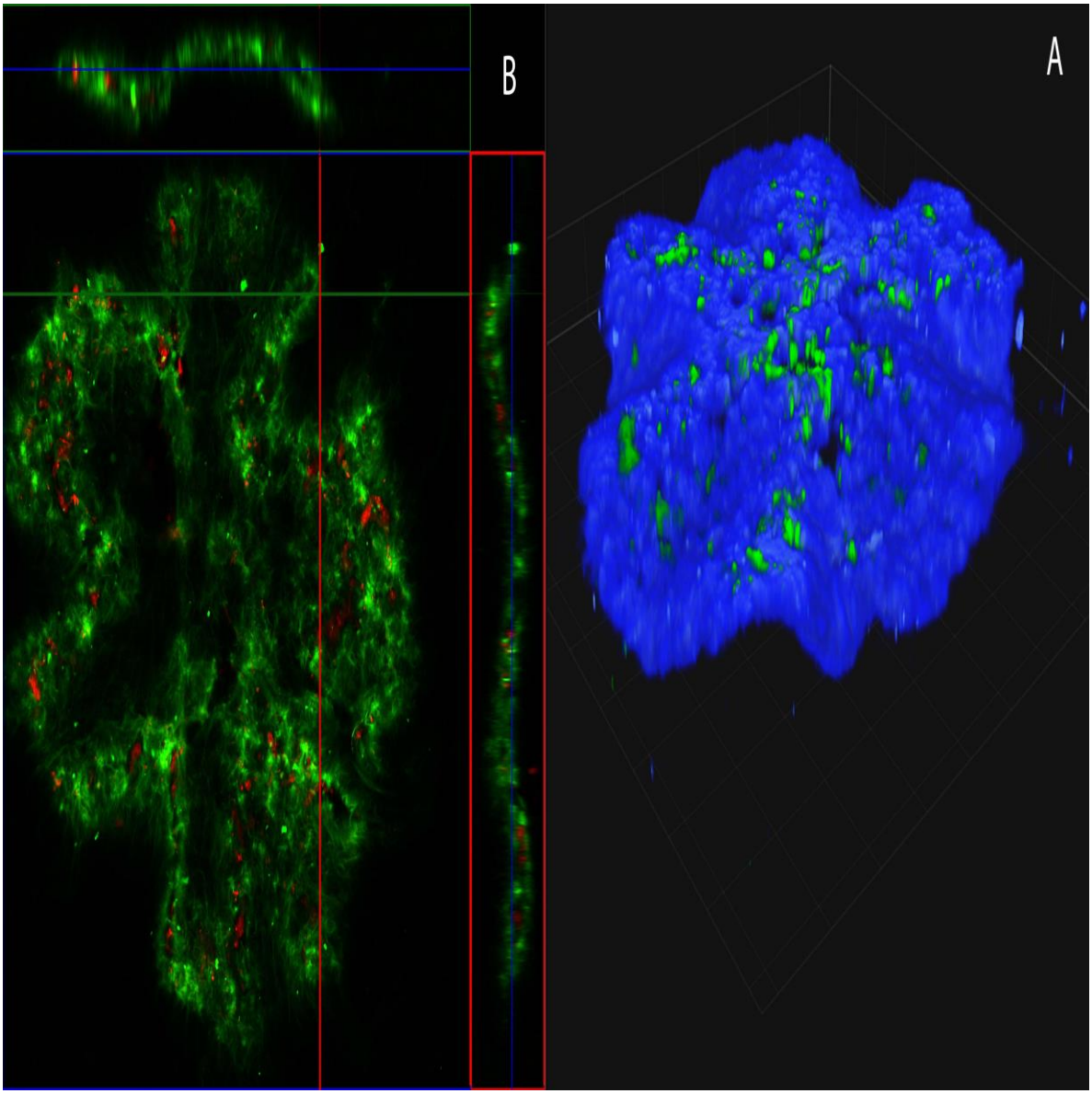


**Figure 1.** Buckling of an acto-myosin sheet . A) Laser scanning confocal micrograph of a three-dimensional view of a buckling gel at steady state(actin-blue,myosid green). B) Laser scanning confocal fluorescence micrographs of the actin gel in (A) in the xy-plane (top view), the xz-plane (top side view), and yz-plane (left side view)(actin-green,myosin-red). Side views (xz and yz-planes) are measured along the white lines. Scale bars: (horizontal) and (vertical) (insets of A) and (B).

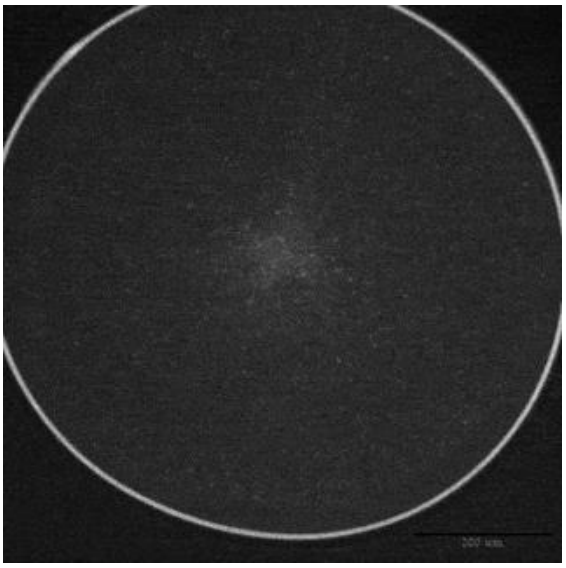

**Figure 2**: Actomyosin network contraction on XY plain. epifluorescence microscope. time scale 5 min. scale bar – 200um.

**References**

[1] C. P. Heisenberg, Y. Bellaïche, *Cell* **2013**, DOI 10.1016/j.cell.2013.05.008.

[2] B. Li, Y.-P. Cao, X.-Q. Feng, H. Gao, *Soft Matter* **2012**, *8*, 5728.

[3] J. A. Gemmer, S. C. Venkataramani, *Nonlinearity* **2012**, *25*, 3553.

[4] B. Audoly, A. Boudaoud, *Phys. Rev. Lett.* **2003**, *91*, 86105.

[5] A. E. Shyer, T. Tallinen, N. L. Nerurkar, Z. Wei, E. S. Gil, D. L. Kaplan, C. J. Tabin, L. Mahadevan, *Science* **2013**, *342*, 212.

[6] J. Dervaux, M. Ben Amar, *Phys. Rev. Lett.* **2008**, *101*, 68101.

[7] U. Nath, B. C. W. Crawford, R. Carpenter, E. Coen, *Science (80-. ).* **2003**, *299*, 1404.

[8] H. Liang, L. Mahadevan, *Proc. Natl. Acad. Sci. U. S. A.* **2011**, *108*, 5516.

[9] C. P. Heisenberg, Y. Bellaïche, *Cell* **2013**, DOI 10.1016/j.cell.2013.05.008.

[10] E. Hannezo, J. Prost, J.-F. Joanny, *Proc. Natl. Acad. Sci.* **2014**, DOI 10.1073/pnas.1312076111.

[11] B. He, K. Doubrovinski, O. Polyakov, E. Wieschaus, *Nature* **2014**, DOI 10.1038/nature13070.

[12] Y. Ideses, V. Erukhimovitch, R. Brand, D. Jourdain, J. Salmeron Hernandez, U. R. Gabinet., S. A. Safran, K. Kruse, A. Bernheim-Groswasser, *Submitted* **2017**.

[13] A. Livshits, L. Shani-Zerbib, Y. Maroudas-Sacks, E. Braun, K. Keren, *Cell Rep.* **2017**, DOI 10.1016/j.celrep.2017.01.036.

[14] Y. Klein, E. Efrati, E. Sharon, *Science* **2007**, *315*, 1116.

[15] F. Backouche, L. Haviv, D. Groswasser, A. Bernheim-Groswasser, *Phys. Biol.* **2006**, DOI 10.1088/1478-3975/3/4/004.

[16] Y. Ideses, A. Sonn-Segev, Y. Roichman, A. Bernheim-Groswasser, *Soft Matter* **2013**, DOI 10.1039/c3sm50309g.

[17] J. Alvarado, M. Sheinman, A. Sharma, F. C. MacKintosh, G. H. Koenderink, *Nat. Phys.* **2013**, DOI 10.1038/nphys2715.

[18] M. P. Murrell, M. L. Gardel, *Proc. Natl. Acad. Sci.* **2012**, DOI 10.1073/pnas.1214753109.

[19] M. Lenz, T. Thoresen, M. L. Gardel, A. R. Dinner, *Phys. Rev. Lett.* **2012**, DOI 10.1103/PhysRevLett.108.238107.

[20] X. Xu, S. A. Safran, *Phys. Rev. E - Stat. Nonlinear, Soft Matter Phys.* **2015**, *92*, 1.

---

Parallel Sessions II: LIFE SCIENCES

## CORRELATIVE CRYO X-RAY MICROSCOPY SHEDS LIGHT ON HEME DETOXIFICATION AND THE MECHANISM OF DRUG ACTION IN THE MALARIA PARASITE *PLASMODIUM FALCIPARUM*

**Sergey Kapishnikov**[1], Leslie Leiserowitz[2], Jens Als-Nielsen[1], Eva Pereiro[4], Yang Yang[5], Daniel Grolimund[6], James G. McNally[3], Gerd Schneider[3,7]

[1]*X-ray and Neutron Physics, Niels Bohr Institute - University of Copenhagen, Copenhagen, Denmark*

[2]*Department of Materials and Interfaces, Weizmann Institute of Science, Rehovot, Israel*

[3]*Soft Matter and Functional Materials, Helmholtz Zentrum Berlin, Berlin, Germany*

[4]*MISTRAL Beamline–Experiments Division, ALBA Synchrotron Light Source, Barcelona, Spain*

[5]*ID16A beamline, European Synchrotron Radiation Facility (ESRF), Grenoble, France*

[6]*Swiss Light Source, Paul Scherrer Institute, Villigen, Switzerland*

[7]*Institute of Physics, Humboldt University, Berlin, Germany*

Alarming signs of the malaria parasite resistance to current drug treatments highlight the need for identification of efficient targets to improve present antimalarial therapies. Residing in a human red blood cell the malaria parasite consumes hemoglobin and digests it in an organelle called the digestive vacuole. Hemoglobin digestion liberates large quantities of heme. This iron-containing molecule is toxic to the parasite. The parasite detoxifies heme by turning it into inert hemozoin crystals. This waste-disposal mechanism is a promising drug target. How heme is crystallized remains uncertain, but current models predict very different rates of crystallization. To this end we have developed a unique correlative X-ray absorption cryo-tomography and X-ray fluorescence cryo-microscopy method that enables us to determine the distribution and concentration of chemical elements relative to the three-dimensional cellular structure of instantly frozen snapshots of the malaria parasites in red blood cells.[1] Our measurements of heme crystallization rate and our discovery of considerable amounts of hemoglobin in the digestive vacuole suggest an assembly line process of heme detoxification: heme monomers liberated from hemoglobin are dimerized via the heme detoxification protein (HDP) and the dimers crystallize into hemozoin.[2] According to this model, the rates of heme monomer release, heme dimerization and hemozoin formation must closely match. Thus, two targets for drug development become apparent: inhibition of HDP, a subject of ongoing studies, and inhibition of hemozoin crystallization. Both targets will lead to accumulation of toxic heme monomers and self-poisoning of the parasite. Indeed, quinoline-family drugs are believed to act by targeting hemozoin crystallization. Specifically, molecular simulation studies predict that the drugs adsorb onto the surface of hemozoin crystals thereby inhibiting their growth[3,4]. In order to investigate this model, we used our X-ray cryo-microscopy method to quantitatively map the distribution of bromoquine, an analog of the classical chloroquine drug, within the malaria parasites. To avoid altering distribution of chemical elements due to sample preparation, the parasites were rapidly vitrified by cryo-freezing avoiding chemical fixation, staining, embedding or sectioning. Our results strongly support the predicted affinity of bromoquine to hemozoin crystals (see Figure 1). Interestingly, we also detect accumulation of bromoquine at the nucleus of the parasite indicating an additional antimalarial activity.

In conclusion, our correlative X-ray cryo-microscopy method establishes a new approach for the measurement of element-specific concentrations within intact cellular ultrastructure at high spatial resolutions of ~50 nm or better. This, in-turn, enables us to further investigate heme metabolism, antimalarial drug action and resistance in the malaria parasites.

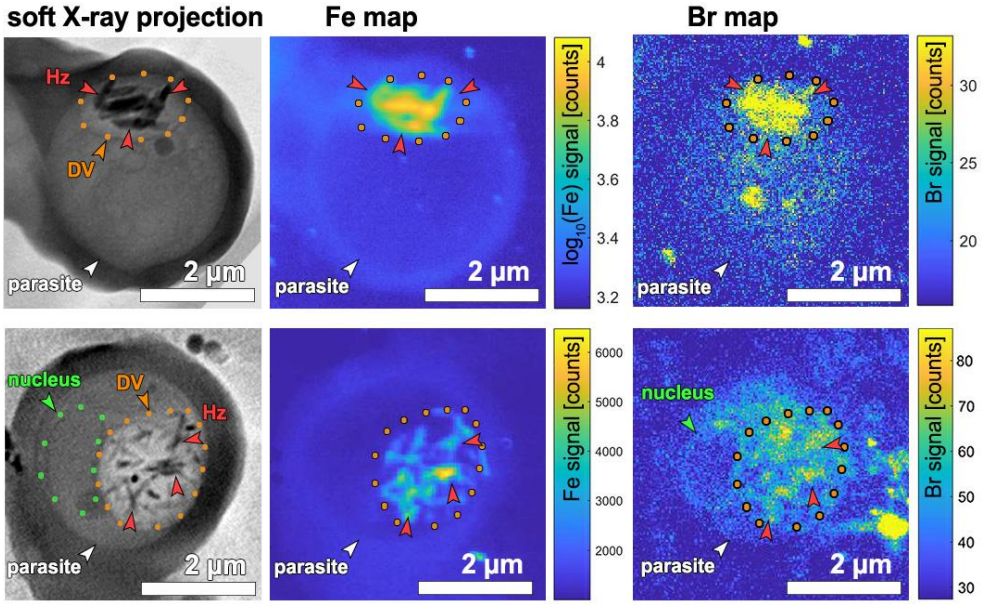


**Figure 1.** Soft X-ray cryo-tomography (SXT) re-projection images and X-ray fluorescence maps of two malaria parasite-infected red blood cells. Left: SXT maps. Center: iron (Fe) maps. Right: bromine (Br) maps. DV – digestive vacuole delineated with orange dots containing iron-dense hemozoin (Hz) crystals.

**References:**

1 Kapishnikov, S. *et al. Scientific Reports* **7**, 802 (2017).
2 Kapishnikov, S. *et al. Scientific Reports* **7**, 7610 (2017).
3 Dubar, F. *et al. ACS Chemical Biology* **6**, 275-287 (2011).
4 Buller, R. *et al. Cryst Growth Des* **2**, 553-562 (2002).

---

# CRYO-SCANNING TRANSMISSION ELECTRON TOMOGRAPHY REVEALS THE EXTRACELLULAR MATRIX AGAINST ORGANELLE ULTRASTRUCTURE

**Zipora Lansky**[1], Yael Mutsafi[1], Lothar Houben[2], Tal Ilani[1], Sharon G. Wolf[2], Deborah Fass[1]

[1]*Structural Biology, Weizmann Institute of Science, Rehovot, Israel*

[2]*Chemical Research Support, Weizmann Institute of Science, Rehovot, Israel*

Cryo-scanning transmission electron tomography (CSTET) is a novel method for creating three dimensional images of biological samples at nanometer resolution, while keeping the samples in their native hydrated state, without fixation, dehydration, or other perturbation[1–3]. We apply this technique to map the organization of the extracellular matrix (ECM) in cell cultures while simultaneously visualizing the underlying cell ultrastructure. Such snapshots can lead to insights about how the cells deposit and interact with the ECM, processes crucial for healthy physiology and which are perturbed by diseases such as cancer and myopathy[4,5]. The most abundant ECM components deposited by fibroblasts, collagen VI and fibronectin, were labeled with gold beads for contrast and identification. This enabled us to see collagen VI networks and fibronectin filaments together with intracellular organelles, cytoskeletal elements, and cell surface features such as caveolae (figure 1). Microfibril network patterns of collagen VI were analyzed quantitatively, showing the characteristic repeats of globular domains within individual fibrils and presenting novel information on fibril organization and turnover in the cell microenvironment. Specifically, cells appeared to migrate into collagen VI that had been widely dispersed in the cell vicinity following secretion, and collagen VI network fragments containing a few dozen globular repeats were taken up and recycled into large intracellular vesicles. This work demonstrates that CSTET is complementary to super-resolution light microscopy for the study of extracellular matrix in cell biology, highlighting labeled extracellular elements against a backdrop of unlabeled but morphologically identifiable cellular features with nanometer resolution detail.

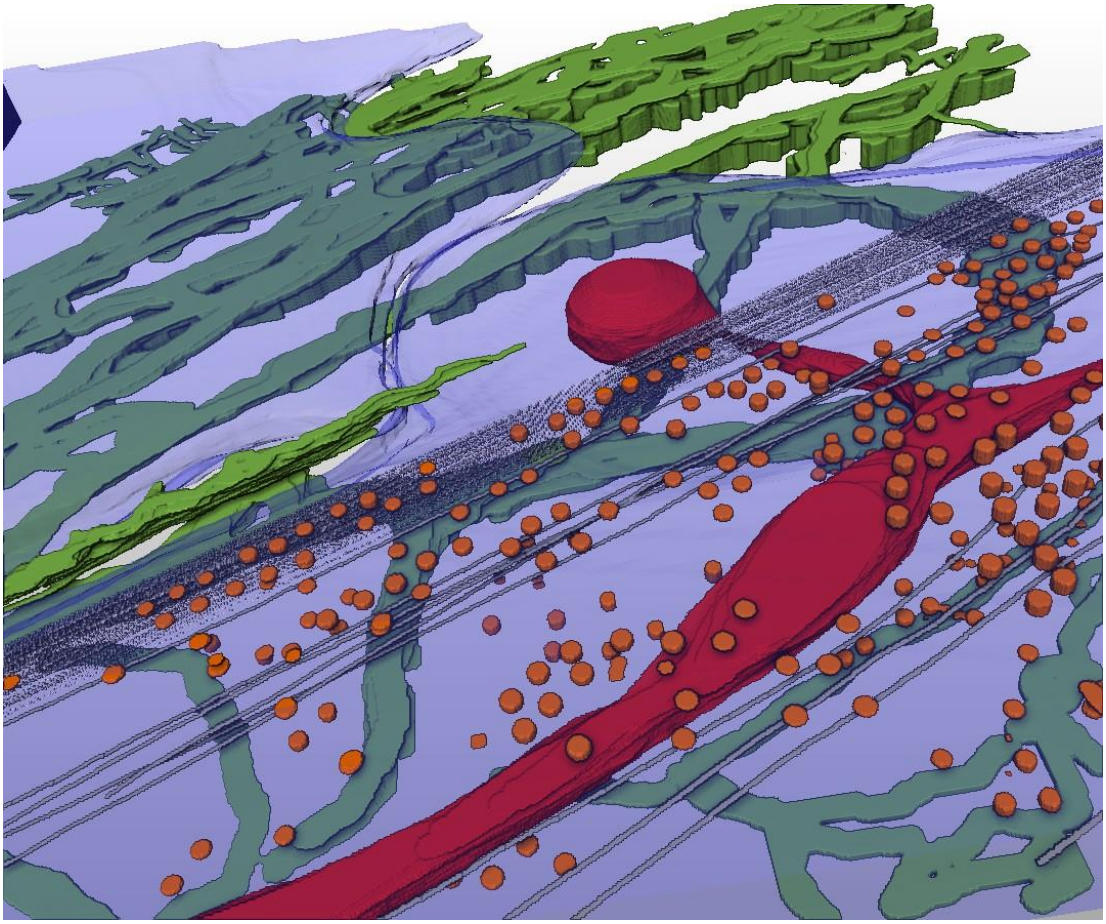

References:

[1] S.G. Wolf, L. Houben, M. Elbaum, Cryo-scanning transmission electron tomography of vitrified cells, Nat Meth. 11 (2014) 423–428.

[2] S.G. Wolf, P. Rez, M. Elbaum, Phosphorus detection in vitrified bacteria by cryo-STEM annular dark-field analysis, J. Microsc. 260 (2015) 227–233.

[3] S.G. Wolf, Y. Mutsafi, T. Dadosh, T. Ilani, Z. Lansky, B. Horowitz, S. Rubin, M. Elbaum, D. Fass, 3D visualization of mitochondrial solid-phase calcium stores in whole cells, Elife. 6 (2017) 1–18.

[4] L.K. Zamurs, M.A. Idoate, E. Hanssen, A. Gomez-Ibanez, P. Pastor, S.R. Lamande, Aberrant mitochondria in a bethlem myopathy patient with a homozygous amino acid substitution that destabilizes the Collagen VI α2(VI) chain, J. Biol. Chem. 290 (2015) 4272–4281.

[5] W.K. You, P. Bonaldo, W.B. Stallcup, Collagen VI ablation retards brain tumor progression due to deficits in assembly of the vascular basal lamina, Am. J. Pathol. 180 (2012) 1145–1158.

---

## Parallel Sessions II: LIFE SCIENCES

*Invited Lecture*

### QUANTUM ENHANCED SUPERRESOLUTION MICROSCOPY

**Dan Oron**, Ron Tenne, Yonatan Israel, Uri Rossman, Batel Rephael, Yaron Silberberg
*Physics of Complex Systems, Weizmann Institute, Rehovot, Israel*

Far-field optical microscopy beyond the Abbe diffraction limit, making use of nonlinear excitation (e.g. STED), or temporal fluctuations in fluorescence (PALM, STORM, SOFI) is already a reality. In contrast, overcoming the diffraction limit using non-classical properties of light is very difficult to achieve due to the fragility of quantum states of light. Here, we experimentally demonstrate superresolution microscopy based on quantum properties of light naturally emitted by fluorophores used as markers in fluorescence microscopy. Our approach is based on photon antibunching, the tendency of fluorophores to emit photons one by one rather than in bursts. Although a distinctively quantum phenomenon, antibunching is readily observed in most common fluorophores even at room temperature.

This nonclassical resource can be utilized directly to enhance the imaging resolution, since the non-classical far-field intensity correlations induced by antibunching carry high spatial frequency information on the spatial distribution of emitters. Detecting photon statistics simultaneously in the entire field of view, we were able to detect non-classical correlations of the second and third order, and reconstructed images with resolution significantly beyond the diffraction limit.

Alternatively, we demonstrate the utilization of antibunching for augmenting the capabilities of localization-based superresolution imaging in the presence of multiple emitters, using a novel detector comprised of an array of single photon detectors connected to a densely packed fiber bundle. These features allow us to enhance the spatial and temporal resolution with which multiple emitters can be imaged compared with other techniques that rely on CCD cameras.

Finally, new modalities for harnessing quantum photon statistics for super-resolved imaging will be discussed.

---

*Invited Lecture*

## MINIMISING DOSE (-RATE) IN THE STEM WHILE MAXIMISING INFORMATION CONTENT

**Lewys Jones**[1,2], Jakob Spiegelberg[3], Clive Downing[1], Annick DeBacker[4], Aakash Varambhia[5], Jan Rusz[3], Peter D. Nellist[5], Sandra VanAert[4]
[1]*Advanced Microscopy Laboratory (CRANN), Trinity College Dublin, Dublin, Ireland*
[2]*School of Physics, Trinity College Dublin, Dublin, Ireland*
[3]*Department of Physics and Astronomy, University of Uppsala, Uppsala, Sweden*
[4]*EMAT, University of Antwerp, Antwerp, Belgium*
[5]*Department of Materials, University of Oxford, Oxford, UK*

The scanning transmission electron microscope (STEM) yields many imaging and spectroscopic signals fully simultaneously and at very high-resolution. With the aberration corrected STEM now readily delivering atomic resolutions in these signals, the new frontier becomes sensitivity – the ability to detect more reliably and at lower imaging doses than before. The enemy of sensitivity is uncertainty, and in a scanned instrument this can come from spatial-uncertainty (scanning distortions); or from signal-uncertainty, the finite signal-to-noise which limits the data.

Previously we have shown how scanning distortions in annular dark-field (ADF) images can be compensated for by using non-rigid registration across a series of individual scans [1]. Going further, by analytically expressing this scanning-uncertainty along with the Poisson-limited uncertainty [2] and with the probability of introducing sample-damage, the experiment design can be optimised by minimising the combined uncertainty a function of electron-dose.

Shifting to a multi-frame regime, in practice, introduces many new experiment design parameters and these will be discussed. If the imaging conditions of these scans is not changed, then this process intrinsically increases the total sample exposure many times over. We can instead reduce the dwell-time and maintain a fixed total-dose, or we can reduce the beam current and reduce also the dose and dose-rate. Where the inherent cross-section is small for spectroscopic mapping, then multi-frame approaches can be used to accumulate signal over many frames while allowing time for heat or charge to dissipate leading to an overall reduction in damage [3]. However, left unchecked this spawns a new problem of unmanageable data-rates in the recording and approaches to mitigate this will be presented.

Lastly, we will present a new method to form ADF images using digital (electron counting) approach [4]. This pushes down the noise-floor to zero, improves the ADF MTF and DQE and returns images natively calibrated in an absolute greyscale units of electrons.

[1] L. Jones et al., *Adv. Struct. Chem. Imaging* **1**, 8 (2015).

[2] A. De Backer et al, *Ultramicroscopy* **151**, 56 (2015).

[3] L. Jones et al., *Microscopy* **67**, Supp. 1, (2018).

[4] R. Ishikawa et al., *Microsc. Microanal*. **20**, 99 (2014).

---



## ATOMIC-STRUCTURE REORGANIZATION AT THE SURFACE OF $BaTiO_3$ NANOPARTICLES

**Maya Barzilay**[1,2], Yachin Ivry[1,2]
[1]*Department of Materials Science and Engineering, Technion - Israel Institute of Technology, Haifa, Israel*
[2]*Solid State Institute, Technion - Israel Institute of Technology, Haifa, Israel*

Ferroelectrics are attractive materials for various low-power applications at the nanoscale thanks to the reversible spontaneous polarization they exhibit. The spontaneous polarization originates from collective

interactions of ion that are displaced off-center. In the non-centrosymmetric tetragonal structure of ferroelectrics, bound charges accumulate at the material surface to form depolarization field opposite to the bulk polarization direction. The ion organization at the surface is also responsible to reduce mechanical strain, giving rise to a unique electro-mechanical coupling. In the absence of surface-charge compensation, the ferroelectric state is unstable. To-date, full realization of the surface structure has remained elusive, hindering the theoretical and even conceptual understanding of ferroelectricity as well as the technological potential of ferroelectric materials.

Here, we report on direct observation of an unpredicted formation of a thin cubic TiO shell that helps stabilize the ferroelectric polarization of tetragonal $BaTiO_3$ nanoparticles. Moreover, we showed and quantified the dynamic evolution of this surface structure growth during exposure time to the electron beam, along with Ba escape. Our structural and chemical observations were confirmed using HRTEM/STEM equipped with HAADF as well as iDPC (integrated differential phase contrast) and atomic-resolution EDX detectors that allowed us to image the 20-pm ion displacement and to record the growth of 3-6 atomic layers of TiO shell on the $BaTiO_3$ surface. Finally, the effect of temperature was also examined, allowing us to demonstrate directly how the surface affects the ferroelectric phase transformation.

---

Parallel Sessions I: MATERIALS SCIENCE

## CHARACTERIZATION OF MATERIAL INTERACTION AND COMPOSITIONAL ANALYSIS OF NANOMACHINING AND NANODEPOSITION USING A $Cs^+$ FOCUSED ION BEAM – A SOURCE TECHNOLOGY CANDIDATE FOR FUTURE CIRCUIT EDIT PLATFORMS

**Yariv Drezner**[1], Yuval Greenzweig[1], Roy Hallstein[2], Rick Livengood[2], Amir Raveh[1], Adam Steele[3], Brenton Knuffman[3], Andrew Schwarzkopf[3]

[1]*Intel Israel (74), Ltd., P.O. Box 1659, Haifa, Israel*

[2]*Intel Corporation, 2200 Mission College Blvd., Santa Clara, CA 95054 , USA*

[3]*zeroK, Nanotech, Gaithersburg, MD 20879, USA*

The use of focused ion beam (FIB) instruments has become essential for the semiconductor and microelectronic industries in recent years. Transmission electron microscopy (TEM) sample preparation [1,2], failure analysis (FA) [1,3], and nanofabrication of miniature prototypes [3,4] are all performed using FIBs. Another indispensable FIB application field is circuit edit (CE), where FIB has been used to fix faulty circuitry and verify layout modifications prior to lithography masks remanufacturing [5]. In addition, CE provides working chips prior to the next manufacturing round, thus expediting time to market of semicoductor products [6]. Frequent CE FIB activities are signal rerouting and device bypassing [5,6]. These involve FIB gas assisted etch to designated metal lines, followed by ion beam induced deposition (IBID) of oxides (for isolation where required) and metals (for connections). The requirements from the IBID material here are relatively low resistivity for conductors, and high resistivity for the insulators - both depend on the material purity of the deposit [5].

In order to enable the fine micro- and nano-machining required for the above applications, FIB source technologies have been developed over the past three decades. To date, the $Ga^+$ liquid metal ion source (LMIS) and $Xe^+$ plasma cusp ion sources provide the horsepower behind fine machining and bulk micro-machining, respectively [6,7]. Gas field ionization source (GFIS) based FIBs were introduced in the last decade, providing small probe-size and highly localized nano-machining solutions for mask-defect repairing and fine re-wiring [6]. These tools are in different development and comercialization phases.

Alternative emerging FIB source technologies based on the magneto-optical trap were recently introduced [8,9]. These “cold beam” technologies, involve the ionization of deep sub-Kelvin laser-cooled atoms, and formation of low energy spread focused ion beams. One of the most promissing candidates for cold beam is the $Cs^+$ Low Temperature Ion Source (LoTIS), introduced by zeroK Nanotech [8].

In this talk we shall present and discuss our recent findings on gas assisted nano-machining and IBID using the proof of concept $Cs^+$ LoTIS installed on zeroK’s test platform. TEM images of nano-mchining features will be shared, as well as energy dispersive spectroscopy (EDS) composition measurements taken from IBID lines. Further nano-machining attributes will be discussed.

- R. Young and M. V. Moore, Introduction to Focused Ion Beams (Springer, New York, 2005), pp. 247–268.
- L. Giannuzzi, B. W. Kempshall, S. M. Schwartz, J. K. Lomness, B. I. Prenitzer, and F. A. Stevie, Introduction to Focused Ion Beams (Springer, New York, 2005), pp.201–228.
- N. Yao, Focused Ion Beam Systems: Basics and Applications (Cambridge University, Cambridge, England, 2007), pp. 268-280.
- A. A. Tseng, Small 1, 924 (2005)
- J. Melngailis, J. Vac. Sci. Technol., B **5**, 469 (1987).
- S.Tan and R. Livengood, He Ion Microscopy (Springer, Switzerland, 2016), pp. 479–490.
- M.M.V. Taklo, A. Klumpp, P. Ramm, L. Kwakman and G. Franz, Microscopy and Analysis **9** (November 2011)
- B. Knuffman, A. V. Steele, J. J. McClelland, J. Appl. Phys. **114** 044303 (2013)
- J. J. McClelland, A. V. Steele, B. Knuffman, K. A. Twedt, A. Schwarzkopf, and T. M. Wilson, Appl. Phys. Rev. **3** 011302 (2016)


---

Parallel Sessions I: MATERIALS SCIENCE

## INVESTIGATION OF THE STRUCTURE OF A NEW ND-RE-AL PHASE USING ELECTRON CRYSTALLOGRAPHY METHODS


**Gili Yaniv**, Louisa Meshi

*Department of Materials Engineering and Ilse Katz Institute for Nanoscale Science and Technology, Ben-Gurion University of the Negev, Beer-Sheva, Israel*


In the framework of the Nd-Re-Al phase diagram study, new ternary phase was discovered with the 2:3:15 stoichiometry. Although alloy of an interest was exposed to prolonged (one month) heat treatment (at 800°C), it did not attained equilibrium state, and contained multiple binary and ternary phases. Therefore, structure solution of the new phase was essentially impossible using traditional X-ray diffraction methods. Electron crystallography, in this case, was the only viable tool applicable for structure solution. Methodology summarized in [1] was successfully applied for characterization of the structure of this aluminide. Classical electron diffraction patterns taken from the particles of this phase exhibited interesting features, attributed to structural defects. Geometry of the unit cell and partial atomic model were deduced applying direct methods (utilized in Sir2014 [2]) on electron diffraction tomography dataset. Structure of the new Nd-Re-Al phase was found to be related to the $Ln_{7+x}Re_{12}Al_{61+y}$ (where Ln = lanthanide element) family [3]. Structural model as well as structure relationship to the $Ln_{7+x}Re_{12}Al_{61+y}$ family will be presented.

References


1. Samuha, Y. Krimer L. Meshi, J. Appl. Cryst. 47 (2014) 1032.

2. C. Burla, R. Caliandro, M. Camalli, B. Carrozzini, G. L. Cascarano, C. Giacovazzo, M. Mallamo, A. Mazzone, G. Polidori, and R. Spagna, J. Appl. Crystallogr. 45 (2012) 357.

3. Niemann, W. Jeitschko, J. Alloys Compd. 221 (1995) 235.


---

*Invited Lecture*

## ELECTRON BEAM-INDUCED CURRENT ELUCIDATES PHOTOVOLTAIC MECHANISMS IN HALIDE PEROVSKITE SOLAR CELLS

**Gary Hodes**
*Materials and Interfaces, Weizmann Institute of Science, Rehovot, Israel*

Halide perovskite (HaP) solar cells have reached ~23% conversion efficiency in the 6 years since serious research began in the field. In spite of the enormous research being carried out on these cells, there are still many outstanding questions. One of these is: What is the operating mechanism that dominates in HaP cells? By careful choice of experimental conditions and procedures, necessary because of the electron beam sensitivity of the materials to the electron beam, we succeeded to use electron beam-induced current (EBIC) to understand the photovoltaic operating mechanisms of the cells. The mechanisms are found to be dependent on the specific HaP used, while also the metal contact can affect the nature of the cell. As part of these studies we demonstrate effects of both the electron beam and of light on both the HaP itself and on cells made using the HaPs.

---



*Invited Lecture*

## STATISTICAL METHODS AND MACHINE LEARNING OF DIFFRACTION DATA FOR MICROSTRUCTURE ANALYSIS

**Alexander Eggeman**[1], Ben Martineau[2], Paul Midgley[2]
[1]*School of Materials, University of Manchester, Manchester, UK*
[2]*Department of Materials Science and Metallurgy, University of Cambridge, Cambridge, UK*

Data science approaches have been successfully applied to a variety of electron microscopy measurements, resulting in highly detailed analysis of composition, electronic structure, crystallography and atomic structure of complex materials systems. The goal in all of these approaches is to take a large set of measurements from a sample and then to utilise the redundancy in the data to recover a model, or set of significant factors that can be associated with the physically distinct components in the material. In the case of diffraction data the goal is to identify the unique diffraction pattern associated with each component or region within a microstructure and which can be used to characterise that component.

Statistical decompositions are one widely used method for this, using matrix factorisation methods to isolate those particular signals that describe the majority of the structured part of the data as efficiently as possible. This has proven a valuable approach in the analysis of scanning diffraction data, especially in the fairly common situation where individual diffraction patterns can contain information about one or more overlapping phases in the microstructure being studied. The value of these approaches for analysing both simulated as well as experimental data will be addressed.

Further to this, the decomposition stage can also be thought of as a means of lowering the dimensionality of the data-analysis problem. This allow new approaches such as C-means or ‘fuzzy’ clustering to be applied. In high dimensional data the `distance` between two points (measurements) can become quite a complicated problem, whereas in low dimensions this becomes a more understandable quantity. Using such distance metrics allows like and unlike patterns to be distinguished via computational means alone. The distribution , shape and interaction between these clusters of measurements offers not only a way to improve the separation of overlapping signal but also a tantalising possibility of a machine learnable method for identifying different microstructural features.

---

# DIRECT IMAGING OF CARBON NANOTUBES IN SUPER-ACID SOLUTIONS AND LIQUID CRYSTALLINE PHASES

**Olga Kleinerman**

*Chemical Engineering, Technion - Israel Institute of Technology, Haifa, Israel*

During recent years it has been demonstrated that carbon nanotubes (CNTs) spontaneously dissolve in chlorosulfonic acid (Davis et al., 2009), and at high concentrations form a liquid crystalline phase (Davis et al., 2004). Actually, chlorosulfonic acid (CSA) is the only solvent for CNT, to form thermodynamically stable solutions and liquid crystalline phases, from which carbon nanotube fibers can be spun. Fiber spinning from a liquid crystal state is essential for the high degree of CNT orientation in the fibers, and hence preserving the intrinsic unique properties of individual CNT (such as an exceptional strength and electrical conductivity) in the spun fiber (Behabtu et al., 2013).

The transition between the isotropic and the liquid crystalline phases depends strongly on the CNT type, concentration, and solvent strength. Combination of direct cryogenic transmission- and cryogenic scanning-electron microscopy (cryo-TEM and cryo-SEM) of CNT/CSA solutions at different concentrations allowed us, for the first time to follow phase transformation at nanometric level; from diluted solution to the isotropic phase, through the biphasic region, to the pure liquid crystalline phase, used as the "dope" for fiber spinning (Kleinerman et al., 2017). This work presents the first direct validation of Onsager`s and Flory`s models describing phase transitions in rigid-rod polymers (Onsager, 1949, Flory, 1956) in CNT/super-acid systems.

To allow direct imaging of superacid solutions we developed novel cryo-EM specimen preparation and imaging methodologies, suitable for highly acidic systems. Those techniques preserve the native nanostructure in the system, without harming the expensive equipment and the operator (Kleinerman et al., 2015), and were successfully applied to study CNTs (Davis et al., 2009, Kleinerman et al., 2017) and boron nitride nanotubes (Kleinerman et al., 2017) in CSA in their native state.

The correlation between direct imaging of the "dope" in its liquid state and of fiber, spun from the "dope" allowed us to study the effect of CNT behavior in the solution on final fiber structure and alignment, which are directly related to fiber mechanical and electrical properties. By a combination of x-ray analysis, with a focused ion beam (FIB) fiber cross-sectioning, and high-resolution electron microscopy for morphological and chemical analysis, we have provided nanometric structural information of the individual CNTs and CNT fibers, in terms of the basic nanotube properties, the degree of fiber alignment, the degree of purity and porosity.

**References:**

Davis, V. A.; Parra-Vasquez, A. N. G.; Green, M. J.; Rai, P. K.; Behabtu, N.; Prieto, V.; Booker, R. D.; Schmidt, J.; Kesselman, E.; Zhou, W.; Fan, H.; Adams, W. W.; Hauge, R. H.; Fischer, J. E.; Cohen, Y.; Talmon, Y.; Smalley, R. E.; Pasquali, M. True Solutions of Single-Walled Carbon Nanotubes for Assembly into Macroscopic Materials. Nat. Nanotechnol. 2009, 4, 830–834.

Davis, V. A.; Ericson, L. M.; Parra-Vasquez, a. N. G.; Fan, H.; Wang, Y.; Prieto, V.; Longoria, J. A.; Ramesh, S.; Saini, R. K.; Kittrell, C.; Billups, W. E.; Adams, W. W.; Hauge, R. H.; Smalley, R. E.; Pasquali, M. Phase Behavior and Rheology of SWNT in Superacids. Macromolecules 2004, 37, 154–160.

Behabtu, N.; Young, C. C.; Tsentalovich, D. E.; Kleinerman, O.; Wang, X.; Ma, A. W. K.; Bengio, E. A.; ter Waarbeek, R. F.; de Jong, J. J.; Hoogerwerf, R. E.; Fairchild, S. B.; Ferguson, J. B.; Maruyama, B.; Kono, J.; Talmon, Y.; Cohen, Y.; Otto, M. J.; Pasquali, M. Strong, Light, Multifunctional Fibers of Carbon Nanotubes with Ultrahigh Conductivity. Science 2013, 339, 182–186.

Kleinerman, O.; Liberman, L.; Behabtu, N.; Pasquali, M.; Cohen, Y.; Talmon, Y. Direct Imaging of Carbon Nanotube Liquid-Crystalline Phase Development in True Solutions. Langmuir 2017, 33, 4011–4018.

Onsager, L. The Effects of Shape on the Interaction of Colloidal Particles. Ann. N. Y. Acad. Sci. 1949, 51, 627–659.

Flory, P. J. Phase Equilibria in Solutions of Rod-Like Particles. Proc. R. Soc. A Math. Phys. Eng. Sci. 1956, 234, 73–89.

Kleinerman, O.; Parra-Vasquez, A. N. G. N. G.; Green, M. J. J.; Behabtu, N.; Schmidt, J.; Kesselman, E.; Young, C. C. C.; Cohen, Y.; Pasquali, M.; Talmon, Y. Cryogenic-Temperature Electron Microscopy Direct Imaging of Carbon Nanotubes and Graphene Solutions in Superacids. J. Microsc. 2015, 259, 16–25.

Kleinerman, O.; Adnan, M.; Marincel, D. M.; Ma, A. W. K.; Bengio, E. A.; Park, C.; Chu, S.-H.; Pasquali, M.; Talmon, Y. Dissolution and Characterization of Boron Nitride Nanotubes in Superacid. Langmuir 2017, 33.

---

Parallel Sessions II: MATERIALS SCIENCE

## SUPER-FERROMAGNETISM OF IRON DISILICIDE NANO-ISLANDS

**Matan Dascalu**, Federico Cesura, George Levi, Oswaldo Dieguez, Ilan Goldfarb
*Materials Science and Engineering, Tel Aviv univeristy, Tel-Aviv, Israel*

We demonstrate control over super-magnetic response of tetragonal iron disilicide epitaxial and coherent nano islands on vicinal Si(111) surfaces. We utilize two epitaxial growth modes - solid phase epitaxy (SPE) and reactive deposition epitaxy (RDE) - to grow structurally equivalent but morphologically different iron disilicide nano islands: orientated, ordered matrix vs. isotropic and randomly scattered. The structure and chemistry of these surfaces is investigated using scanning tunneling microscopy (STM), low energy electron diffraction (LEED), x-ray photo-electron spectroscopy (XPS), and transmission electron microscopy (TEM). The effect of surface arrangement on magnetic response is studied using superconducting quantum interference device (SQUID) magnetometry. We show that the periodic ordering of the islands along the vicinal surface of the Si(111) substrate is the primer reason for the emergence of the superferromagnetic behavior of the islands; who are otherwise superparamagnetic.

---

Parallel Sessions II: MATERIALS SCIENCE

## IMAGING ORGANIC CRYSTALLIZATION IN AQUEOUS MEDIA

**Yael Tsarfati**, Haim Weissman, Shaked Rosenne, Boris Rybtchinski
*Organic Chemistry, The Weizmann Institute of Science, Rehovot, Israel*

Organic crystals are of primary importance in pharmaceuticals, functional materials, and biological systems. Nevertheless, the understanding of organic crystallization mechanism is still limited. Understanding the transformation from “Non-classical” Prenucleation phases into crystals is a key challenge. In this study a Perylene Diimide (PDI) crystallization, within aqueous solution, is studied by optical spectroscopy and cryogenic electron microscopy, in order to address this challenge. Direct imaging of evolving prenucleation phase reveals a fascinating complexity of a nonclassical crystallization path, providing new insights into organic crystallization mechanism.

---

Parallel Sessions II: MATERIALS SCIENCE

## PHOTON-INDUCED FAR-FIELD AND NEAR-FIELD ELECTRON MICROSCOPY

**Kangpeng Wang**[1], Giovanni Vanacore[2], Enrico Pomarico[2], Ivan Madan[2], Gabriele Berruto[2], Francisco de Abajo[3,4], Ido Kaminer[1], Fabrizio Carbone[2]
[1]*Faculty of Electrical Engineering, Technion-Israel Institute of Technology, Haifa, Israel*
[2]*Institute for Condensed Matter Physics (ICMP), École Polytechnique Fédérale de Lausanne (EPFL), Laussane, Switzerland*
[3]*ICFO-Institut de Ciencies Fotoniques, The Barcelona Institute of Science and Technology, Barcelona, Spain*
[4]*ICREA, Institució Catalana de Recerca i Estudis Avançats, Barcelona, Spain*

The development of four-dimensional ultrafast electron microscopes (4D UEM) breaks the time resolution limit of conventional transmission electron microscopy techniques and enables sample imaging with fs temporal and nanometer spatial resolutions [1]. This promising capability is based on photon-electron interactions mediated by the evanescent field localized around the imaged nanostructure [2-4] and is known as photon-induced near-field electron microscopy (PINEM) [1-3]. Despite many reports on ultrafast dynamics of plasmons and phonons [5-6], the full potential of imaging via the interactions between electrons and the light field is not completely understood yet. In this work, we developed the PINEM technique for novel imaging capabilities in two new scenarios: Scanning resonant near-field electron microscopy and Semi-infinite far-field electron microscopy.

In scanning resonant near-field electron microscopy [7] many nanostructures have spectral responses that are highly sensitive to the excitation frequency. To enable coupling into such resonant modes with PINEM, a tunable wavelength laser for excitation is required. Here we demonstrate this technique with a silver nanowire by employing an optical parametric amplifier as a wavelength-tunable light source. The plasmonic mode energy was resolved down to the laser linewidth; 20 meV in this work. This scanning resonant electron microscopy not only reveals the ultrafast dynamics of a nanostructure, but can also determine the oscillatory energy with meV resolution. Moreover, it becomes possible to directly image optically sensitive low-energy modes such as phonons and Raman vibrations which are too weak to be observed by conventional PINEM and EELS.

In semi-infinite far-field electron microscopy [8] we investigated electron-photon interactions in the semi-infinite vacuum far-field rather than using the evanescent near-field of a nanostructure as the medium for photon-electron energy exchange as in PINEM. We observed the depletion of the zero-loss peak (ZLP) in EELS and the broadening of the electron energy distribution as the tilt angle increased. Remarkably, this implies that almost all electrons interacted with the photon field. This strong coupling in the far-field greatly extends the reach of PINEM by increasing the overall photon-electron interaction cross-section and thus producing a significantly enhanced signal. This work implies a potential imaging technique assisted by refracting, absorbing, or reflecting interfaces.

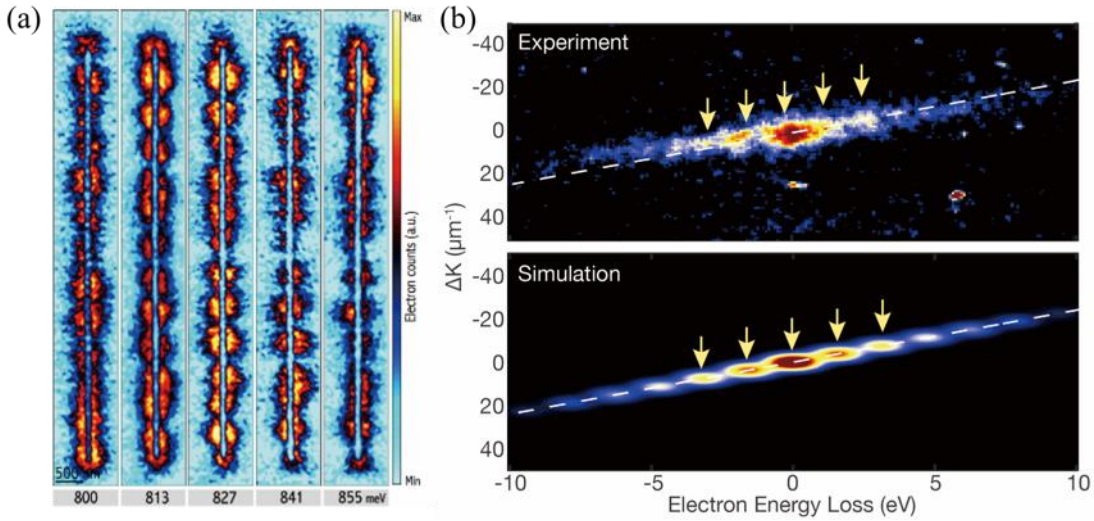


Fig. 1 New imaging capabilities through the PINEM technique in two new scenarios: (a) Imaging plasmonic standing waves by a tunable excitation in the UEM (b) Observation and simulation of the energy and momentum exchanges between electron and photon in UEM diffraction mode.

**References**

[1] A. Zewail, “Four-Dimensional Electron Microscopy”, Science 328, 187-193. (2010)
[2] B. Barwick, D. Flannigan and A. Zewail, "Photon-induced near-field electron microscopy". Nature 462, 902-906. (2009)
[3] S. T. Park, et. al., "Photon-induced near-field electron microscopy (PINEM): theoretical and experimental." New J. Phys. 12, 123028 (2010).
[4] F. de Abajo. “Optical excitations in electron microscopy.” Rev. Mod. Phys. 82, 209. (2010)
[5] D. Cremons, et. al., "Defect-mediated phonon dynamics in TaS2 and WSe2." Struct. Dyn. 4, 044019. (2017)
[6] L. Piazza, et. al., “Simultaneous observation of the quantization and the interference pattern of a plasmonic near-field.” Nat. Commun. 6, 6407. (2015)

[7] E. Pomarico, et. al., “meV resolution in laser-assisted energy-filtered transmission electron microscopy”, ACS Photonics. (2017)
[8] GM Vanacore et. al., “From attosecond to zeptosecond coherent control of free-electron wave functions using semi-infinite light fields”. arXiv:1712.08441

---

Parallel Sessions II: MATERIALS SCIENCE

*Invited Lecture*

## ABERRATION CORRECTION IN TRANSMISSION ELECTRON MICROSCOPES USING SCULPTED MEMBRANES

**Ady Arie**
*Physical Electronics, Tel Aviv University, Tel Aviv, Israel*

A sculpted thin membrane of silicon nitride can be used as a phase-mask [1] to induce specific aberrations into an electron beam probe [2]. Specifically, it can be used to correct the inherent spherical aberration of the standard, spherically symmetric lenses that are used in the electron column, by inducing opposite spherical aberration with a thin film corrector. The advantage of this concept is that it enables an immediate and low-cost upgrade to an existing non-corrected electron microscope, by placing the corrector in one of the available aperture ports of the microscope.

We validated this concept by designing and fabricating (by focused ion beam milling) a corrector that was installed in the condenser 2 aperture of a 300 kV FEI Titan scanning transmission electron microscope. The non-corrected spherical aberration of the microscope, with a coefficient Cs=2.7mm, determined the convergence semi-angle of 7.4 mrad for achieving optimal resolution. However, when our corrector was added, this optimal angle was increased to 12 mrad. This correction reduced the probe size from 183 pm to 124 pm, thus enabling to resolve details that could not be observed with the uncorrected microscope. For example, the silicon dumbbells, separated by 136 pm could be resolved only when the corrector was used [3].

The method we present can be further extended to correct other types of aberrations and in addition to probe correction, it may also be also used for image correction.

[1] R. Shiloh, Y. Lereah, Y. Lilach and A. Arie , “Sculpturing the electron wave-function using nanoscale phase masks”, Ultramicroscopy 144, 26-31 (2014).

[2] R. Shiloh, R. Remez and A. Arie, “Prospects for electron beam aberration correction using sculpted phase masks”, Ultramicroscopy 163, 69-74, (2016).

[3] R. Shiloh, R.Remez, P.-H. Lu, L. Jin, Y. Lereah, A. H. Tavabi, R. E. Dunin-Borkowski and A. Arie, “Spherical aberration correction in a scanning transmission electron microscope using a sculpted foil”, Ultramicroscopy 189, 46-53 (2018).

---

P-1

## CYTOKINETIC ABSCISSION IN EARLY ZEBRAFISH EMBRYOGENESIS

**Shai Adar**, Dikla Nachmias, Ramon Birnbaum, Natalie Elia
*Life Sciences, Ben Gurion University, Beer Sheva, Israel*

Cytokinetic abscission is the last step of cell division where two daughter cells are separated. After membrane constriction, the cells remain connected by an intercellular bridge of membrane and microtubules. Abscission is mediated by fission of the microtubules and membrane driven by the ESCRT proteins complex. The spatiotemporal organization of ESCRTs during abscission was mapped in cytokinesis of mammalian tissue-culture-cells. However, little is known about the ESCRTs role during embryonic development. In this study, we tracked the spatiotemporal dynamics of intercellular bridges at different division cycles of developing zebrafish embryos. We found that abscission is delayed prior to the $10^{th}$ cell cycle. During the first 10 division cycles, cells maintain their intercellular bridges as they enter the following cycle. The $10^{th}$ division cycle in zebrafish termed MidBlastula-Transition (MBT), and characterized by translation of zygotic genes, appearance of G1 phase and by loss of synchronized division. ESCRTs are expressed prior to MBT due to maternal expression. Moreover, we detected ESCRT candidates localize to the midbody in stages prior to MBT, where abscission is inhibited. It therefore appears that the abscission machinery is present, however abscission is still inhibited. Study this unique abscission inhibition will shed light on ESCRT regulation processes, and will contribute to understand ESCRT machinery during development.

---



P-2

## BIOORTHOGONAL LABELING OF ESCRT PROTEINS USING FLUORESCENT ORGANIC DYES

**Ariel Alon**
*Life Sciences, Ben-Gurion University of the Negev, Beer Sheva, Israel*

ESCRT is a machinery that enables the severing of membrane necks in a variety of cellular processes. Among the ESCRT family, ESCRT-III is thought to be the driving force for the membrane fission reaction by polymerizing into helical structures. Until recently, the main technique used to label these complexes, and other proteins, in live cells was by tagging them with fluorescent (Fl) proteins. The main problem with such approach is that Fl-proteins are larger than most ESCRT-III subunits and consistently tagging ESCRT-III with Fl-proteins interferes with proper function of these proteins. We therefore, set to apply a more direct approach for labeling these proteins in live cells.

---



P-3

## ROLE OF LAMIN A PROTEIN IN DIFFUSION PROPERTIES OF CHROMATIN IN EMBRYONIC STEM CELLS AND NEURON PRECURSORS

**Irena Bronshtein**[1,2], Efrat Shoham[2], Ron Goldstein[2], Hodaya Hochberg[2], Yaron Shav-Tal[2], Yuval Garini[1]
[1]*Physics Department and Nanotechnology Institute, Bar Ilan University, Ramat Gan, Israel*

[2]*The Mina & Everard Goodman Faculty of Life Sciences, Bar Ilan University, Ramat Gan, Israel*

The organization of the genome in the nucleus is believed to be crucial for cellular functions such as gene regulation and the maintenance of genome integrity along the cell cycle. We used live cell imaging to examine the organization of the genome in living cells. We analysed the diffusion of different genomic sites by measuring their trajectories through Single Particle Tracking (SPT) and thoroughly characterized their diffusion characteristics also under depletion of different nuclear proteins.

We found that chromatin diffusion in differentiated cells is slow and anomalous; in vast contrast, absence of lamin A protein leads to a significant increase in chromatin mobility, and induces a dramatic transition of genome dynamics from slow anomalous diffusion to fast and normal diffusion.

Constrained chromatin mobility can have an important role in maintaining the chromosomal territories, which in turn prevents chromosomal entanglement and aberrations. Indeed, by using SKY (Spectral Karyotyping) technique, we found that $Lmna^{-/-}$ cells have a higher frequency of genomic aberrations compared to normal cells.

While B-type lamins are expressed in all cells, A-type lamins are developmentally regulated and they do not express in ESCs cells. Diffusion analysis of chromatin motion in ESCs and hNP1 (Neuron Precursors) cells indicates that chromatin scan much large volume in the nucleus compared to differentiated cells, while the expression of lamin A in these cells restricts chromatin local freedom of motion. More than this, the dynamics of chromatin loci in Embryonic stem cells (ESCs) was found to be normal diffusion, similar to lamin A depleted cells. The expression of lamin A protein in hNP1 cells switched the type of diffusion from normal to anomalous diffusion. It means that lamin A protein acts as key in the cells that able to switch on /switch off the chromatin diffusion type.

We now try to understand the functional reason for the drastic increased freedom of chromatin motion in undifferentiated cells compare to differentiated cells.

---

POSTER SESSION - Life Sciences

P-4

## TIME RESOLVED INTENSITY PHOTOBLEACHING – A NOVEL METHOD FOR STUDYING PROTEINS IN LIVE CELLS

**Eugene Brozgol**, Irena Bronshtein, Itamar Kantor, Yuval Garini
*Physics Department, Bar Ilan University, Ramat Gan, Israel*

We present a method for exploring proteins in living cells. In a single measurement, the method enables to reveal a significant number of quantitative properties of the proteins dynamics including the diffusion coefficient, bound and free fraction, protein concentration and binding-unbinding kinetics. The method combines in a single measurement quantitative photobleaching, fluorescence correlation spectroscopy and fluorescence lifetime imaging. After labeling the protein of interest with a fluorescent protein, we use time correlation single photon counting to measure the fluorescence intensity at fixed points in the sample. The information provides both the fluorescent intensity as a function of time for ~60 seconds, the rapid intensity fluctuations (KHz) and the decay time of each arriving photon. This information is processed according to a procedure that takes the biophysical dynamic model of a protein into account and the full kinetic behavior of the protein is revealed.

---

P-5

# UNDERSTANDING THE MECHANISMS UNDERLYING CHOLESTEROL CRYSTAL FORMATION IN ATHEROSCLEROSIS

**Jenny Capua Shenkar**[1], Neta Varsano[1], Eyal Shimoni[2], Ifat Kaplan-Ashiri[2], Katya Rechav[2], Lia Addadi[1]
[1]*Structural Biology, Weizmann Institute of Science, Rehovot, Israel*
[2]*Chemical Research Support, Weizmann Institute of Science, Rehovot, Israel*

Atherosclerosis is a chronic progressive disease characterized by the sub-endothelial accumulation of Low Density Lipoproteins (LDL), cholesterol-esters and cholesterol crystals [1]. Cholesterol crystals are difficult to dissolve by means of known physiological mechanisms and hold pro-inflammatory properties perpetuating the atherogenic process. The combination of these factors facilitates the instability and the eventual rupture of the atheromatous plaque leading to arterial thrombosis. Macrophage cells have a crucial role in LDL metabolism in the atheromatous tissue and the process of cholesterol crystal formation [2]. However, the exact mechanism by which crystals form in atherosclerotic plaques is not yet understood.

Cholesterol crystals are formed by J774 macrophages fed with CE-droplets, presumably intracellularly, from lipid loaded lysosomes [3]. Crystals formed within J774 macrophages are characterized by a needle or plate like appearance. Similar characteristics of cholesterol crystals are observed in intracellular locations of human macrophages and the extracellular matrix of human atherosclerotic lesions. We have studied cholesterol crystals formation in macrophages nucleating from cholesterol nano-domains segregating within the cell plasma membrane or from intracellular locations [4,5].

The main objective of this research is to elucidate the possible mechanisms responsible for cholesterol crystals formation in macrophages. Here we demonstrate that cholesterol crystals are formed within viable J774A.1 macrophages fed with Ac-LDL, implying that the crystallization process may occur during the initial stages of LDL accumulation and is not necessarily associated with or is a product of macrophage cell death. To allow 3D observation and analysis of macrophage foam cells and atherosclerotic tissues under cryogenic conditions, we employ cryo-Focused Ion Beam/Scanning (cryo-FIB-SEM) block face serial imaging [6]. We are currently developing a method comprising cryo-SEM combined with Cathodoluminescence for studying cholesterol crystals formation in macrophage cell culture models (J774A.1/Human monocyte derived macrophages) and rabbit atherosclerotic tissues. Cathodoluminescence signal provided by cholesterol crystals and/or fluorescently labeled cholesterol crystal-specific antibodies is being assessed.

Understanding the underlying mechanisms of cholesterol crystals formation in macrophage model cells and atherosclerotic plaques can provide useful information toward possible therapeutic approaches.

**References**:

- Kruth, H.S., *Lipoprotein cholesterol and atherosclerosis.* Current molecular medicine, 2001. **1**(6): p. 633-653.
- Kruth, H., *Macrophage foam cells and atherosclerosis.* Frontiers in bioscience: a journal and virtual library, 2001. **6**: p. D429-55.
- Tangirala, R.K., et al., *Formation of cholesterol monohydrate crystals in macrophage-derived foam cells.* Journal of lipid research, 1994. **35**(1): p. 93-104.
- Varsano, N., et al., *Development of Correlative Cryo-soft X-ray Tomography and Stochastic Reconstruction Microscopy. A Study of Cholesterol Crystal Early Formation in Cells.* Journal of the American Chemical Society, 2016. **138**(45): p. 14931-14940.
- Varsano N., et al., *Two Polymorphic Cholesterol Monohydrate Crystal Structures Form in Macrophage-derived Foam* Relevance to Atherosclerosis PNAS, under revision.

- Vidavsky, N., et al., *Cryo-FIB-SEM serial milling and block face imaging: Large volume structural analysis of biological tissues preserved close to their native state.* Journal of structural biology, 2016. **196**(3): p. 487-495.


---

POSTER SESSION - Life Sciences

P-6

## PUTTING HIGH CONTENT SCREENS INTO FOCUS – A NOVEL APPROACH FOR PERFORMING GENETIC SCREENING AT ELECTRON MICROSCOPY RESOLUTION


**Nir Cohen**[3], Yury Bykov[1,2], Maya Schuldiner[3], John Briggs[1,2]

[1]*Structural and Computational Biology, European Molecular Biology Laboratory, Heidelberg, Germany*

[2]*Structural Studies, MRC Laboratory of Molecular Biology, Cambridge, UK*

[3]*Department of Molecular Genetics, Weizmann Institute of Science, Rehovot, Israel*


In recent years, genetic screens performed using high throughput fluorescent microscopes have generated large data-sets that contributed many insights into cell biology. However, such approaches cannot tackle question of ultra-structure that are below the resolution limit of fluorescent microscopy. Electron microscopy (EM) overcomes this resolution limit and generates high-resolution, ultra-structure, imaging. However, this advantage comes at a cost, as EM requires long and expensive sample preparation limiting throughput. To overcome this obstacle, we suggest a robust method to perform high(er) content screening using correlative light and EM. Our approach is based on pooling together different yeast populations for EM sample preparation and subsequent identification if each cell's genotype using fluorescent barcodes. Coupled with easy to use software for correlation, segmentation and computer image analysis, our method currently allows us to extract 15 different yeast populations from a single sample preparation. Such a methodology is not restricted to yeast and can be utilized in multiple ways to enable EM to become a powerful screening methodology.

---

POSTER SESSION - Life Sciences

P-7

## GREEN SYNTHESIS OF SINGLE CRYSTALLINE GOLD NANOPLATES: UNVEILING AN UNEXPECTED POTENTIAL OF BEET ROOT WASTE A MECHANISTIC STUDY


**Girish Deokar**, A.G. Ingale

*Dept. of Biotechnology, School of Life Sciences, North Maharashtra University, Jalgaon, Maharashtra, India*


A mechanistic approach toward unveiling a mechanism of formation of single crystalline gold (Au) nanoplates via a novel green synthetic route, using an aqueous extract of red beetroot waste (BRW) i.e peel, at room temperature(Deokar and Ingale, 2018). However, use of chemical methods for the synthesis of nanoparticles exhibited many drawbacks including harmful nature of solvents, reagents and the reducing environment that might result in the contamination in end product or may generate some risky by-product. Application of the green chemistry principles for nanostructure synthesis is a challenging task. No doubt there are varieties of reports of green synthesis of the nanoparticles using a plant material(Shankar et al., 2004), but using waste material from the plant is the novelty of this work. Previous reports on waste mediated nanoparticle synthesis includes our major contribution like banana peel(Deokar and Ingale, 2016) and the crystallinity dependent study focusing the potential of the beetroot peel aqueous extract(Deokar and Ingale, 2017)

Here in we report a novel green method for mechanical study of the single crystalline triangular nanoplates. The green method examined using UV-VIS spectroscopy, the existence of metallic gold validated using EDS and XPS, structure and orientation of the gold nanostructures examined using XRD. The active biomolecules present in the BRW aqueous extract that are responsible for reduction, confirmed using XPS and FTIR spectroscopy. These significant characterisations, unveiled a probable three-step mechanism for nanoplate synthesis. First, formation of the nanosphere, second its transformation into icosahedrons and finally its fragmentation into triangular nanoplates. The green synthetic mechanism for these nanoplates is investigated, validated and evidenced by both HR-TEM and XRD studies. The selected area electron diffraction (SAED) patterns and the assessment of Moire´ fringes confirmed that the nanoplates formed in this manner found single crystalline efficiently oriented in {111} lattice plane as their basal planes.

References

Deokar, G.K., Ingale, A., 2017. Green synthesis and study of crystallinity of AuNps. Acta Crystallogr. Sect. A Found. Adv. 73, C496–C496. doi:10.1107/S2053273317090775

Deokar, G.K., Ingale, A.G., 2018. Unveiling an unexpected potential of beetroot waste in green synthesis of single crystalline gold nanoplates: A mechanistic study. Arab. J. Chem. doi:10.1016/j.arabjc.2018.03.016

Deokar, G.K., Ingale, A.G., 2016. Green synthesis of gold nanoparticles (Elixir of Life) from banana fruit waste extract – An efficient multifunctional agent. RSC Adv. 6, 74620–74629. doi:10.1039/C6RA14567A

Shankar, S.S., Rai, A., Ankamwar, B., Singh, A., Ahmad, A., Sastry, M., 2004. Biological synthesis of triangular gold nanoprisms. Nat. Mater. 3, 482–8. doi:10.1016/j.jcis.2004.03.003

---

POSTER SESSION - Life Sciences

P-8

## STRUCTURAL BASIS FOR LINEZOLID BINDING SITE REARRANGEMENT IN THE *STAPHYLOCOCCUS AUREUS* RIBOSOME

**Zohar Eyal**[1], Matthew J. Belousoff[2], Mazdak Radjainia[3], Tofayel Ahmed[4], Rebecca S. Bamert[2], Donna Matzov[1], Anat Bashan[1], Ella Zimmerman[1], Satabdi Mishra[4], David Cameron[2], Hans Elmlund[3], Anton Y. Peleg[2,5], Shashi Bhushan[4], Trevor Lithgow[2], Ada Yonath[1]

[1]*Structural Biology, Weizmann Institute of Science, Rehovot, Israel*
[2]*Infection & Immunity Program, Biomedicine Discovery Institute & Department of Microbiology, Monash University, Clayton, Australia*
[3]*The Clive and Vera Ramaciotti Centre for Structural Cryo-Electron Microscopy, Monash University, Melbourne, Australia*
[4]*School of Biological Sciences, Nanyang Technological University, Singapore, Singapore*
[5]*Department of Infectious Diseases, Alfred Hospital, Prahran, Australia*

The ribosome, an assembly of RNA and proteins, translates the genetic code into proteins in all living cells. As the ribosomes are essential for cell life, inhibiting their function will damage the cell. As a result, about 40% of the antibiotics, which are in clinical use, target functional centers in the ribosome. The growing burden on human health caused by various antibiotic resistance mutations now includes prevalent pathogen *Staphylococcus aureus* resistance to last line antimicrobial drugs such as linezolid.

Here we present single-particle reconstruction cryo-electron microscopy studies on the structures of the 70S ribosomes from a wild type *Staphylococcus aureus* vs. a clinical isolate [1]. An unorthodox, surprising mechanism of resistance to the antibiotic linezolid was revealed. This high-resolution structural information demonstrated that a single amino acid deletion in ribosomal protein uL3 confers linezolid resistance despite being located 24 Å away from the linezolid binding pocket in the peptidyl-transferase center. The mutation induces a cascade of allosteric structural rearrangements of the rRNA that ultimately results in the alteration

of the antibiotic binding site. This work may provides a step toward the redesign of oxazolidinone antibiotics, a strategy that could thwart known mechanisms of linezolid resistance

Also, new features of the *Staphylococcus aureus* large ribosomal subunit, which were missing in the crystal structure [2], were revealed.


- Belousoff MJ, Eyal Z, Radjainia M, Ahmed T, Bamert RS, Matzov D, Bashan A, Zimmerman E, Mishra S, Cameron D, Elmlund H, Peleg AY, Bhushan S, Lithgow T and Yonath A. 2017. *Structural basis for linezolid binding site rearrangement in the Staphylococcus aureus ribosome*. mBio 8:e00395-17. https://doi.org/10 .1128/mBio.00395-17.

- Eyal Z, Matzov D, Krupkin, M, Wekselman I, Paukner S, Zimmerman E, Rozenberg H, Bashan A, and Yonath A. *Structural insights into species-specific features of the ribosome from the pathogen Staphylococcus aureus* PNAS (2015) 112(43):E5805-14.


---

POSTER SESSION - Life Sciences

P-9

## RESOLVING ESCRT-III SPIRALS AT THE INTERCELLULAR BRIDGE OF DIVIDING CELLS USING 3D STORM


**Inna Goliand**[1], Shai Adar[1], Inbar Segal[1], Dikla Nachmias[1], Tali Dadosh[2], Michael M. Kozlov[3], Natalie Elia[1]

[1]*Department of Life Sciences and NIBN, Ben Gurion University of the Negev, Beer Sheva, Israel*

[2]*Department of Chemical Research Support, Weizmann Institute of Science, Rehovot, Chemical Research Support, Israel*

[3]*Department of Physiology and Pharmacology, Tel Aviv University, Tel Aviv, Israel*



The ESCRT machinery mediates membrane fission in a variety of processes in cells. According to the proposed mechanism, ESCRT-III proteins drive membrane fission by assembling into helical filaments on membranes. Yet, ESCRT-III filaments have never been directly visualized in a process utilizing ESCRTs for its function. Here we used 3D STORM imaging of endogenous ESCRT-III component IST1, to reveal the evolution of the structural organization of ESCRT-III in mammalian cytokinetic abscission. Using this approach, ESCRT-III ring and spiral assemblies were resolved and characterized at different stages of abscission. Visualization of IST1 structures in cells depleted of ESCRT-III components or lacking the microtubule severing enzyme spastin provides further information on the organization and function of the ESCRT-III complex in cells. This work provides the first evidence that ESCRT-III proteins form helical filaments to mediate their function in cells. The new structural information raises new mechanistic scenarios for ESCRT-driven cytokinetic abscission.


---

POSTER SESSION - Life Sciences

P-10

## CRYO-SEM STRUCTURAL CHARACTERIZATION OF CRYO-PLANED MOUSE BONE EPIPHYSEAL GROWTH PLATE


**Heden Haimov**[1], Eyal Shimoni[2], Steve Weiner[1], Lia Addadi[1]

[1]*Structural Biology, Weizmann Institute of Science, Rehovot, Israel*

[2]*Chemical Research Support, Weizmann Institute of Science, Rehovot, Israel*


Vertebrate bone is a specialized connective tissue (1) with a highly organized hierarchical structure (2). Bone consists of carbonated hydroxyapatite nanocrystals formed within an organic matrix of collagenous fibers

and various biological molecules. The elongation of long bones occurs through a mechanism of endochondral ossification which happens exclusively at the growth plate (3). In the endochondral ossification pathway mesenchymal cells differentiate to produce intermediate cartilage tissue, which is later replaced by bone tissue. The growth plate is also a relevant region for bone disorders, infections and a target area for secondary metastases during breast cancer. To date, a high-resolution characterization of the microstructure of the growth plate under near-physiological conditions is missing. This research aims to improve our understanding of both the growth plate structure and endochondral bone formation pathways. In order to explore this clinically crucial region of bone biology, we have avoided the standard freeze-fracture technique used in cryo-SEM, and instead have developed an innovative approach to examine fully hydrated mice tibiae growth plates under cryogenic conditions, using cryo-planing (Figure1). The technique consists of rapid freezing of the tissue after it was infiltrated with a cryo-protectant (glycerol) and then cryo-planing followed by block-face imaging. This technique allows visualization of both the growth plate chondrocytes (GPC) and the mineralization front (MF) up to the resolution of a few nanometers. Integration of these images with fully hydrated microCT analysis will, in the future, provide a micrometer-scale 3D characterization of both the non-mineralized soft-tissue and the mineralized components of the hard tissue.

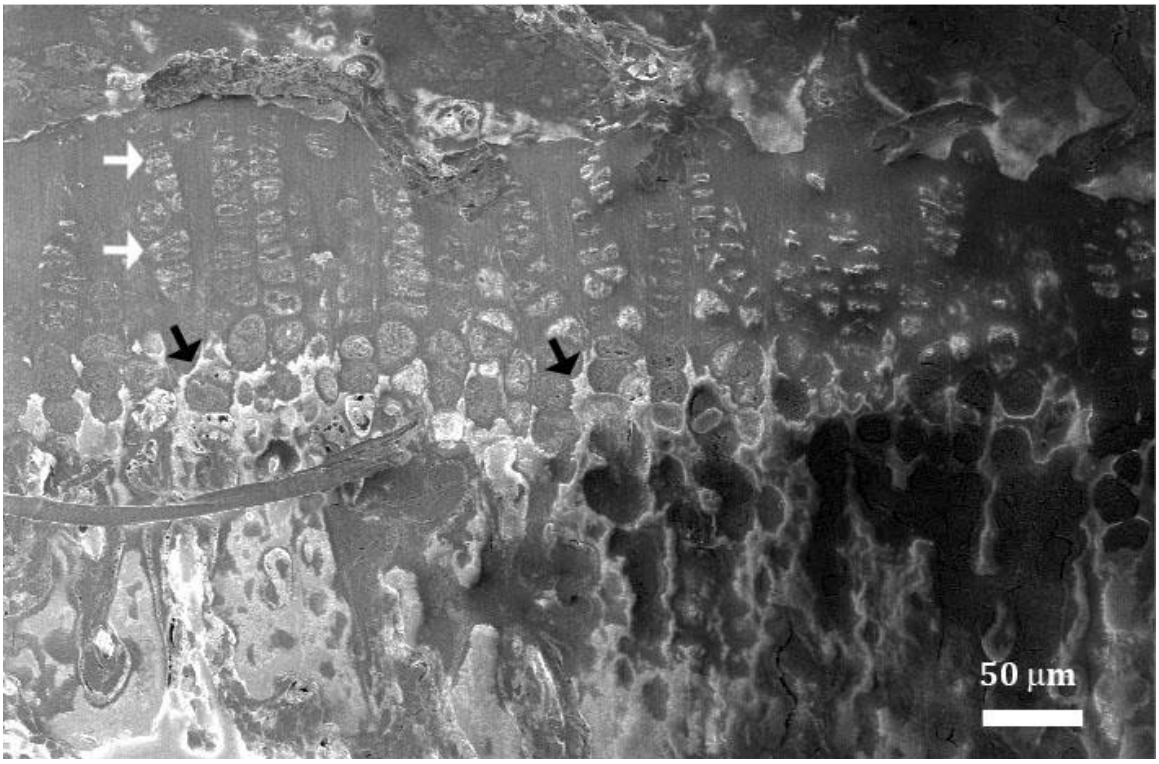


**Figure 1.** Cryo-SEM block-face micrograph of a mouse tibia showing the growth plate chondrocytes (white arrows) and the mineralization front (black arrows).

**References:**


- Bourne GH (1957) *The Biochemistry and Physiology of Bone* (Elsevier).
- Weiner S & Traub W (1992) Bone structure: from angstroms to microns. *The FASEB Journal* 6(3):879-885.
- Irving J (2012) *Calcium and phosphorus metabolism* (Elsevier).


---

P-11

# OPTIMIZATION OF 3D NEURON-SURFACE INTERFACE IMAGING BY SEM/FIB MICROSCOPE

**Itai Henn**[1,2,3], Ayelet Atkins[1,3], Amos Markus[1,2], Yossi Mandel[1,2,3]
[1]*Mina and Everard Goodman Faculty of Life Sciences, Bar-Ilan University, Ramat Gan, Israel*
[2]*School of Optometry and Vision Science, Bar-Ilan University, Ramat Gan, Israel*
[3]*Bar Ilan institute for Nanotechnology and Advance Materials (BINA), Bar-Ilan University, Ramat Gan, Israel*

## Introduction

In the last decade there is increasing in the use of SEM/FIB for imaging and studying the neural-surface[1,2,34] or neural-electrode[5,6,7,8]. Studying the cell interface is important for various applications such as tissue culture engineering, electrical stimulation and more. However, it is of critical importance to preserve the cellular morphology during the fixation and dehydration process. The aim of the current research is to optimize drying, membrane staining and imaging techniques for the study of the neuron-electrode or neuron-surface interface.

## Materials and Methods

Retinal Pigmented Epithelium (ARPE) and photoreceptor precursors (PRP) cells were cultured on glass for 24hrs. We evaluated 4 different drying techniques (critical point drying machine (CPD)[9,10], hexamethyldisilazane (HMDS) [11], Resin[12] and OTOTO[13] air dry and four different staining techniques (Osmium[14], Osmium+salts, OTOTO, osmium + uranil[15,16,17]) the cell morphology was investigated by the FIB/SEM technique. The ARPE are characterized by fine protrusions, which are easily broke in response to change in cellular morphology and thus can serve for evaluating the drying and fixation effect on cellular structures. Scanning electron microscope (SEM) imaging was used to measure the preservation of the cell-surface interface by analyzing the percentage of broken protrusions. In addition, $Ga^+$ Focus Ion beam (FIB) milling, SEM and HR-SEM imaging were used to evaluate the cellular membrane structure contrast when stained by the various staining techniques. Furthermore, we studied the cell interface with a micro-well scaffold fabricated by SU-8 photolithography and with a gold mushroom-shaped electrodes printed by a 3D two-photon based nano-printing (Nanoscribe GmbH, Germany).

## Results and Discussion

The percentage of broken cellular extensions in the resin drying technique (22.57%,±13.3) and OTOTO air dry (27.74%,±14) were significantly lower as compared with CPD (59.73%, ±10.3) and HMDS (61.42%,±13.7) (mean, STDEV, p  0.001). Furthermore, the inner cellular structures contrast was enhanced by the resin drying and OTOTO staining accompanied with a higher membrane contrast and with the lowest shrinkage (less artifacts).

## Conclusion

We optimized the fixation and staining protocols and studied cells interface with different surfaces including 3D surfaces and structures. Our results reveal that the resin and OTOTO air dry technique significantly preserve cellular structure as compared with CPD or HMDS techniques. The OTOTO staining yields the most detailed images of the cell, enables the visualization of cell organelles and membrane. Finally, this study highlights that a proper drying and fixation method is vital for the preservation of natural cellular morphology which is of great importance for the study of cell-surface interface.

## References

- Santoro, F. *et al.* Revealing the Cell–Material Interface with Nanometer Resolution by Focused Ion Beam/Scanning Electron Microscopy. *ACS Nano* **11,** 8320–8328 (2017).

- Xie, C., Lin, Z., Hanson, L., Cui, Y. & Cui, B. Intracellular recording of action potentials by nanopillar electroporation. *Nat. Nanotechnol.* **7,** 185–190 (2012).
- Hanson, L., Lin, Z. C., Xie, C., Cui, Y. & Cui, B. Characterization of the Cell–Nanopillar Interface by Transmission Electron Microscopy. *Nano Lett.* **12,** 5815–5820 (2012).
- Farah, N., Reutsky, I. & Shoham, S. Patterned Optical Activation of Retinal Ganglion Cells. in *2007 29th Annual International Conference of the IEEE Engineering in Medicine and Biology Society* **2007,** 6368–6370 (IEEE, 2007).
- Hai, A., Shappir, J. & Spira, M. E. In-cell recordings by extracellular microelectrodes. *Nat. Methods* **7,** 200–202 (2010).
- Ojovan, S. M. *et al.* A feasibility study of multi-site,intracellular recordings from mammalian neurons by extracellular gold mushroom-shaped microelectrodes. *Sci. Rep.* **5,** 14100 (2015).
- Santoro, F. *et al.* Interfacing electrogenic cells with 3D nanoelectrodes: Position, Shape, and Size Matter. *ACS Nano* **8,** 6713–6723 (2014).
- Nakano, T. *et al.* Self-Formation of Optic Cups and Storable Stratified Neural Retina from Human ESCs. *Cell Stem Cell* **10,** 771–785 (2012).
- Technologies, Q. *Technical Brief Critical Point Drying*. (2009).
- Critical Point Drying Principles. Available at: https://www.emsdiasum.com/microscopy/technical/datasheet/critical_drying.aspx. (Accessed: 22nd August 2017)
- Hazrin-Chong, N. H. & Manefield, M. An alternative SEM drying method using hexamethyldisilazane (HMDS) for microbial cell attachment studies on sub-bituminous coal. *J. Microbiol. Methods* **90,** 96–99 (2012).
- Belu, A. *et al.* Ultra-thin resin embedding method for scanning electron microscopy of individual cells on high and low aspect ratio 3D nanostructures. *J. Microsc.* **263,** 78–86 (2016).
- LEŠER, V., DROBNE, D., PIPAN, Ž., MILANI, M. & TATTI, F. Comparison of different preparation methods of biological samples for FIB milling and SEM investigation. *J. Microsc.* **233,** 309–319 (2009).
- Williams, Y. *et al.* Comparison of three cell fixation methods for high content analysis assays utilizing quantum dots. *J. Microsc.* **232,** 91–98 (2008).
- Eltoum, I., Fredenburgh, J., Myers, R. B. & Grizzle, W. E. Introduction to the Theory and Practice of Fixation of Tissues. *J. Histotechnol.* **24,** 173–190 (2001).
- Rolls, G. Fixation and Fixatives (3) – Fixing Agents Other than the Common Aldehydes. (2012).
- Rando, T. Molecular Mechanisms and Models of Aging. Annals of the New York Academy of Sciences, Vol 1119. *J. Neuropathol. Exp. Neurol.* **67,** 633.1-633 (2008).


---

POSTER SESSION - Life Sciences

P-12

## AOPW1, A TYPE III-SECRETED EFFECTOR FROM *ACIDOVORAX CITRULLI*, IS TRANSLOCATED INTO THE PLANT CELL DISRUPTING THE ACTIN CYTOSKELETON AND RELATED PROCESSES


**Irene Jiménez-Guerrero**, Monica Sonawane, Saul Burdman
*Plant Pathology and Microbiology, The Hebrew University of Jerusalem, Rehovot, Israel*

Plant pathogenic bacteria employ the type III secretion system (T3SS) to deliver sets of protein effectors into the cytoplasm of the host cell. These effectors promote bacterial virulence through alteration of the host cell metabolism and/or suppression of host defense responses (Mansfield 2009). *Acidovorax citrulli* is a Gram-negative bacterium that causes bacterial fruit blotch of cucurbits, a devastating disease that threatens watermelon and melon production worldwide (Burdman and Walcott 2012). Based on genetic, biochemical and host preferential association, the *A. citrulli* population is divided into three groups: group I includes strains that are moderately to highly aggressive on a wide range of cucurbits strains (isolated mainly from melon and other non-watermelon cucurbits), group II strains are highly aggressive on watermelon (mainly isolated from watermelon), and group III strains possess relatively weak virulence on melon, watermelon and pumpkin (Walcott et al. 2000, Eckshtain-Levi et al. 2014). Sequence analysis of genes encoding type III-secreted effectors (T3Es) from a global population of strains revealed that the *A. citrulli* groups significantly differ each from the other, based on effectors' repertoire and sequences (Eckshtain-Levi et al. 2014). Gene *aopW1*, homologous to *Pseudomonas syringae hopW1-1*, is an example of a T3E gene that may be involved in the specialization of *A. citrulli* groups to different hosts. *aopW1* (1455 bp) is relatively conserved among the three *A. citrulli* groups, with the exception of a 138-bp hypervariable region (HVR) located at nucleotide positions 439 to 576. Heterologous expression of *aopW1* genes in yeast revealed that the group I and III versions exerted strong growth inhibition and lethality, while the group II version of this effector had only a subtle effect. In this sense, similar effects were shown when this effector was expressed *in planta*. Besides, confocal microscopy analysis revealed that AopW co-localizes with chloroplasts, actin cytoskeleton, endoplasmic reticulum (ER) and plant endosomes. However, the group I AopW1, but not the group II AopW1, disrupts actin cytoskeleton *in vivo*.

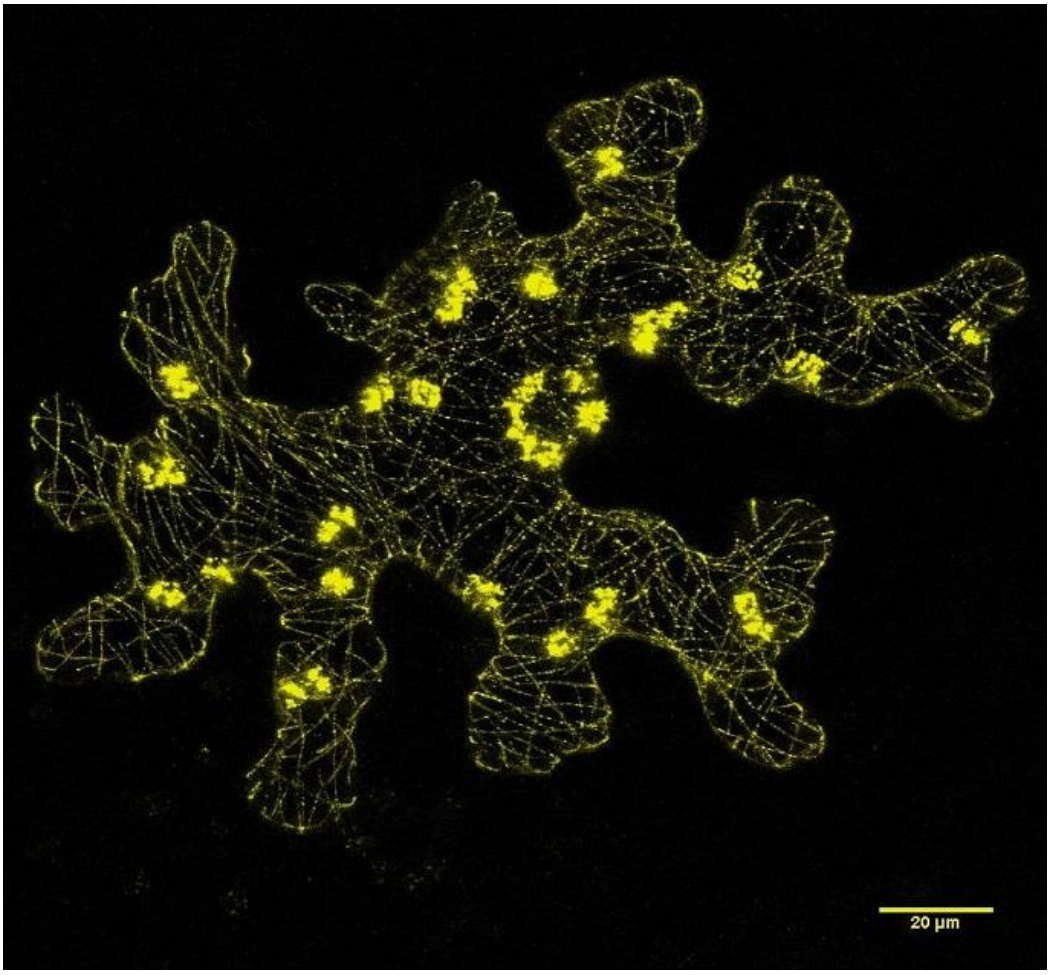


Figure 1: Subcellular localization of the AopW1 group I effector in *Nicotiana benthamiana* leaves.

References: Mansfield JW. (2009) Mol Plant Pathol 10:721-34. Burdman S, Walcott R. (2012) Mol Plant Pathol 13:805-815. Walcott RR, Langston DB, Sanders FH, et al. (2000) Phytopathology 90:191-196. Eckshtain-Levi N, Munitz T, Zivanovic M, et al. (2014) Phytopathology 104:1152-62.
This work has been supported by grant US-4734-14C from the US-Israel Binational Agricultural Research and Development (BARD) Fund.

---

P-13

# CHARACTERIZATING MINERAL-BEARING VESICLES IN SEA URCHIN EMBRYOS USING CRYO-SOFT X-RAY MICROSCOPY AND QUANTITATIVE CRYO-EDS

**Keren Kahil**[1], Neta Varsano[1], Andrea Sorrentino[2], Eva Pereiro[2], Lia Addadi[1], Steve Weiner[1]
[1]*Structural Biology, Weizmann Institute of Science, Rehovot, Israel*
[2]*MISTRAL Beamline−Experiments Division, ALBA Synchrotron Light Source, Barcelona, Spain*

Sea urchin larvae have endoskeletons comprised of two calcitic spicules. Large amounts of calcium must assemble in the larva to build the spicules, requiring substantial calcium uptake from the water or the food into spicule-forming cells (PMCs). PMCs uptake seawater through endocytosis[1] into a complex network of vacuoles. Within the PMCs, calcium ions are translocated from the seawater vacuoles to various organelles and vesicles where they accumulate, and subsequently precipitate as a mineral[2]. The amorphous precipitates are finally translocated to the spicule, where they crystallize.

Here we address the question of the form in which calcium ions are stored in different locations in the cell – dissolved, solid and if so what is the solid phase? In order to locate and characterize calcium content in individual vesicles we apply cryo-soft X-ray microscopy on PMCs. The presence of concentrated calcium ions was detected by imaging the cells in the energy range before and after the calcium L-absorption edge (Figure 1). We characterized the chemical environment of the calcium ions using X-ray absorption spectroscopy and determined that some of these particles are composed of different forms of highly disordered calcium carbonate. We also developed a method for quantitative measurement of ion concentrations by EDS, whereby we follow the development of vesicle content. These data shed light on the intracellular transport and concentration pathways of calcium ions, eventually leading to a deeper understanding of mineral formation.

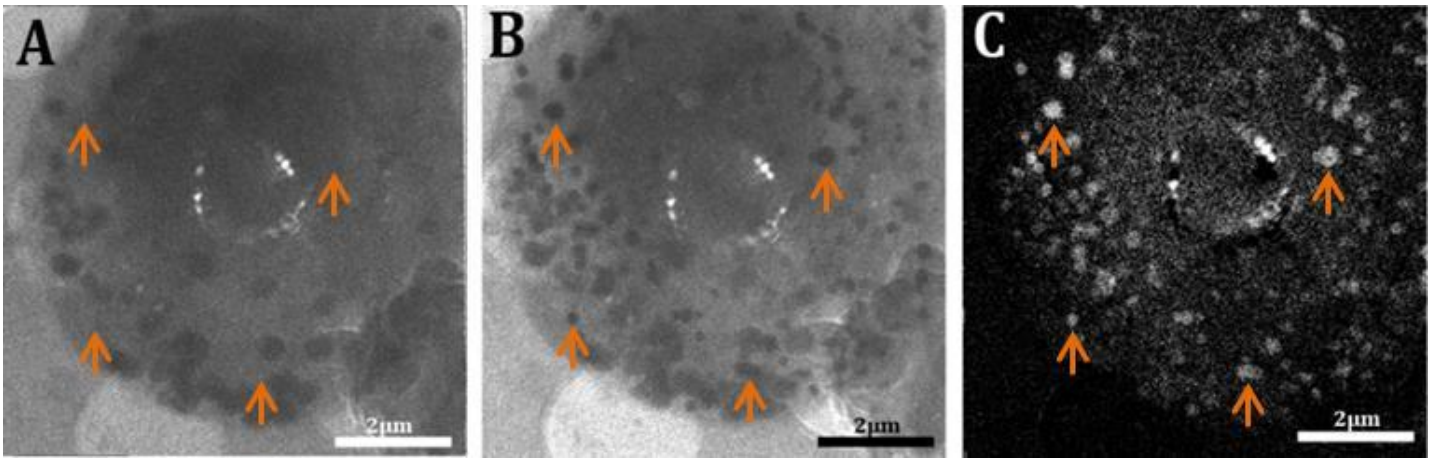


Figure 1 - (A) A spicule-forming cell imaged at 342eV, below the Ca L-absorption edge. (B) The same cell imaged on the Ca-absorption edge at 352.1eV. Many particles appear to absorb at this energy (dark particles) – corresponding to areas containing concentrated Ca. (C) "Ca-map" of the same cell. The map was obtained by subtracting the image in (A) from the image in (B). Representative Ca-containing particles are marked by arrows. The varying intensities of these particles are indicative of varying Ca concentrations

References

- Vidavsky, S. Addadi, A. Schertel, D. Ben-Ezra, M. Shpigel, L. Addadi, S. Weiner, Calcium transport into the cells of the sea urchin larva in relation to spicule formation. Proc. Natl. Acad. Sci. U.S.A, 113(45), 12637-12642,2016.
- Beniash, J. Aizenberg, L. Addadi, S. Weiner, Amorphous calcium carbonate transforms into calcite during sea urchin larval spicule growth. P. Roy. Soc. B-Biol. Sci., 264 (1380), 461-465, (1997).

---

P-14

## LIVE CELL AND SUPER-RESOLUTION IMAGING OF ESCRT PROTEINS LABELED WITH MINIMAL TAGS *VIA* GENETIC CODE EXPANSION

**Andres Koenig**[1,3], Inbar Segal[1,3], Eyal Arbely[1,2,3], Natalie Elia[1,3]
[1]*Faculty of Natural Sciences, Department of Life Sciences, Ben-Gurion University of the Negev, Beer-Sheva, Israel*
[2]*Department of Chemistry, Faculty of Natural Sciences, Ben-Gurion University of the Negev, Be'er Sheva, Israel*
[3]*The National Institute for Biotechnology in the Negev, Ben-Gurion University of the Negev, Beer-Sheva, Israel*

Much has been leaned about the spatiotemporal organization of ESCRTs in cells through quantitative high-resolution imaging techniques. Yet, the mechanism for ESCRT induced membrane remodeling remained unknown. This may stem from the inability of current imaging techniques to document the entire process with sufficient resolution in live cells. On top of that, tagging ESCRT proteins with fluorescent proteins may influence the physiological function of the ESCRT membrane fission machine, which is composed of relatively small proteins that polymerize to mediate their function. Genetic code expansion and bioorthogonal labeling offer, for the first time, a non-invasive way to directly attach fluorescent dyes to proteins in live cells. Employing the superb photophysical properties and small size of fluorescent dyes to high resolution imaging of ESCRTs is expected to improve the spatiotemporal resolution of the techniques and at the same time to better preserve physiological context. Recently, we have demonstrated the applicability of this approach for studying cellular polymers in live cells, using tubulin as a benchmark. Fluorescent dye labeling the ESCRT proteins CHMP4B and IST1 indicate that this approach is also applicable for imaging ESCRTs in live cells. We now expand the applicability of this labeling approach and adapt it to live super-resolution imaging which will ultimately be applied to study ESCRTs in a manner that better recapitulate their natural state and in a yet unprecedented spatiotemporal resolution.

---



P-15

## COLOCALIZATION AND DISPOSITION OF BACTERIAL CELLULOSOMES REVEALED BY CORRELATIVE SUPERRESOLUTION IMAGING, SCANNING AND TRANSMISSION ELECTRON MICROSCOPY

**Lior Artzi**[1], Tali Dadosh[2], Elad Milrot[2], Sarah Moraïs[1], Smadar Levin-Zaidman[2], Ely Morag[1], Edward A. Bayer[1]
[1]*Biomolecular Sciences, Weizmann Institute of Science, Rehovot, Israel*
[2]*Chemical Research Support, Weizmann Institute of Science, Rehovot, Israel*

Lior Artzi[a] - Margulis Prize applicant

Tali Dadosh - was involved in the design of the project and co-performed the superresolution and correlative imaging

Elad Milrot helped prepare samples and SEM imaging, co-performed correlative imaging.

Sarah Moraïs[a] helped calibrate immunolabeling of the cells.

Smadar Levin-Zaidman helped perform sample preparations and TEM imaging experiments

Ely Morag[a] - participated in the project design

Edward A. Bayer[a] – the principal investigator

[a]Department of Biomolecular Sciences, The Weizmann Institute of Science, Rehovot, Israel Department of Chemical Research Support, The Weizmann Institute of Science, Rehovot, Israel

The plant cell wall is the most abundant carbon source on earth and comprises a variety of polysaccharides, mainly cellulose, which is highly resistant to enzymatic degradation (1). Cost-effective strategies to break down cellulose will provide soluble sugars that can be fermented to biofuels, thus alleviating our reliance on fossil fuels (2).

Cellulosomes are large multienzyme complexes produced by certain anaerobic bacteria to degrade plant cell wall polysaccharides, including cellulose. The cellulosome is composed of a large set of hydrolytic enzymes organized by non-catalytic, structural proteins called scaffoldins into a highly efficient degradative machine (3, 4). *Clostridium clariflavum* is an anaerobic thermophile, that produces the largest assembled cellulosome complex known in nature, composed of 185 enzymatic and structural subunits (5). This 4-tiered cell surface-attached complex is composed of a cell-anchoring scaffoldin (ScaC), 4 adaptor scaffoldins (ScaB) that allow multiplication of the enzymes in the complex, and 20 primary scaffoldins (ScaA), that interact with 160 enzymatic subunits (Figure 1A). This architectural flexibility multiplies the cellulosomal enzyme compositions in this bacterium.

To investigate these surface-associated cellulosomes, we used monoclonal and polyclonal antibodies against 4 representative cellulosome components, one from each tier (Figure 1A), to define their relative subcellular localization. By using superresolution microscopy (STORM), we observed co-localization among the successive cellulosomal components. The cells were labeled by monoclonal and polyclonal antibody pairs to study their relative localization in the complex (Figure 1C-F). By taking this approach, we were able to localize ScaC at the most proximal level of the complex, relative to the cell surface. ScaB is situated between ScaC and ScaA, ScaA is distal to ScaB and the enzymatic subunits were located at the most external layer of the complexes. This is the first time that the hierarchical organization of cellulosomes could be presented visually *in vivo*. By quantifying the clusters of ScaC on the cell surface of cells grown on different soluble (e.g., cellobiose) and recalcitrant insoluble (cellulose and wheat straw) carbon sources, we revealed large variations in the number of surface-associated cellulosomes depending on the carbon source used for cell growth, suggesting novel control mechanism(s) for cellulosome surface display and assembly.

In addition, we investigated the morphological localization of cellulosomes. Cell-surface protuberances had previously been observed SEM and TEM. We showed by TEM that cellulosome components are localized exclusively on the cell surface (Figure 2). SEM revealed a similar pattern of protuberances, as we observed by immunolabeling of cellulosomes, and correlative STORM-SEM (CLEM) showed that cellulosomes are specifically localized in these protuberances, indicating that the bacterium creates specialized cell-surface compartments for cellulosomes (Figure 3).

The results of this study provide definitive experimental proof of the presumed architecture of a cellulosome system, which had previously been based on the logical assessment of the biochemically determined interactions of the cellulosome component parts. Our results thus provide conclusive insight into the spatial organization of cellulosomes on the bacterial cell surface and reveal that the bacterial cell requires closely attached surface cellulosomes to break down cellulosic substrates. This information is crucial for designing efficient plant cell wall deconstruction processes, whereby the bacterial cell, together with the secreted proteins, plays an important role in polysaccharide degradation (6).

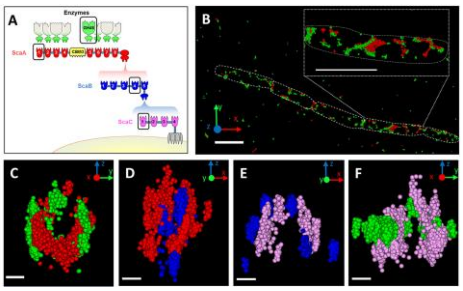


**Figure 1**: Hierarchical organization of cell-surface cellulosome components. (A) Schematic illustration of the major cellulosome system of *C. clariflavum*. Color-coded cohesins (Coh) and enzyme (GH48) components circled in black were immunolabeled during experiments. (B) Representative 3D STORM image of cellobiose-grown cells labeled with anti-GH48 (green) and anti-CohA (red). Scale bar, 2 μm. (C to F) Representative cross-sectioned STORM images of selected bacterial cells immunolabeled with pairs of antibodies (scale bars, 300 μm). A portion of each bacterium was sectioned and rotated 90° for viewing

through its long axis. (C) Anti-GH48 (green) and anti-CohA (red); (D) anti-CohA (red) and anti-CohB (blue); (E) anti-CohB (blue) and anti-CohC (pink); (F) anti-CohC (pink) and anti-GH48 (green).

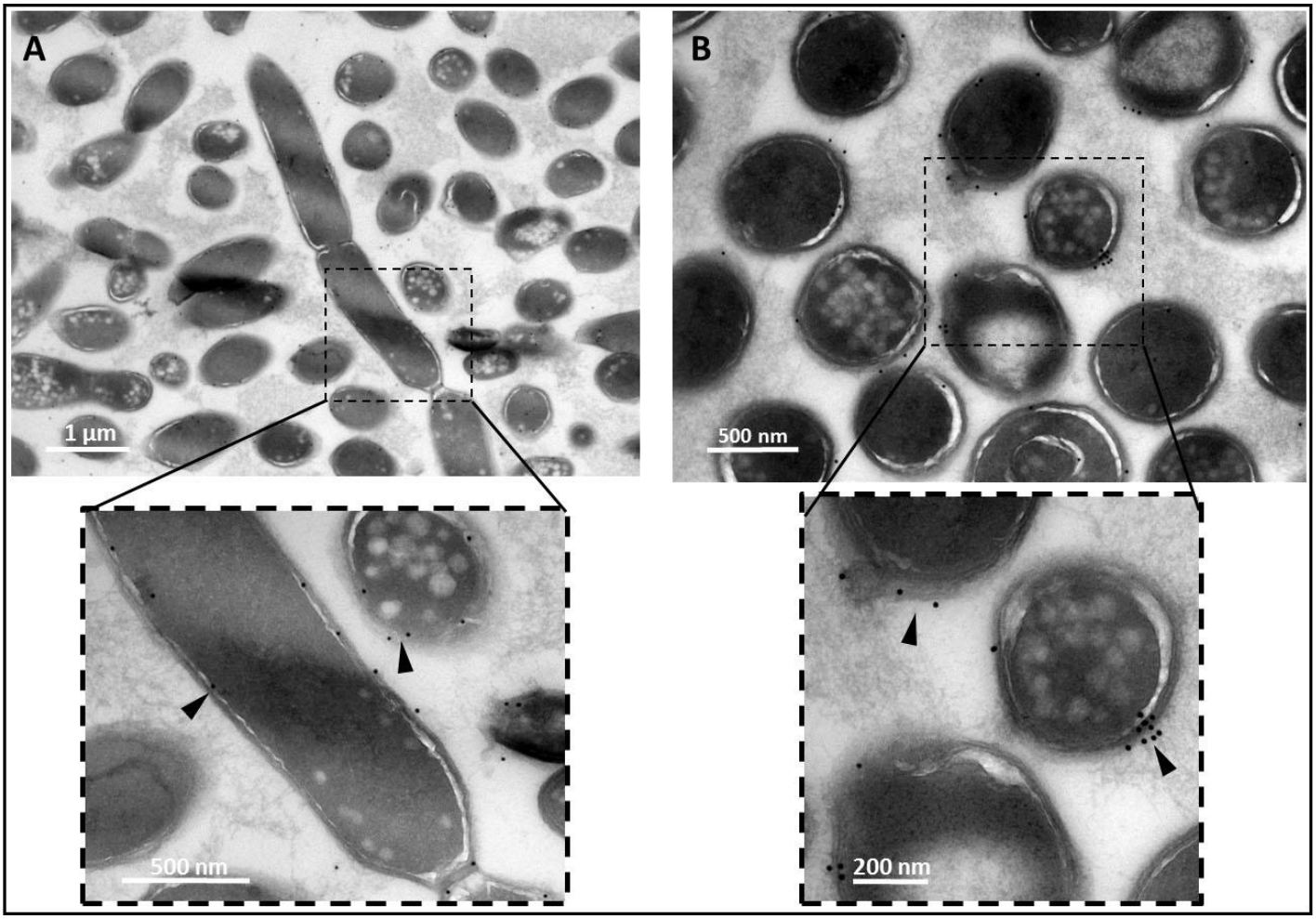


**Figure 2**: TEM immunolabeling of *C. clariflavum*. Cells were immunolabeled (arrows) with gold-derivatized anti-CohB4 (A) or anti-GH48 (B). (C) Cellulosome particles are exclusively localized to the cell surface (cells labeled by anti-CohB4 n=217 and by anti-GH48 n=269).

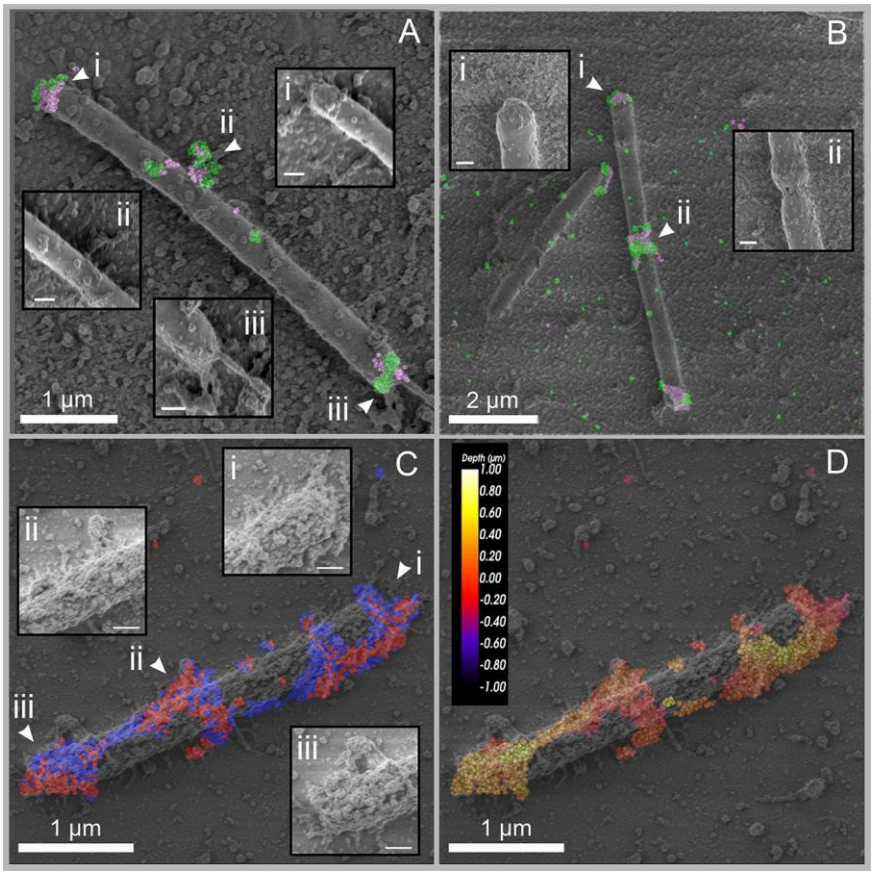

**Figure 3:** CLEM images of *C. clariflavum*. (A and B) Cellobiose-grown cells were immunolabeled with anti-GH48 (green) and anti-CohC (pink). (A) Scale bars, 1 µm (200 nm in each inset). (B) Scale bars, 2 µm (200 nm in each inset). (C and D) Wheat straw-grown cell, immunolabeled with anti-CohA and anti-CohB. (C) Labeling is colored according to the specific probes: anti-CohA, red; anti-CohB, blue. (D) The depth of labeling is presented for the two combined probes, color-coded from yellow (shallow labeling) to dark red (deep labeling, closer to the slide). Scale bars, 1 µm (200 nm in each inset in panel C).

**References**


- Gilbert HJ. 2010. The biochemistry and structural biology of plant cell wall deconstruction. Plant Physiol 153:444–55.
- Bayer EA, Lamed R. 1992. The cellulose paradox: pollutant par excellence and/or a reclaimable natural resource? Biodegradation 3:171–88.
- Bayer EA, Shoham Y, Lamed R. 2013. Lignocellulose-decomposing bacteria and their enzyme systems, p. 215–266. *In* Rosenberg, E, DeLong, EF, Lory, S, Stackebrandt, E, Thompson, F (eds.), The Prokaryotes. Springer Berlin Heidelberg, Berlin, Heidelberg.
- Artzi L, Bayer EA, Moraïs S. 2016. Cellulosomes: bacterial nanomachines for dismantling plant polysaccharides. Nat Rev Microbiol 15:83–95.
- Artzi L, Dassa B, Borovok I, Shamshoum M, Lamed R, Bayer EA. 2014. Cellulosomics of the cellulolytic thermophile *Clostridium clariflavum*. Biotechnol Biofuels 7:100.
- Artzi L, Dadosh T, Milrot E, Moraïs S, Levin-Zaidman S, Morag E, Bayer EA. 2018. Colocalization and disposition of cellulosomes in *Clostridium clariflavum* as revealed by correlative superresolution imaging. *mBio* 9:e00012-18.


---

POSTER SESSION - Life Sciences

P-16

## THE CRYO-EM STRUCTURE OF HIBERNATING 100S RIBOSOME DIMER FROM PATHOGENIC *STAPHYLOCOCCUS AUREUS*


**Donna Matzov**[1], Shintaro Aibara[2], Arnab Basu[3], Ella Zimmerman[1], Anat Bashan[1], Mee-Ngan F Yap[3], Alexey Amunts[2], Ada Yonath[1]

[1]*Structural Biology, Weizmann Institute of Science, Rehovot, Israel*

[2]*Science for Life Laboratory, Department of Biochemistry and Biophysics, Stockholm University, Solna, Sweden*

[3]*Edward A. Doisy Department of Biochemistry and Molecular Biology, Saint Louis University School of Medicine, St. Louis, Missouri, USA*



Formation of 100S ribosome dimer is generally associated with translation suppression in bacteria. Trans-acting factors RMF and HPF were shown to directly mediate this process in *E. coli*. Gram-positive *S. aureus* lacks an RMF homologue, and the structural basis for its 100S formation was not known. Here we report the cryo-EM structure of the native 100S ribosome from *S. aureus*, revealing the molecular mechanism of its formation. The structure is distinct from previously reported analogues and relies on the HPF C-terminal extension forming the binding platform for the interactions between both of the small ribosomal subunits. The 100S dimer is formed through interactions between rRNA h26, h40 and protein uS2, involving conformational changes of the head as well as surface regions that could potentially prevent RNA polymerase from docking to the ribosome.


---

P-17

## THE NEWEST ART OF CHILLING: USING CRYO-STEM TOMOGRAPHY TO UNDERSTAND *PLASMODIUM* BIOLOGY

**Debakshi Mullick**[1], Michael Elbaum[1], Katya Rechav[2], Ron Dzikowski[3]
[1]*Chemical and Biological Physics, Weizmann Institute of Science, Rehovot, Israel*
[2]*Electron Microscopy Unit, Weizmann Institute of Science, Rehovot, Israel*
[3]*Department of Microbiology & Molecular Genetics, The Hebrew University-Hadassah Medical School, Jerusalem, Israel*

Malaria is an infectious disease caused by the protozoan parasites-*Plasmodium spp*. The WHO estimated 216 million cases of the disease in 2016 and it continues to be a global burden, despite many measures undertaken to combat it. Of the species that infect humans, *P. falciparum* causes one of the deadliest forms of the disease. The parasites have complex life-cycle alternating between the female *Anopheles* mosquito and the human host, where the early phase of development is asymptomatic and is in the hepatocytes. Following this, the parasites invade red blood cells (RBCs) where they undergo cyclic asexual multiplication that results in the classic clinical symptoms of malaria. Most antimalarial agents are targeted to this stage and a systematic biological understanding of the blood stage becomes both essential and imperative. Classic electron microscopy (EM) methods have been employed to understand the ultrastructure of the parasite and infected host cells but, harsh chemical fixatives and heavy metal stains cause artefacts that can be misleading. Cryo-EM methods preclude undesirable sample preparation steps by use of instantaneous vitrification to preserve biological ultrastructure in the near native state, but pose restrictions on sample thickness. To partially overcome thickness limitation cryo-scanning transmission electron microscopy (Cryo-STEM) can be used. Here a focussed electron probe raster scans the sample and a series of images can be obtained by tilting the sample at various angles (Cryo-STEM tomography). The images are formed by detectors that collect transmitted electrons scattered at various angles. These images can be then subjected to reconstruction and image analysis protocols ultimately resulting in a 3D ultrastructural image of the native state of the parasite. We propose to use this novel technique in understanding various biological aspects of the parasite.

The present works describes encouraging data from the use of Cryo-STEM tomography to visualise and understand the ultrastructure of *P. falciparum*. We are in the process of standardizing the current methods and extend it towards understanding the biology of the parasite.

---



P-18

## MICROSCOPIC DROPLETS ENGULFING BACTERIAL AGGREGATES ON DRYING SURFACES

**Tomer Orevi**, Maor Grinberg, Shifra Levin, Nadav Kashtan
*Department of Plant Pathology and Microbiology, The Robert H. Smith Faculty of Agriculture, Food and Environment The Hebrew University of Jerusalem, Rehovot, Israel*

While water is essential to life, the largest terrestrial microbial habitats – soil, roots, and leaf surfaces – are not constantly saturated with water and are subjected to frequent drying events. In these habitats bacteria experience fluctuations in water availability that routinely reach desiccation conditions, strongly impacting their survival probability. Bacterial cells in these habitats are observed in both solitary and aggregated forms. These surface-attached aggregates differ in size and shape. In this study, we ask how aggregates` size and morphology influence the extent and duration of their local water availability, and as a consequence, affect their survival probability under desiccation. We hypothesize that large-enough aggregates remain hydrated

for longer periods in comparison to solitary cells and as a consequence, increase their survival probability. To this end, we have constructed a dynamic experimental system based on multi-well plates that provides water-saturated conditions where bacteria grow for a defined period of time and then gradually evaporates and becomes dry. Microscopy aided inspection of the surface subsequent to the macroscopic evaporation of the liquid layer revealed three distinct bacterial organization forms: (1) solitary cells; (2) round-shaped dome-like aggregates of different size (10-500 cells); (3) flat aggregates with irregular shape that originate from the water-air interface and have sunk to the surface. Interestingly, while the vacant surface appeared to have completely dried, the surface-attached cells were engulfed with micro-droplets of different sizes and shapes (figure 1). These micro-droplets remained stable for long periods of time (hours to days). The relation between aggregates` characteristics and droplet size was explored by automatic scanning of large surface area (4.25mm x 4.25 mm, thousands of micro-droplets) with adequate resolution for single drop and single-cell analysis. Using advanced image analysis we established a strong correlation between aggregates` features and the surrounding drop size and shape. We found that in comparison to solitary cells, large aggregates retained more water around them and remained hydrated for longer periods. We observed similar results with two distinct bacterial species (*Pseudomonas putida* and *P. fluorescens* – a soil and plant-surface model strains) – supporting the view that this phenomenon is not unique to a specific strain. We employed time-lapse microscopy coupled with fluorescence viability assay (Live/Dead) in order to monitor the viability and recovery rate of individual cells and aggregates on the surface. Currently, we are assessing the survival probability within hydrated aggregates over time and with respect to the microscopic drops size and shape. The formation and retention of such micro-droplets around aggregates, may explain how bacterial cells in terrestrial habitats keep their micro-environment hydrated, a feature that is likely key for their survival.

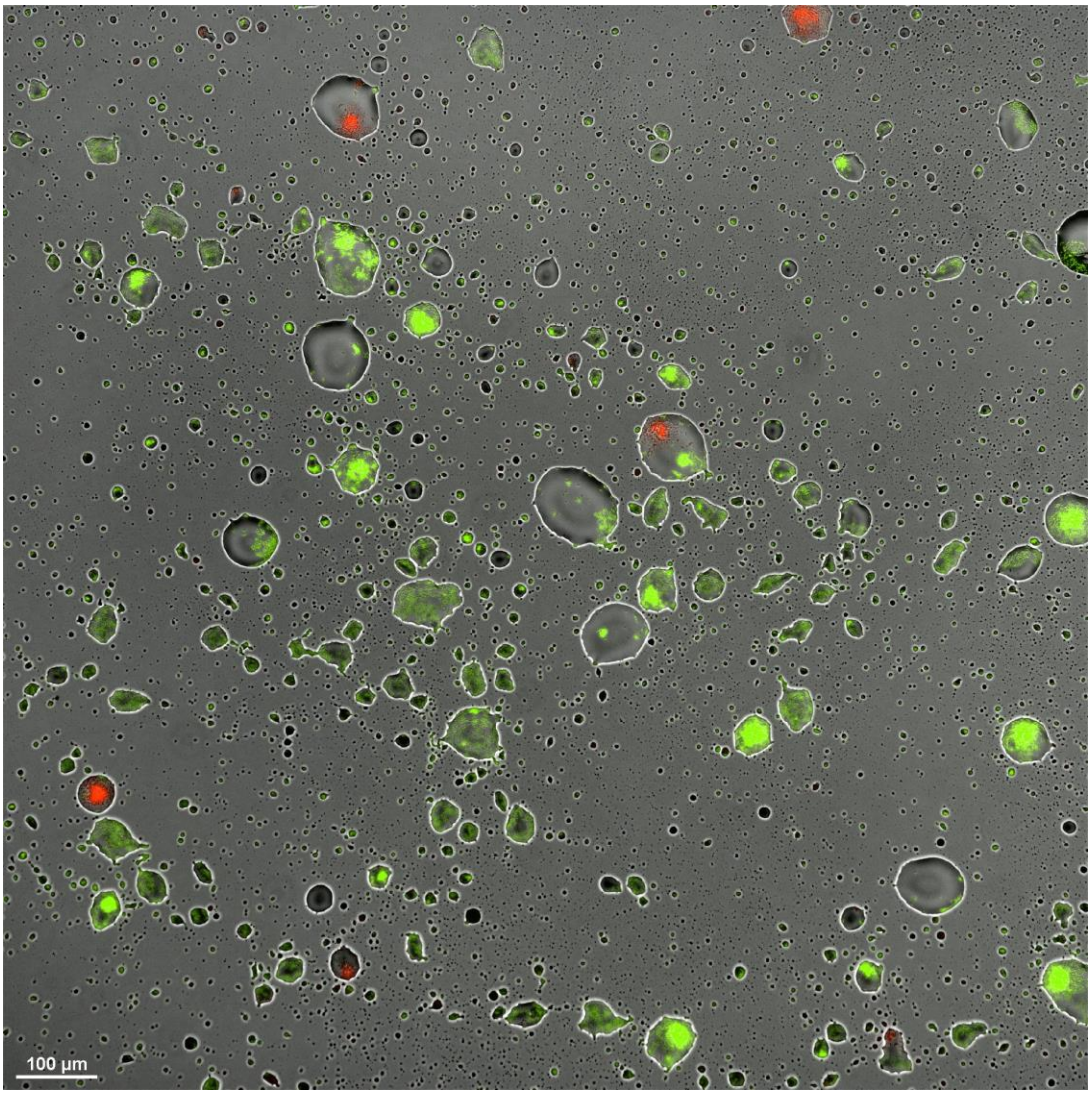


---

P-19

## SPATIAL STRUCTURE OF FEMALE SEMINAL RECEPTACLE SPERM-STORAGE SITE IN DROSOPHILA BY 3-D CORRELATIVE MICROSCOPY

**Katya Rechav**[1], Einat Zelinger[2], Vlad Brumfeld[1], Yael Heifetz[2]
[1]*Chemical Research Support, Weizmann Institute of Science, Rehovot, Israel*
[2]*Faculty of Agriculture, The Hebrew University of Jerusalem, Rehovot, Israel*

Drosophila females have two types of internal sperm storage organs. Spermathecae - a pair of long-term sperm storage and seminal receptacle - a short term storage. The seminal receptacle is an elongated closed end tubular structure. The sperm cells keep motility during storage in it for several weeks with no docking period as in mammalians or further activation. The seminal receptacle provides a microenvironment that maintains the active, motile sperm. Thus, it is possible that motile sperm interact with molecules secreted by the epithelium and that this sperm-female interaction plays a role in maintaining and/or regulating sperm functionality. There is relatively little known and much to be learned about the factors that govern sperm storage in the female reproductive tract.

Using a triple correlative approach of confocal, micro-CT and FIB-SEM we were able to observe the location of sperm in the seminal receptacle and to begin to dissect sperm-epithelium interactions at high resolution.

This is the first attempt to study sperm-female interactions using a correlative approach. Sperm-female interactions are mostly unknown, mainly because they occur within the receptacle`s confined small space (approx. 10-20 microns) which house hundreds of 0.5-micron thick long sperm. The triple correlative approach opens up a window to a completely new level of high-resolution information at the cellular level. Thus, having in hand such a system we can now begin to address questions related to sperm-female interactions. Furthermore, such a system is suitable not only for Drosophila but also for other organisms with soft delicate tissues.

---



P-20

## IMAGE-FORMATION, LIGHT-ENHANCEMENT & CAMOUFLAGE IN THE MIRRORED EYES OF CRUSTACEANS

**Nathan Schiffmann**, Eyal Merary Wormser, Benjamin A. Palmer, Steve Weiner, Lia Addadi
*Department of Structural Biology, Weizmann Institute of Science, Rehovot, Israel*

Some animals use mirrors rather than lenses to form images[1]. Such mirrored eyes are extremely efficient at collecting light and are found in marine animals living in dim-light habitats. A fascinating example of such an eye is found in decapod crustaceans: the reflective superposition compound eye (Fig. 1A). Previously it was known that each eye contains two types of reflector: (i) an image-forming “distal mirror” in the upper part of the eye which focuses light onto the retina (comprised of the photosensitive rhabdoms); (ii) an intensity-enhancing “tapetum reflector” underlying the retina which back-scatters light onto the rhabdoms, giving the retina a second chance to capture dispersed light. We recently reported that, in freshwater crayfish and prawns, these reflectors are formed from highly reflective crystals of isoxanthopterin[2] – a previously unknown optically functional bio-crystal.

Here, we report the discovery and characterization of a third “proximal” reflector in the eye of the whiteleg shrimp *L. vannamei* (Fig. 1B-F). The reflector is located below the tapetum within the nerve layer of the eye (lamina ganglionaris). The reflector is separated from the retina by a thick pigment layer and does not contribute to image-formation, since light impinging along the eye-axis will be absorbed before reaching the reflector. Instead, we suggest the reflector acts to camouflage the eye by back-scattering off-axis light away

from the highly conspicuous eye-pigments. Using X-ray micro-CT, light and fluorescent microscopy and cryo-SEM in combination with confocal Raman microspectrometry, we show that this reflector is constructed from crystalline nanoparticles of isoxanthopterin and functions by diffuse light-scattering. We also report the identification of isoxanthopterin crystals in numerous infraorders across the decapoda including Astacidea, Caridea and Dendrobranchiata, confirming that this material is found widely in decapod crustaceans. These results call for the investigation of crystalline pteridines more widely in the animal kingdom.

In conclusion, we unearth a remarkable and unique multi-functional natural optical device containing three types of reflector associated with three optical functions: image-formation, light-enhancement and camouflage. Understanding how organisms control the formation and arrangement of organic crystalline materials to manipulate light could pave the way for the development of novel bio-inspired organic optical materials.

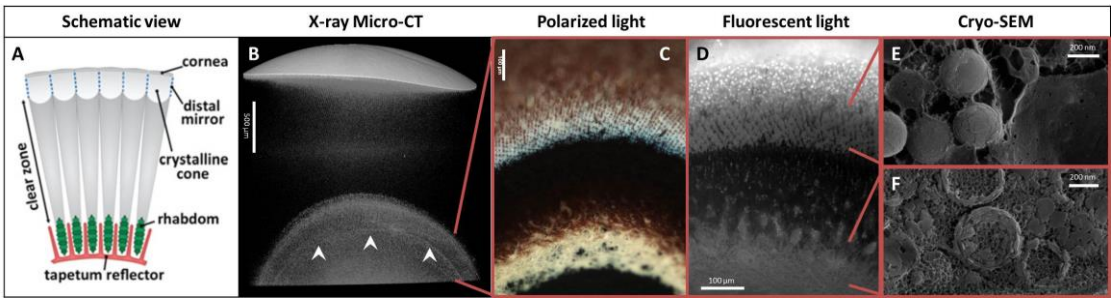


**Figure 1**: **Millimeter-to-nanometer scale architecture of the tapetum and proximal reflectors**. (**A**) Schematic of the reflecting compound eye viewed along the optic axis. (**B**) X-ray microCT scan of part of an eye, showing four high contrast features: the cornea (uppermost), distal mirror (immediately below cornea), tapetum (lower, between red lines) and proximal reflector (arrowheads, between red lines). (**C**) Polarized light micrograph of the highly birefringent tapetum (upper) and proximal (lower) reflectors. (**D**) DAPI stained fluorescent microscopy image of the tapetum and proximal reflectors, showing cell nuclei (tapetum layer), isoxanthopterin auto-fluorescence (tapetum and proximal layers) and myelin auto-fluorescence (proximal layer). (**E**) - (**F**) Cryo-SEM images from the tapetum (E) and the proximal reflector (F) regions displaying crystalline isoxanthopterin nanoparticles.

**References:**

[1] Palmer BA et al., *Science*. **2017** 358, 1172-1175.

[2] Palmer BA et al., *Proc. Natl. Acad. Sci. U. S. A.* **2018** 115, 2299-2304.

---

POSTER SESSION - Life Sciences

P-21

## JUDGE THE BOOK BY THE COVER- STEM BIOMECHANICS ARE GOVERNED BY MORPHOLOGY RATHER THAN INTERNAL STRUCTURE AND CELL WALLS COMPOSITION

**Ilana Shtein**[1,4,5], Alex Koyfman[2,5], Amnon Schwartz[3], Zoe A Popper[4], Benny Bar-On[5]
[1]*Agriculture and Oenology Department, Eastern Region R&D Center, Ariel, Israel*
[2]*Nuclear Research Center, Nuclear Research Center-Negev, Beer-Sheva, Israel*
[3]*The Robert H. Smith Institute of Plant Sciences and Genetics in Agriculture, The Hebrew University of Jerusalem, Rehovot, Israel*
[4]*Ryan Institute for Environmental, Marine and Energy Research, National University of Ireland Galway, Galway, Ireland*

[5]*Department of Mechanical Engineering, Ben-Gurion University of the Negev, Beer-Sheva, Israel*

Growth strategy of climbers depends on external support, as opposed to erect self-supporting plants. Self-supporting plants and climbers exhibit numerous differences in their morphology, vascular anatomy and biomechanical properties. Fundamental functional differences supposedly should originate at the tissue and cell walls levels.

In this study we compared three non-woody evolutionarily close Solanales species with different growth habits: a self-supporting plant (potato, *Solanum tuberosum*), a trailing plant (sweet potato, *Ipomoea batatas*) and a twining climber (morning glory, *Ipomoea tricolor*). Several biomechanical analyses were combined with structural and immunocytochemical approach, always comparing the uppermost mature stem internode.

The stems showed large morphological differences, with the climber morning glory stem being the most slender and least circular. Stem anatomy was somewhat similar in all three species- being herbaceous, mostly unlignified with inner phloem and collenchyma at the stem periphery. Potato stems were hollow and xylem was organized in small separate vascular bundles, while in morning glory and sweet potato the xylem was continuous around the stem. Cell wall composition was very similar. The highest fraction of the cell wall were the hemicelluloses (~60%), α-cellulose constituted around 25% of the cell wall, and pectins constituted 5-8%. In morning glory hemicellulose a content was a bit lower, and α-cellulose content was slightly higher. Immunohistochemistry of specific cell wall components also showed little variation among the species, with some differences in hemicelluloses allocation. According to tensile and flexural tests, potato stems were significantly the stiffest and the morning glory stems the most compliant, while Elastic modulus values were not sufficiently different. Stiffness parameter takes into account the morphology of the organ, while the elastic modulus depends mainly on the material properties of measured stem. Apparently, mainly morphology influences the biomechanical function.

In this case, closely related species diverged into different stem types, while generally preserving their ancestral traits of anatomical structure and cell wall composition. Function was changed by simple changes in stem morphology. However, in other taxonomic groups the biomechanics could be changed by other factors.

Immunolocalisation of pectins in Solanum tuberosum stem.

---

POSTER SESSION - Life Sciences

P-22

## STUDY OF THE S. CEREVISIAE KINESIN-5 MOTORS BY CRYO–ELECTRON MICROSCOPY

**Sudhir Kumar Singh**[1,2], Nurit Siegler[1,2], Ran Zalk[4], Gabriel Frank[3,4], Leah Gheber[1,2]
[1]*Departments of Chemistry, Ben-Gurion University of the Negev, Beersheva, Israel*
[2]*The Ilse Katz Institute for Nanoscale Science and Technology, Ben-Gurion University of the Negev, Beersheva, Israel*
[3]*Life Sciences, Ben-Gurion University of the Negev, Beersheva, Israel*
[4]*The National Institute for Biotechnology in the Negev, Ben-Gurion University of the Negev, Beersheva, Israel*

*S. cerevisiae* cells express two kinesin-5 motors Cin8 and Kip1. These motors share a bipolar homotetrameric structure involved in mitotic spindle dynamics by crosslinking and sliding apart antiparallel microtubules. Interestingly, recent studies from our and other groups demonstrated the bidirectional motility for yeast kinesin-5 motors, Cin8 and Kip1, that can switch directionality under a number of conditions (Duselder et al., 2015; Fridman et al., 2013; Gerson-Gurwitz et al., 2011). These findings were in contrast to the previous dogma stating that N-terminal kinesin motors are exclusively plus-end directed. We aim to

understand the structural and biochemical features of yeast kinesin-5 motors that promote directional switching of motility. To investigate the mechanistic basis for the bidirectional motility of Cin8, we cloned and purified the dimeric constructs of Cin8 and Kip1. For Cin8, the constructs include the native dimer and the Loop 8 (L8) deletion variant. The deletion of Loop 8 construct induces a strong bias towards minus-end directed motility and affects the stoichiometric microtubule binding (Bell et al., 2017; Gerson-Gurwitz et al., 2011). Further we are using Cryo–Electron microscopy (Cryo-EM), which uniquely allows for high-resolution 3D reconstructions of Cin8 bound to microtubules in the presence of different nucleotides. We present preliminary results of decoration of microtubules by Cin8 and Kip1. We believe that the Cryo-EM studies will reveal the unique structural elements involved in the bidirectional motility of Cin8 and Kip1.

***References:***

1-Z. Shang, K. Zhou, C. Xu, R. Csencsits, J.C. Cochran and C.V. Sindelar. 2014. High-resolution structures of kinesin on microtubules provide a basis for nucleotide-gated force-generation Elife, 3, p. e04686

2-Roostalu, J., C. Hentrich, P. Bieling, I.A. Telley, E. Schiebel, and T. Surrey. 2011. Directional switching of the Kinesin cin8 through motor coupling. *Science*. 332:94-99.

3-Gerson-Gurwitz, A., C. Thiede, N. Movshovich, V. Fridman, M. Podolskaya, T. Danieli, S. Lakamper, D.R. Klopfenstein, C.F. Schmidt, and L. Gheber. 2011. Directionality of individual kinesin-5 Cin8 motors is modulated by loop 8, ionic strength and microtubule geometry. *Embo J*. 30:4942-4954

---

POSTER SESSION - Life Sciences

P-23

## DYNAMICS OF GERMINAL CENTER EGRESS REVEALED BY WHOLE ORGAN IMAGING

**Liat Stoler-Barak**[1], Adi Biram[1], Chiara Medaglia[1], Amir Giladi[1], Eyal David[1], Natalia Davidzohn[1], Yoseph Addadi[2], Ofra Golani[2], Tomer Meir Salame[2], Ido Amit[1], Ziv Shulman[1]
[1]*Immunology, Weizmann Institute of Science, Rehovot, Israel*
[2]*Life Sciences Core Facilities, Weizmann Institute of Science, Rehovot, Israel*

Enduring protection from pathogens depends on generation of long-lived memory and antibody-secreting plasma cells in germinal centers (GC). The GC is segregated into a dark zone, where B cells proliferate and mutate their antibodies, and a light zone (LZ) where T cells select B cells for clonal expansion. However, the selection mechanism for GC-egress and the precise departure site remain unclear. Using light-sheet fluorescence microscopy for large-scale imaging of intact lymph nodes, we demonstrate that individual GCs generate highly heterogeneous numbers of departing cells. Combining whole-organ imaging, photo-labeling and single-cell-RNA sequencing revealed that B cells depart GCs through the LZ in a transitional differentiation state. Furthermore, we show that selection for GC-egress is dictated by intrinsic-B cell receptor affinity. Our findings provide a unifying model for the role of T cells in expansion of clones available for GC-egress, and the requirement for intrinsic B cell functions for antibody-mediated immunity.

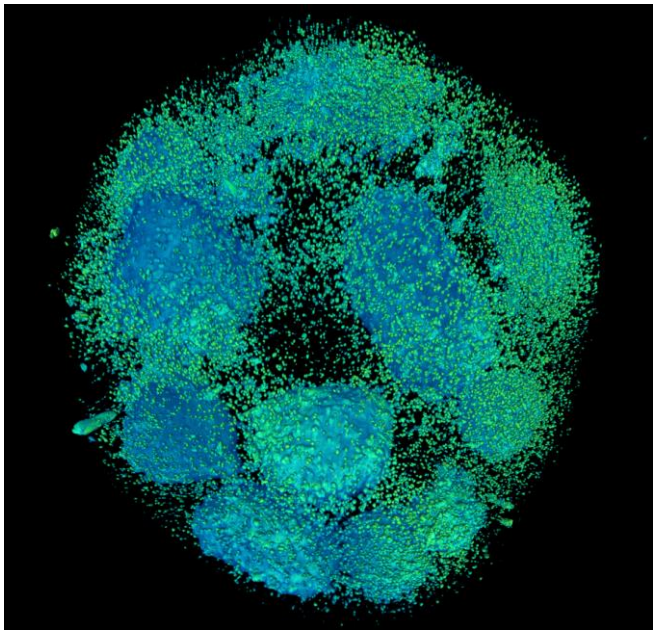

---

POSTER SESSION - Life Sciences

P-24

## THREE-DIMENSIONAL RECONSTRUCTION OF BACTERIAL FLAGELLAR FILAMENTS WITH A SEAM

**Shlomo Trachtenberg**, Yair Ben Shaul
*Microbiology&Molecular Genetics, The Hebrew University, Jerusalem, Israel*

Non-helically perturbed polymers are a product of pairwise reduction along symmetry lines of uneven Bessel orders. The result is a discontinuity in the form of a helical seam. Seams have been shown to occur in TMV [1], microtubules [2] and bacterial flagellar filaments [3]. Only the structure of seamed microtubules was fully analyzed.

The right-handed flagellar filament of *Salmonella typhimurium* sjw23 (serotype gt) is non-helically perturbed. removing the outer, D3, flagellin domain from the *fliC23* gene or replacing it with a domain from an unperturbed strain (sjw1655) restores helical symmetry (as indicated by the disappearance of the typical layer-line clusters (*n*= -2.5, -13.5, 8.5) from the power spectrum). This suggests that the non-helical perturbation is, likely, a product of unique interactions in the inner part of the outer D2/D3 domains. To specify the sub-molecular interactions leading to the perturbation, we need a full three-dimensional reconstruction.

Microtubules are assembled from globular alpha and beta tubulin dimers, are thin-walled, hollow tubes with long, nearly vertical, helical repeats. bacterial flagellar filaments, in comparison, are dense polymers with a narrow central channel and a complex, four domained radial mass distribution.

using the underlying symmetry of the perturbed filament we develop a streamlined, compact and efficient reconstruction procedure. It is based on the long range helical order of the seam and the shorter repeats as ‘single particles’. We utilize the short helical repeat (*n*=11, 393Å) and the long helical repeat of the seam (393x11=4323Å). The method, compared to microtubule reconstructions, (1) does not require an external reference, (2) does not require prior knowledge of the location of the seam, (3) can handle short independent segments as single particles, (4) helical averaging of the protofilaments is done in one step and (5) brings

into account the relation between the seam ‘s angular position and the tube’s radius. Determining the polymer`s symmetry allows restoring, or ‘reverse engineering’ helicity so as to compensate for the perturbation and reconstruct the structure. The perturbation can be reconstructed as a straight or helical seam.

[1] E.M. Mandelkow, R. Schultheiss, R. Rapp, M. Muller, E.M. Mandelkow, M. Müller, On the surface lattice of microtubules: helix starts, protofilament number, seam, and handedness, J Cell Biol. 102 (1986) 1067–1073. doi:10.1083/jcb.102.3.1067.

[2] J. Cope, S. Gilbert, I. Rayment, D. Mastronarde, A. Hoenger, Cryo-electron tomography of microtubule–kinesin motor complexes, J. Struct. Biol. 170 (2010) 257–265. doi:10.1016/j.jsb.2009.12.004.

[3] K. Nisani-Bizer, S. Trachtenberg, Unperturbing a non-helically perturbed bacterial flagellar filament: Salmonella typhimurium SJW23, J. Mol. Biol. 416 (2012) 367–388. doi:10.1016/j.jmb.2012.01.003.

[4] D.L. Caspar, K.C. Holmes, Structure of dahlemense strain of tobacco mosaic virus: a periodically deformed helix., J. Mol. Biol. 46 (1969) 99–133. http://www.ncbi.nlm.nih.gov/pubmed/5358645 (accessed August 22, 2016).

---

POSTER SESSION - Life Sciences

P-25

## INTENSIFY3D: NORMALIZING SIGNAL INTENSITY IN LARGE HETEROGENIC IMAGE STACKS

**Nadav Yayon**[1,2], Amir Dudai[2,3], Nora Vrieler[2,3], Oren Amsalem[2,3], Michael London[2,3], Hermona Soreq[1,2]

[1]*Department of Biological Chemistry, The Life Sciences Institute, The Hebrew University of Jerusalem, Jerusalem, Israel*

[2]*The Edmond and Lily Safra Center for Brain Sciences (ELSC), The Hebrew University of Jerusalem, Jerusalem, Israel*

[3]*Department of Neurobiology, The Life Sciences Institute, The Hebrew University of Jerusalem, Jerusalem, Israel*

**Introduction** - Fluorescence microscopy once relied on single plane images from relatively small areas and yielded limited amounts of quantitative data. Nowadays, many imaging experiments encompass some form of depth or a Z-stack of images, often from distinct regions in the sample. Hence, much like biochemical and molecular experimental datasets[2], accurate normalization, beyond background subtraction[3] of imaging signals, could reduce tissue-derived and/or technical variation. Specifically, 2-Photon (2P) and Light-Sheet (LS) microscopes enable the acquisition of images from both deep and wide tissue dimensions (Fig 1a, c, left panel). However, every biological sample and imaging technique introduces its own acquisition aberrations: beyond mirror and lens distortions[4], the imaged preparations combine different characteristics (of e.g. cell density and lipid composition) that affect the optical penetration and light scattering at diverse tissue depths. Experimental limitation (antibody penetration, clearing efficiency) also constrain the ability to extract information from imaging experiments. Taken together, these difficulties call for the development of universal post-acquisition image correction/normalization tools that account for signal-carrying pixels and which estimate the specific heterogeneity of each image individually. To achieve 3D normalization, we developed a new algorithm, Intensify3D (Fig 1. b), Intensify3D aims to detect and use the background for correct normalization of the signal. Consequently, our normalization algorithm initiates with an estimation of the background by removing as much as possible of the imaged signals (as defined by the experimenter). Then, the background intensity gradients are used for correction by local transformation (correction by division) of both signal and background, without compromising the signal-to-noise ratio (Fig 1. a, b).

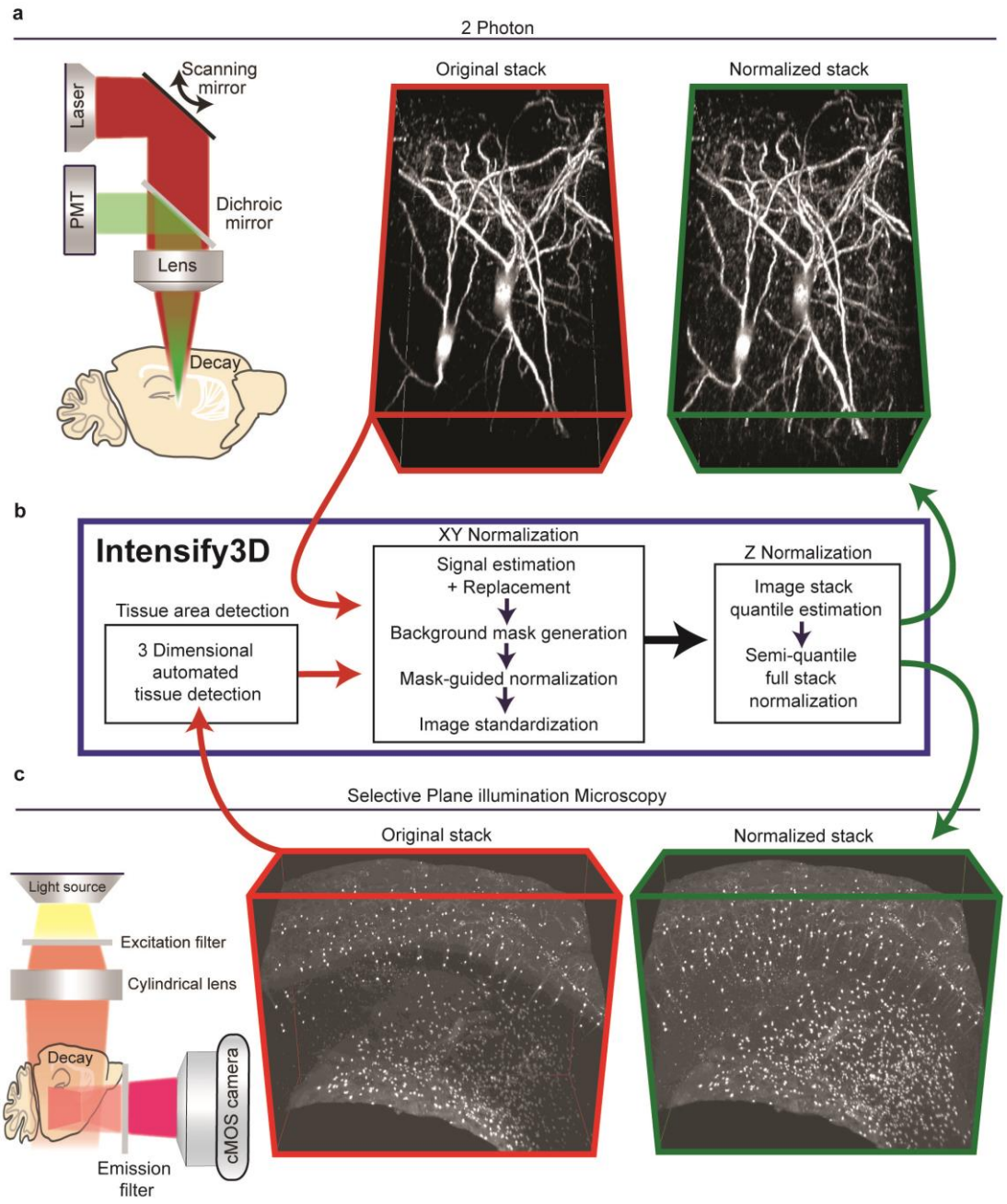


**Figure 1. The basic normalization process of Intensify3D for 2-Photon and Light-Sheet 3D imaging. a. Left panel.** 2-photon imaging setup illustrating the decay in excitation laser (red) and emitted light (green) through the imaged tissue. **Red frame, middle panel.** 3D projection of *In vivo* 2-photon Z-stack of cortical cholinergic interneurons (CChIs) up to 300µm depth, bottom portion is deeper. **Green frame, right panel.** 3D projection of image stack post normalization with Intensify3D; note the enhanced visibility of deep neurites. **b.** Intensify 3D processing pipeline for 2-Photon and light sheet image stacks. The latter requires an additional step to only account for tissue pixels in the image. The images in the stack are normalized one by one (XY normalization). After all the images are corrected the entire stack is corrected (Z Normalization) by semi-quantile normalization (other options exist). **c. Left panel.** Light-Sheet imaging setup where the excitation light is orthogonal to the imaged surface. **Red frame, middle panel.** iDISCO immunostaining and clearing of CChIs as well as striatal Cholinergic interneurons. Original image suffers from fluorescence decay at increasing tissue depth. **Green frame, right panel.** Intensify3D Normalized image stack. Images before and after normalization are presented at the same brightness and contrast. levels.

**Results** - We tested Intensify3D in two state-of-the-art imaging platforms (2-Photon and Light-Sheet) and demonstrated that it can overcome common sample heterogeneity in large image stacks using both of these technologies and correct significant dataset errors. Specific advantages of our algorithm include its capacity

to distinguish between the signal and background with minimal parameters defined by the experimenter and avoiding distorting one at the expense of the other, as well as enabling applicability to various imaging platforms. The resulting avoidance of imaging errors and improvements in signal homogeneity are therefore an important asset for fluorescence microscopy imaging studies of all cells and tissues, especially in the brain. **2-photon imaging** - Intensify3D normalization enabled homogenous representation across the entire image stack. Additionally, Intensify3D corrected significant errors in the estimation of deep dendrite diameters. Thus, normalized images offer a better representation of both imaged cell bodies and their thin extensions and serve as a superior platform for reconstructions and possibly modeling of the electrical properties of these neurons. Hence, this algorithm may offer a special added value to world-wide leading brain research projects. **Light-Sheet imaging** - Appling Intensify3D on LS data obtained from cleared[5] adult mouse brains dramatically improved the detection and visualization of the barrel fields, indicating its applicability for such studies. At the microscale, we demonstrated that post-normalized scans of detected CChIs somata represent their real-life density, distribution, and composition compared to original scans, highlighting the importance of image normalization. Finally, to test the applicability of Intensify3D to diverse tissues we selected the mammary gland and heart, both of which present considerable challenges. We showed that with normalization we could extract the morphology of the milk ducts and buds by "simple" auto fluorescence.

**Conclusions** - Our current findings and analyses demonstrate that the Intensify3D tool may serve as a user-guided resource, correct sample- and technology-driven variations, improve the reproducibility, and add extractable information to numerous imaging studies in neuroscience research as well as in life sciences at large. Given these advantages, we hope that our work will open an active discussion on matters of image normalization. We believe that image normalization has an integral role in any imaging experiment where numerical data is extracted. As in other fields of life sciences, normalization reduces variability between samples even when the experimental conditions are superb. Finally, Intensify3D might further be of value to time lapse fluorescence imaging platforms such as time lapse structural imaging or calcium imaging in which the fluorescence of the imaged sample is often compromised during imaging.


- Yayon, N. *et al.* Intensify3D: Normalizing signal intensity in large heterogenic image stacks. *Sci. Rep.* **8,** 4311 (2018).
- Bolstad, B. M., Irizarry, R. ., Astrand, M. & Speed, T. P. A comparison of normalization methods for high density oligonucleotide array data based on variance and bias. *Bioinformatics* **19,** 185–193 (2003).
- Dunn, K. W., Kamocka, M. M. & McDonald, J. H. A practical guide to evaluating colocalization in biological microscopy. *Am. J. Physiol. Cell Physiol.* **300,** C723-42 (2011).
- Dong, C.-Y., Koenig, K. & So, P. Characterizing point spread functions of two-photon fluorescence microscopy in turbid medium. *J. Biomed. Opt.* **8,** 450–459 (2003).
- Renier, N. *et al.* iDISCO: A Simple, Rapid Method to Immunolabel Large Tissue Samples for Volume Imaging. *Cell* **159,** 896–910 (2014).


---

POSTER SESSION - Life Sciences

P-26

## OLD FASHION VS. NEW GENERATION- CORRELATIVE METHODS FROM ORGAN TO CELL


**Einat Zelinger**[1], Yulia Pollak[1], Olga Raskina[2], Yuval Cinnamon[3], Smadar Harpaz[4], Oded Yarden[5], Yael Heifetz[6]

[1]*CSI Center for Scientific Imaging of The Robert H. Smith Faculty of Agriculture, Food and Environment, Hebrew University, Rehovot, Israel*

[2]*Institute of Evolution and Department of Evolutionary and Environmental Biology, University of Haifa, Haifa, Israel*

[3]*Department of Poultry and Aquaculture Sciences, Agricultural Research Organization, The Volcani Institute, Reshon Le Tzsion, Israel*
[4]*The Robert H. Smith Institute of Plant Sciences and Genetics in Agriculture, The Hebrew University of Jerusalem, Rehovot, Israel*
[5]*The department of Plant Pathology and Microbiology, The Hebrew University of Jerusalem, Rehovot, Israel*
[6]*The department of Entomology, The Hebrew University of Jerusalem, Rehovot, Israel*

Sometimes new is the well forgotten old! Sophisticated and unique high resolution methods can be found across literature. Yet, not all studies require the finest resolution. Here, we explore the combination of good "old fashion" techniques like cryostat thick sectioning and confocal as well as "new generation" light microscopy based 3D method.

The correlative microscopy methods are presented at three biological levels: whole organ, tissue and intracellular. For the whole organ we use HREM, High-Resolution Episcopic Microscopy (developed by Tim Mohun, CR-UK). Using HREM we can visualize embryos, plants and small organs. Its resolution allows the identification of individual nuclei, nerves and blood vessels, which may not be detectable using lower-resolution techniques such as optical projection tomography (OPT), micro-MRI or micro-CT. It allows histological staining that can be segmented and quantified in 3D.

For the tissue level we used a combination of thick 10-20 micron cryostat sections either pre- or post-stained with fluorescent markers. Following dry/wet fluorescence imaging samples were further prepared for SEM. This combination allows spatial assessment of fluorescent markers in the larger context of the tissue in EM resolution. Looking at tissues such as Drosophila reproductive organs, Fruit cuticle & cell wall and Fungal sexual fruiting bodies indicated a very friendly and versatile method.

For the intracellular level, fluorescent in situ hybridization (FISH) with specific DNA probes in somatic and meiotic cereal anther tissues were used. Following confocal imaging samples were dehydrated and prepared for corresponding HRSEM via XY specific coordinates. This method proved useful for the study of nuclear and chromosomal patterns of tandem repeats and loose-end DNA fragments.

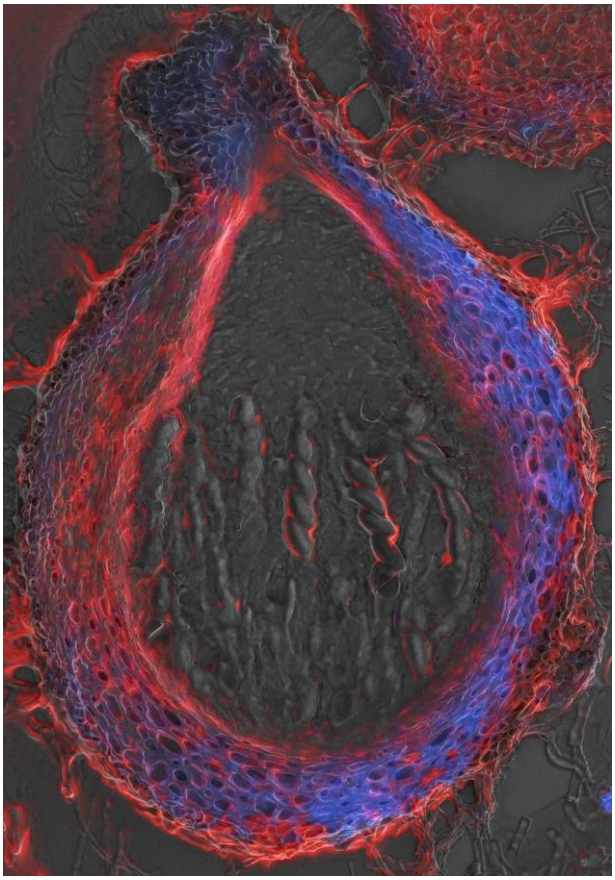

---

P-27

# THE EFFECT OF OXYGEN CONCENTRATION ON THE ELECTRICAL RESISTIVITY OF TANTALUM OXIDE THIN FILMS

**Tamir Amrani**, Amit Kohn, Ilan Goldfarb
*Materials Science and Engineering, Tel Aviv University, Tel Aviv, Israel*

The phenomenon of resistivity change in transition metal oxide insulators under an electric-field was first demonstrated back in 1962. More than thirty years later, the concept of resistive switching was proposed resulting in a new field of research with applications towards non-volatile memory [1].
Among a wide group of materials exhibiting resistive switching is the binary metal oxide of TaOx, which is studied widely for resistance-change random access memory (RRAM). One major reason for the Ta-O system being a leading candidate for RRAM applications is because it contains only a single equilibrium oxide phase, tantalum pentoxide ($Ta_2O_5$), which allows an excellent switching characteristics such as very high endurance [2].

Classified as a Fermi-glass material, amorphous $Ta_2O_5$, is an insulator in which electrical conduction is by a variable-range hopping (VRH) mechanism. Thus, according to Mott`s theory – the electrical conductance is strongly dependent on the hopping length between one conduction-center to another [3].

We investigate the effect of oxygen concentration during sputter deposition (O/Ar flow-rate) on the structure and properties of the amorphous TaOx thin films: electrical resistivity and the electronic band structure.

Related to Mott`s equation, the temperature-dependent hopping lengths must be evaluated in different Ta/O systems in order to show a trend between the electronic properties and the amorphous structure.

Oxygen vacancies serve as conduction-center for the VRH mechanism, so the hopping length can be determined from the inter-atomic distances in the short-range order of the Ta oxide. Moreover, since the memristive behavior exists only in a nano-layered structures, transmission electron microscopy (TEM) is a favorable method for characterizing the short range structural order. Illuminating a nanoscale region of the amorphous thin layer with a parallel electron beam in order to collect an electron diffraction, enables to calculate the radial distribution function (RDF).

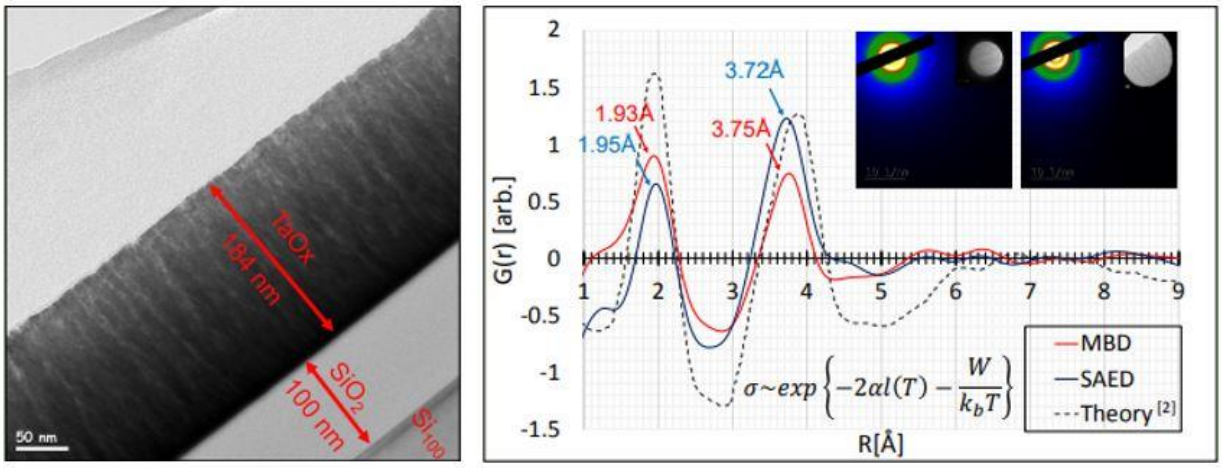


Figure 1: (left) - bright field TEM image of TaOx amorphous thin film sputter deposited with a 30%-Oxygen-flow. (right) radial distribution function curves of Ta2O5 based on micro-beam electron diffraction and selected area electron diffraction [5]. Conductivity $\boldsymbol{\sigma}$ is proportional to the hopping probability as $\boldsymbol{\alpha}$ is the decay length of the localized-electron wave function in r.s, W is the activation energy for hopping, and ($\boldsymbol{T}$) is the hopping length [3].

The chemical bonding states and electronic band structure were characterized by X-ray photoemission spectroscopy (core-level and valence band measurements), Resistivity was measured by a four-point-probe

method. We will discuss the role of oxygen flow during sputter deposition on the structure and functional properties of TaOx thin films.

References

[1] D. Zhu, Yi Li, W. Shen, Z. Zhou, L. Liu , and X. Zhang, Journal of Semiconductors, Vol. 38 (2017).

[2] I. Goldfarb, F. Miao, J. Joshua Yang, W. Yi, J.P. Strachan, M.-X. Zhang, M.D. Pickett, G. Medeiros-Ribeiro, R. Stanley Williams. Appl. Phys A, Vol. 107 (2012).

[3] N.F. Mott, E.A. Davies, Electronic Processes in Non-crystalline Materials, Clarendon (1979).

[4] R. Bassiri, K. B. Borisenko, D. J. H. Cockayne, J. Hough1, I. MacLaren, and S. Rowan. Applied Physics Letters, Vol. 98 (2011).

[5] J. Shanmugam, K. B. Borisenko, Y. Chou, A. I. Kirkland, SoftwareX, Vol. 6 (2017)

---

POSTER SESSION – Materials Science

P-28

## MEASURING THE MEAN INNER POTENTIAL OF $Al_2O_3$ USING OFF-AXIS ELECTRON HOLOGRAPHY

**Avi Auslender**[1], Mahdi Halabi[2], George Levi[1], Oswaldo Diéguez[1], Amit Kohn[1]
[1]*Department of Materials Science and Engineering, Tel Aviv University, Tel Aviv, Israel*
[2]*Department of Materials Engineering, Ben-Gurion University of the Negev, Beer-Sheva, Israel*

The mean inner potential (MIP) of a material is the volume averaged electrostatic (Coulomb) potential between the bulk and vacuum. Thus, the MIP is a fundamental material property, which depends on both composition and structure. Knowledge of MIP values also has significant implications for electron microscopy.[1]

However, measurements of the MIP are lacking for a wide range of materials due to the experimental complexity. One such materialis α-$Al_2O_3$ sapphire, which is also of scientific and technological importance. Here, for the first time, we report the MIP value of sapphire, measured using a novel sample preparation methodology and off-axis electron holography.

We prepared a TEM sample of a polished α-$Al_2O_3$(0001) wedge specimen at an angle of approximately 45°. The wedge sample enabled to improve the accuracy of the determined MIP by measuring the gradient of the phase variation of the reconstructed electron wave. The angle of the wedge was measured to an accuracy of better than 1° by both confocal optical microscopy and by subsequent perpendicular sectioning of the TEM sample in a focused ion beam. The validity of the proposed methodology was first verified on a Si(001) sample resulting in a MIP value of 13.16±0.45V in agreement with previous reports.

Our preliminary measurements, accounting for dynamical contributions, determined that the MIP of sapphire is 16.7±0.2V. We have also performed density-functional theory calculation of the MIP of $Al_2O_3$ slabs cut along (0001) and (1-100) planes, obtaining 15.7V and 16.7V, respectively. This measured MIP of sapphire depends on the degree of ionicity, which lies between theoretical calculations of charged ionic and neutral covalent bonding based on Dirac-Fock and Radi methods.[2] Since sapphire is predominantly an ionic material [3], our measured MIP indeed tends toward the ionic value.

**References**

- M. Gajdardziska-Josifovska, M.R. McCartney, W.J. de Ruijter, David J. Smith, J.K. Weiss, J.M. Zuo, Accurate measurements of mean inner potential of crystal wedges using digital electron holograms, Ultramicroscopy. 50 (1993) 285-299.

- Edgar Volkl, Lawrence F.Allard , David C.Joy, Introduction to electron holography, Kluwer Academic. (1998) ISBN 0-306-44920-X.
- W.E. Lee, K.P.D. Lagerlof, Structural and Electron Diffraction Data for Sapphire (α-Al2O3), Journal of electron microscopy technique. 2 (1985) 247-258.


---

POSTER SESSION – Materials Science

P-29

## CONTROLLING THE DEWETTING MECHANISM AND KINETICS OF Ni THIN FILMS BY SMALL AMOUNT OF ADDITIVES


**Hagit Barda**, Eugen Rabkin
*Materials science and engineering, Technion - Israel Institute of science, Haifa, Israel*


Thin metal films deposited on ceramic substrates tend to undergo dewetting (agglomeration) as a response to an increase of the homological temperature. The driving force for this process is the reduction of the total surface and interface energy of the system. The solid state dewetting process of Ni on several ceramic substrates (sapphire, MgO, and Yittria Stabilized Zirconia) has been carefully studied in the past. Yet, the influence of small amount of additives on the dewetting of Ni films has received much less attention.

In this work we characterized the dewetting of 40 nm thick Ni films in the temperatures range of 700°C-900°C and explored the influence of some additives using mainly HRSEM and STEM methods. We propose new ways to control the morphology of the dewetted Ni films, and the rate of the Ni film agglomeration.

---

POSTER SESSION – Materials Science

P-28

## STRUCTURAL ORIGIN OF PERPENDICULAR MAGNETIC ANISOTROPY IN ULTRA-THIN $Co_2MnSi$ FILMS STUDIED BY TRANSMISSION ELECTRON MICROSCOPY


**Adham Basha**[1], Wenhong Wang[2], You Caiyin[3], Fu Huarui[3], Amit Kohn[1]
[1]*Department of Materials Science and Engineering, Tel Aviv University, Tel Aviv, Israel*
[2]*Institute of Physics, Chinese Academy of Sciences, Beijing, China*
[3]*Materials Science and Technology, Xi'an University of Technology, Xi'an, China*


Spintronics exploits the electron spin as an additional degree of freedom in solid state devices, thus enhancing functionalities. Amongst these are novel opto-electronic devices in which injection of perpendicularly spin polarized electrons from a ferromagnetic electrode into a light emitting diode is expected to yield circularly polarized photons [1]. Butler *et al.* [2] propose that such high polarization electron injection can be achieved in an ultrathin (2-3nm) chemically ordered (B2 or $L2_1$) $Co_2MnSi$ (CMS) full Heusler due to a combination of perpendicular magnetic anisotropy (PMA) and half-metallicity. PMA is expected due to tetragonal distortion of cubic CMS on epitaxial MgO(001).

Here, we correlate between the structure and magnetic properties of magnetron sputter-deposited ultra-thin CMS electrodes with varying thicknesses and annealing temperatures using transmission electron microscopy (TEM: phase contrast, energy-loss spectroscopy, scanning TEM, HAADF) and magnetometry.

Magnetometry measurements show clear PMA in the ultra-thin layers (Fig.1). Structural characterization using aberration corrected high resolution phase contrast imaging indicates almost complete absence of ordered phases in the CMS layer, consistent with the relatively low magnetic saturation moment (Fig.1). Compositional analysis using sub-nm resolution STEM-EELS indicates chemical intermixing of the Heusler

layer with both the MgO and Pd adjacent layers (Fig.2). Consequently, PMA is mostly attributed in this case to interface intermixing anisotropy comparable to Co/Pd multilayers [3] or to Co-Pd alloying [4].

We also note that previous reported structural analyses of these Heusler alloys are undertaken on thin layers (20-50nm), which is then assumed to be comparable in ultra-thin layers (2-3nm). According to our results, this assumption is not valid, and hence these type of ultra-thin film require state-of-the-art TEM analysis.

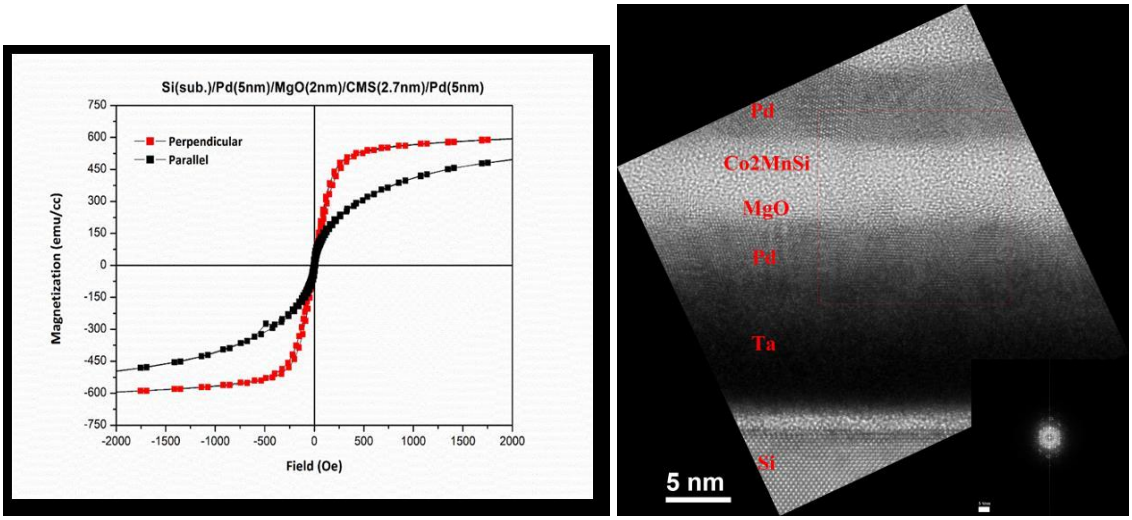


**Fig. 1-(Left) M-H loops measured at 300K (SQUID) for sample with Co2MnSi (2.7nm) on top of MgO (2nm) annealed at 350 °C; (Right) Cs corrected HR TEM image (Phase contrast)-(Si Z.A. [110]) (inset: Power spectrum of area denoted by red square).**

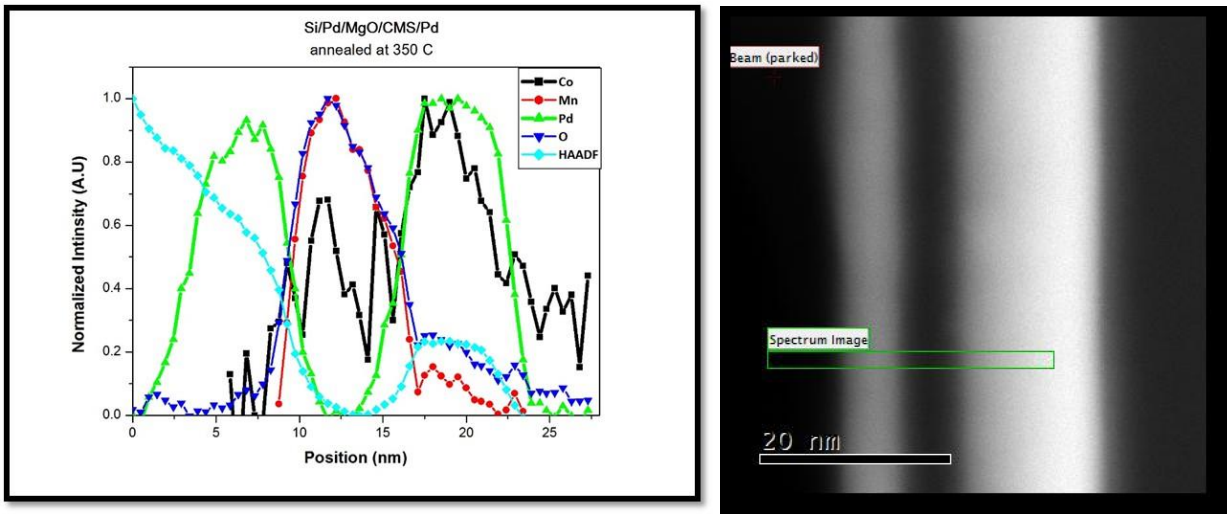


**Fig. 2- STEM EELS line scan: (left) Elemental distribution (Right) HAADF STEM cross-sectional image showing area from which EELS line scans were obtained denoted schematically by the green rectangle**


1. Farshchi, Rouin, *et al.*, *Applied Physics Letters*98(16) (2011).

2. Munira, Kamaram, Jonathon Romero, and William H. Butler, *Journal of Applied Physics*115(17) (2014).

3. Den Broeder, F. J. A., *et al.*, *Journal of Applied Physics* 61(8) (1987).

4. Shunichi Hashimoto *et al.*, *Japanese Journal of Applied Physics* 28 1596 (1989).


---

P-31

# STRUCTURAL PECULIARITIES IN REGULAR DILUTED SOLID Ar-Kr SOLUTIONS

**Viktor Danchuk**[1], Mikhail Strzhemechny[2], Angelina Solodovnik[2], Nataly Mysko[2], Iryna Lehchenkova[3]

[1]*Exact Sciences Faculty, Department of Physics, Ariel University, Ariel, HaMerkaz (Central), Israel*

[2]*ILTPE, B. Verkin Institute for Low Temperature Physics and Engineering of the National Academy of Sciences of Ukraine, Kharkov, Kharkov, Ukraine*

[3]*Engineering Faculty, Chemical Engineering, Biotechnology and Materials Department, Ariel University, Ariel, HaMerkaz (Central), Israel*

Rare gas binary alloys are suitable objects for investigation into basics of solid state [1]. A unique feature of regular diluted solutions of noble gases is the possibility of experimentally determining the excess volume per impurity, which can be compared with the conclusions of various microscopic theories [2]. A successful theoretical description of the equilibrium properties of mixed crystalline systems is based on several generally accepted postulates, in particular, Vegard's empirical rule, dealing with the lattice parameters. However, in reality, the morphology and structure of cryoalloys strongly depends on the procedure for growing the samples [3].

The transmission high energy electron diffraction (THEED) technique was employed for studying the structure of the regular diluted solid Ar - Kr solutions. The polycrystalline samples of regular diluted solid Ar - Kr solutions (to 15 mol.% of one of the components) were prepared *in situ* by deposition of a precooled gaseous mixture onto an Al and carbon substrates cooled to 20 K. The lattice parameters of solutions were measured.

To explain the experimentally observed structural anomalies in diluted solid Ar - Kr solutions, we calculated the positions of atoms in a nine-layer spherical cluster of krypton with an argon atom in the center and argon cluster with krypton atom in center. The interaction was approximated with the Lenard–Jones potential. The substitution volumes $v_{Ar}$ of an argon atom in the krypton crystal and $v_{Kr}$ a krypton atom in argon crystal were calculated. It was shown that compared to the generally accepted estimates obtained within the nearest-neighbor approximation, the value of $v_{Ar}$ is approximately twice as small. This effect is explained by an additional repulsion of the first coordination sphere of krypton atoms arising as the krypton atoms approach each other upon their inward motion. As for the reverse situation (a krypton atom in the argon cluster), in which the guest particle is larger than the regular one, the experimental and calculated results correlate with the estimates obtained from simple combinatorial considerations.

References

- Rare Gas Solids, M.L. Klein and J.A. Venables (eds.), Academic Press, London, (1976) vol. 1; (1977) vol. 2.
- M. A. Strzhemechny, A. I. Prokhvatilov, and L. D. Yantsevich, Physica B 198, 267 (1994).
- V. V. Danchuk, A. A. Solodovnik, N. S. Mysko, and M. A. Strzhemechny, Fiz. Nizk. Temp. 41, 546 (2015) [Low Temp. Phys. 41, 424 (2015)].

---

P-32

# THE ADVANTAGES AND APPLICATIONS OF A CMOS BASED EBSD DETECTOR

**Keith Dicks**[1], Jenny Goulden[2], Pat Trimby[2], Angus Bewick[3]
[1]*Sales, Oxford Instruments NanoAnalysis, High Wycombe, Buckinghamshire, UK*
[2]*Marketing, Oxford Instruments NanoAnalysis, High Wycombe, Buckinghamshire, UK*
[3]*Research & Develpment, Oxford Instruments NanoAnalysis, High Wycombe, Buckinghamshire, UK*

K. Dicks[1], J. Goulden[1], P. Trimby[1], A. Bewick[1]

[1] Oxford Instruments NanoAnalysis, Halifax Road, High Wycombe, HP12 3SE, UK

CCD-based EBSD detectors have been commercially available for more than 15 years. These detectors are typically either ‘high resolution’ or ‘high speed’. The ‘high resolution’ detectors enable the acquisition of high-quality, megapixel-resolution (1024x1024 pixels) diffraction patterns with good sensitivity, but limited acquisition speed. Alternatively, ‘high speed’ detectors, typically offer a VGA resolution (maximum 640x480 pixels), with much higher maximum speeds. The latest high-speed CCD-based detectors achieve speeds of ~1500 patterns per second (pps), but only by using extreme pixel binning. This binning has two undesirable effects with regard to pattern quality: a reduction in resolution (only ~40x30 pixels at the highest speed); and a reduction in the maximum signal-to-noise ratio (SNR) before pixel saturation. As a result this high pattern binning compromises analysis, reducing both the hit rate and the orientation precision of fast data acquisition. Not all EBSD applications require a detector’s maximum speed. Some applications require high sensitivity, high resolution and high pattern quality.

The development of a CMOS sensor for EBSD detectors has overcome these issues, delivering a step change in performance. The CMOS sensor architecture enables high speed without the need for extreme, on-sensor binning.

Therefore good resolution and good maximum SNR can be achieved during fast data acquisition. Results from a CMOS-based detector can be collected and analysed in real time at speeds in excess of 3000pps, more than double the speed of any existing CCD-based detector. Importantly, this CMOS detector has a superior maximum SNR and 4x the resolution (16x more pixels) at 3000pps than a CCD detector at ~1500pps (Figure 1). As a result this technology delivers significant improvements to both indexing hit rates and to the angular resolution of orientation measurements.

Optimising angular resolution is important in many EBSD applications, resulting in a significant interest in high resolution (HR) EBSD. This technique uses pattern correlation techniques to compare acquired patterns to reference patterns and to calculate small diffraction pattern shifts[1]. This has enabled analyses with significantly improved angular resolution, when compared to standard Hough-based indexing, with angular accuracies routinely reported below 0.01°.

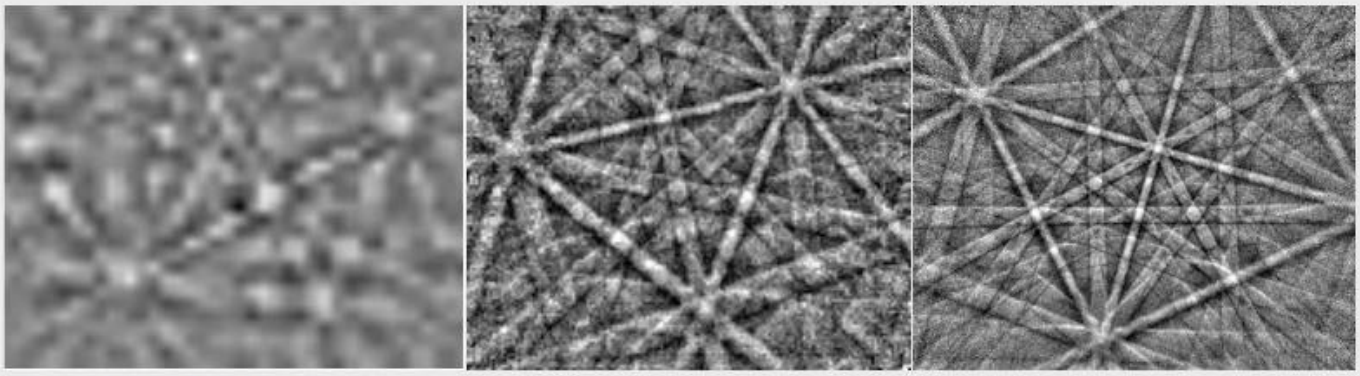

Figure 1 Example EBSPs

40 x 30 pixel EBSP collected at 1580 pps using a conventional CCD-based detector

156 x 128 pixel EBSP collected at 3000 pps using CMOS-based detector

1244 x 1024 pixel EBSP collected at 100 pps from a duplex steel sample using a CMOS-based detector

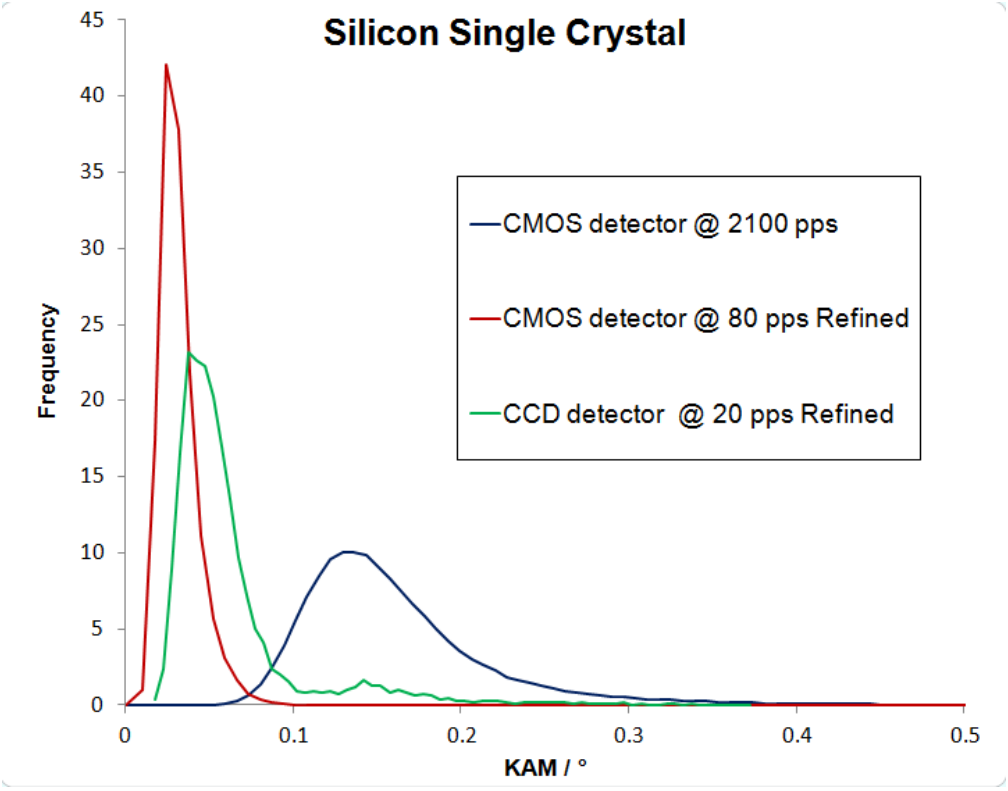


Figure 2. Kernel Average Misorientation distribution plots showing angular accuracy of different analyses / detectors on a Si single crystal. Note the significant improvement in speed and accuracy of a CMOS detector when compared to a CCD detector.

[1] Wilkinson, A. J., Meaden, G. & Dingley, D. J. (2006). Mater. Sci.Technol. 22, 1271–1278

[2] Singh, S., Ram, F. & de Graef, M. (2017). J. Appl. Cryst. 50

[3] Alkorta, J., Marteleur, M. & Jacques, P.J. (2017). Ultramicr. 182, 17-27

---

P-33

## EPMA CHARACTERIZATION OF FLUID MICROINCLUSIONS IN ECLOGITIC GARNET

**Oded Elazar**[1], J-X Huang[2], Ronit Kessel[1], Oded Navon[1]
[1]*The Institute of Earth Sciences, The Hebrew University of Jerusalem, Jerusalem, Israel*
[2]*CCFS, Macquarie University, Macquarie, Australia*

We report preliminary results of a systematic search for fluid/melt microinclusions in mantle minerals. "Dusty" garnets from xenolith XRV6 [1], a heavily metasomatised Type I eclogite from Roberts Victor mine, SA, carry many microinclusions (1 μm). FTIR analyses of the "dusty" zones indicate the presence of molecular water in the inclusions and hydroxyl groups in the garnet. EPMA analysis begins with identification of shallow, subsurface inclusions in backscattered electron imaging and minimal expression in the secondary electron image. Once found, the inclusions (along with the host garnet) are analysed by wavelength dispersion x-ray spectrometry (WDS). Measurements of 136 microinclusions reveal their bulk composition. Compared to the host garnet, they are enriched in $TiO_2$, FeO, CaO, $Na_2O$ and $K_2O$ and depleted in $Al_2O_3$ and MgO. The silica contents seem to be similar to that of the host garnet. Most of the elements form compositional mixing arrays of microinclusion+garnet. Since the proportion of the garnet component is unknown, the composition of the microinclusions cannot be derived directly. The arrays trend away from the compositions of large secondary melt pools or secondary minerals found in healed cracks the xenolith. They point towards the array of silicic to low-Mg carbonatitic high density fluids (HDFs) trapped in diamonds and we derive their composition by intersecting the garnet-inclusions mixing lines with the corresponding arrays of the diamond HDFs. The results indicate close proximity to the fluids known from the diamonds but with lower content of $K_2O$, indicating the important role of HDFs in mantle metasomatism.

[1] Gre´au et al. (2011) *GCA* ***75,*** 6927–6954**.**

---



P-34

## COMPOSITIONAL ANALYSIS OF ULTRA-THIN, ELECTRON-BEAM SENSITIVE FILMS USED IN SEMICONDUCTOR DEVICES BY ENERGY DISPERSIVE X-RAY SPECTROSCOPY IN SCANNING TRANSMISSION ELECTRON MICROSCOPY

**Daniel Fishman**[1,2], Adham Basha[1], Amit Kohn[1]
[1]*Materials Science and Engineering, Tel Aviv University, Tel Aviv, Israel*
[2]*FA Labs, Yield department, Intel F28, Kiryat Gat, Israel*

In the semiconductor industry, the application of Energy Dispersive X-ray spectroscopy (EDS) in the transmission electron microscope (TEM) has been limited to *qualitative* characterization of devices.

New technology in the form of multiple silicon drift detectors (SDD) with large collection angles, high brightness electron sources and rapid statistical computation of large data sets warrant a reevaluation of this analytical methodology. Our question is whether EDS in the Scanning TEM can enable high-throughput *quantitative* analysis of ultrathin, beam sensitive films and structures used in advanced integrated circuits.

We chose a representative structure on a Si (001) wafer of (thickness in brackets): Ti silicide (5 nm), Ti (6.5 nm), and TiN (8.5 nm) films. We compared between the previous technology of a thermally-assisted field-emission gun (FEG) source with a 0.13srad solid angle Si(Li) detector to a high-brightness FEG source with four SDD detectors collecting X-ray photons from a 0.7srad solid angle [1]. Ultrathin films were prepared

both by physical and chemical vapor deposition rendering especially the TiN layer, prepared by the latter method, sensitive to beam damage due to the use of metal-organic compounds.

First, we characterized the onset of electron beam damage to the various layers using an approach described in Refs.[2,3]. These measurements then enabled to define measurement protocols for optimizing X-ray photon count statistics without damaging the layers.

Thus, we utilized the ability of rapid and accurate measurement of the probe current in current TEMs and the sample thickness using a focused ion beam to apply both the Cliff-Lorimer and the Zeta-factor methods for quantitative compositional characterization of the layers.

Quantitative results were compared to electron energy-loss spectroscopy (example in Fig. 1) and X-ray photoelectron spectroscopy measurements. In the case of the TiN layer, energy peak overlaps of X-ray photons from the Ti $L_a$ and N $K_a$ shells still prohibit their reliable quantitative assessment.

We will discuss the combination of high efficiency SDD with high-brightness FEG source in a STEM as a viable method to enable rapid quantitative EDS analysis of semiconductor devices in the microelectronics industry.

Keywords: Energy dispersive X-ray spectroscopy, Scanning Transmission Electron Microscopy, Microelectronic devices, silicon drift detectors, high brightness field emission electron sources

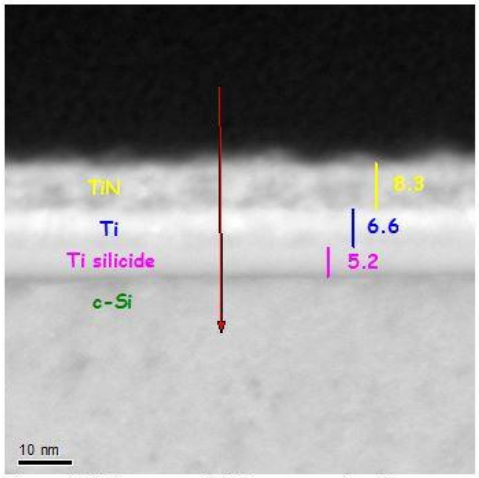


Figure 1 (a) Z-contrast STEM cross-sectional image showing the TiN, Ti and Ti silicide on the Si(001) substrate aligned to a [110] zone axis. The red arrow denotes schematically the direction of the compositional analysis. The numbers denote approximate thickness of layers in nm.

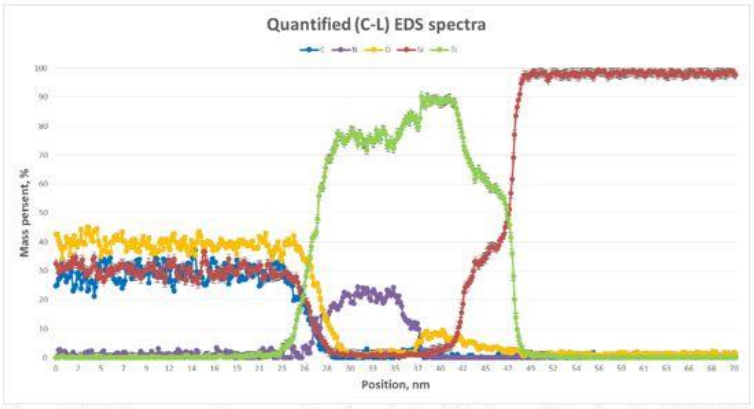


Figure 1 (b) Mass percent compositional analysis of the layers following the STEM EDS line scan seen in (a) and using the Cliff-Lorimer ratio technique.

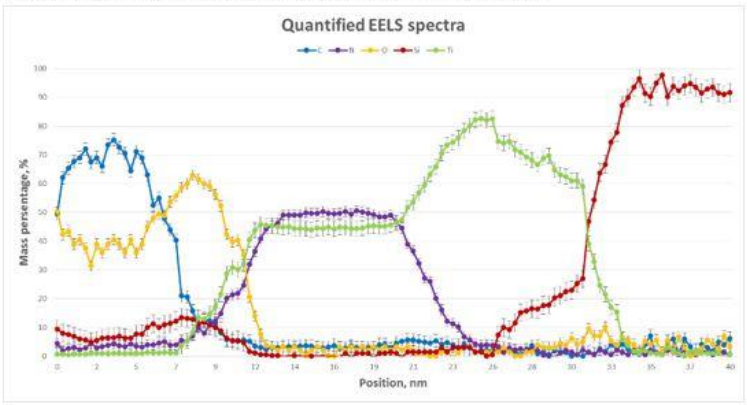


Figure 1 (c) Mass percent compositional analysis of the layers following a STEM EELS line scan seen in (a) and using background subtracted integrated area ratios of the energy-loss peaks.

References:


- FEI Metrios data sheet. http://www.fei.co.jp/_documents/DS0161-02-2014_Metrios-web.pdf
- F. Mansfield, P.R. Okamoto, L.E. Rehn, and N.J. Zaluzec, Radiation effects on X-Ray-microanalysis of a light-element alloy in a medium-voltage electron-microscope, Ultramicroscopy 21 (1987) 13-22
- F. Egerton, F. Wang, and P. A. Crozier, Beam-induced damage to thin specimens in an intense electron probe, Microsc. Microanal. 12 (2006) 65–71


---

P-35

# MAPPING THE SPACE CHARGE REGION IN NANOSCALE MAGNESIUM ALUMINATE SPINEL

**Mahdi Halabi**[1], Amit Kohn[2], Shmuel Hayun[1]
[1]*Department of Materials Engineering, Ilse Katz Institute for Nanoscale Science and Technology, Ben-Gurion University of the Negev, Beer-Sheva, Israel*
[2]*Department of Materials Science and Engineering, Tel Aviv University, Tel Aviv, Israel*

Charge distribution in magnesium aluminate spinel (MAS) results in the formation of a space-charge region, which is then expected to have a critical role in assigning functional properties. Explanations for this phenomenon are reported though quantitative experimental evidence in the case of granular MAS is indirect. To address this topic, we characterized the space charge region in nonstoichiometric nanoscale MAS grains, examining the effect of grain size and applied electric field on the lattice ordering (Fig.1a) and space-charge potential (SCP)[1].

The distribution of cations and point defects [$Al^{\bullet\bullet}_{Mg}$] (inversion parameter) across the grains (Fig.1b) was measured by electron energy-loss spectroscopy (EELS) in scanning transmission electron microscopy (TEM) and compared to the electrostatic potential as measured by off-axis electron holography (EH) in mid-resolution TEM (Fig.1c). We demonstrated quantitatively that regardless of grain size, excess [$Al^{\bullet\bullet}_{Mg}$] defects reside (increased inversion parameter) in the vicinity of grain-surfaces of Al-rich MAS (Fig.1d,e,f). The distribution of electric charge was evaluated by reconstructing the phase shift (Fig.1c) of the electron wave at nanometer-scale resolution. For the same grain, multiple holograms were averaged so that the reconstructed phase was then compared along directions perpendicular to grain surfaces. The contribution of the mean-inner-potential to the phase shifts was evaluated by measuring the relative thickness from the same region using EEL low-loss spectra, as presented in Fig.1d,e,f. Thus, we show that the origin of electrostatic potential difference between the surface and core of the MAS grain is due to the spatial distribution of defects of MAS (Fig.1d,e,f).

We are investigating the effect of grain size on the distribution of the SCP. For grains annealed without applying an external electric field, our measurements show that with decreasing size, the grain core is no longer electrically neutral due to the significant accumulation of charge at surfaces. The effect of an applied electric field on the SCP in $MgO{\cdot}1.27Al_2O_3$ has also investigation when the grain size, sized ~10nm, is comparable to the Debye length (Fig.1b,d). It has been observed that, while grains subjected to thermal annealing (870°C) show significant charge accumulation (potential above 4V), such grains are subjected additionally to dc-electric fields, up to $1000Vcm^{-1}$, and charge accumulation is not detected. Furthermore, since applying a moderate electric field during the annealing process improve lattice ordering (Fig.1a). The origin of this surface charging and its discharge in the presence of an electric field will be discussed.

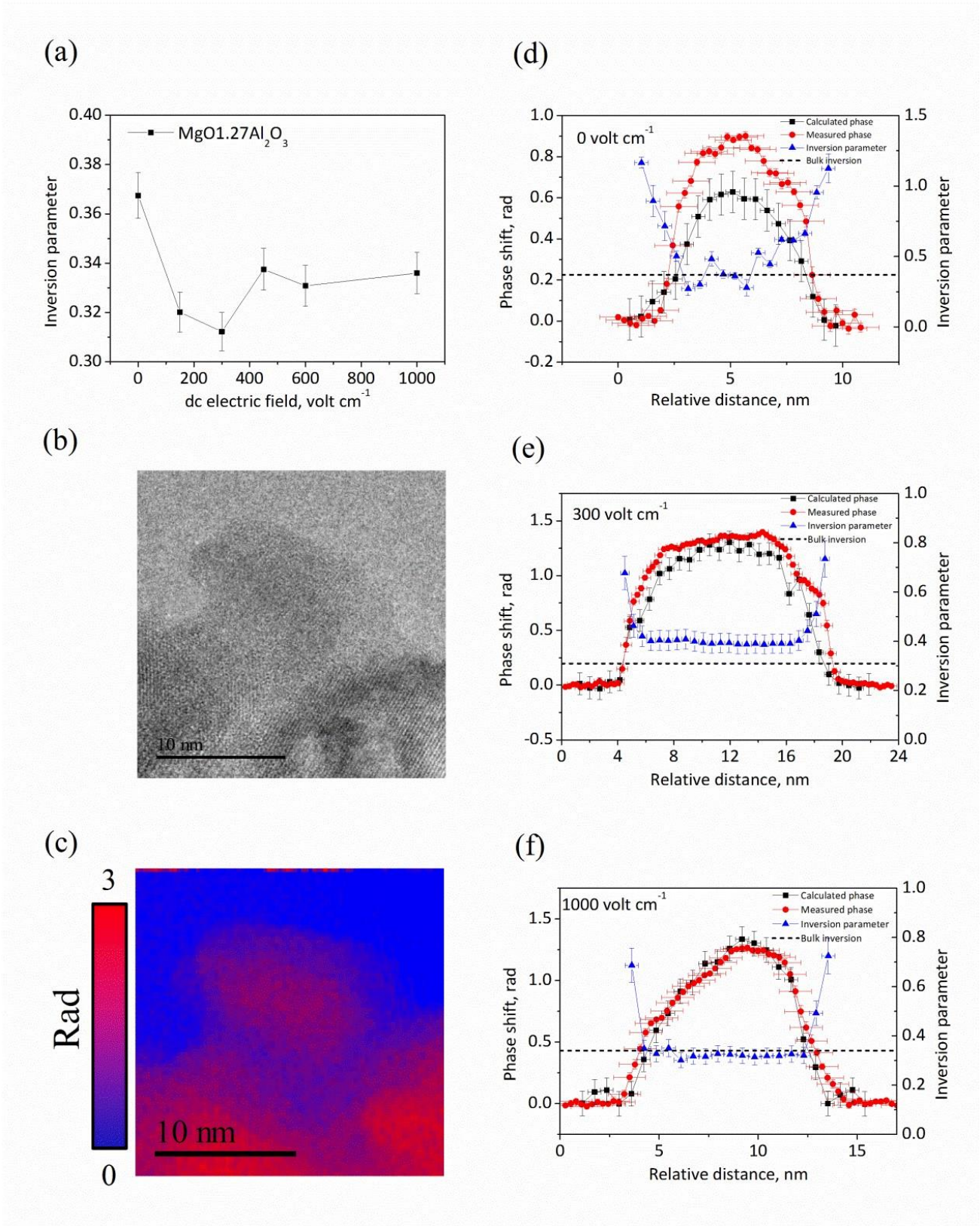


Figure 1. Inversion parameter of $MgO{\bullet}1.27Al_2O_3$ subjected to dc-electric fields, up to $1000Vcm^{-1}$, and an annealing temperature of 870°C (a), BF-TEM image (b) and phase-shift map of the electron wave as measured by EH (c) of as-synthesized MAS grains. Line profile values between grain surfaces of the inversion parameter (blue curves), measured phase-shift (red) and, phase-shift calculated from thickness contribution (black) after annealing at 870°C without (d) and with applying an electric field: $300Vcm^{-1}$ (e) and $1000Vcm^{-1}$ (f)

*References:*


- Halabi, M. *et al.*, *J. Am. Ceram. Soc.* 2017;100:800–811.


---

P-36

## CONTROL OVER SELF-DOPING IN HIGH BANDGAP PEROVSKITE FILMS

**Michael Kulbak**, Gary Hodes, David Cahen
*Materials and Interfaces, Weizmann Institute of Science, Rehovot, Israel*

The effects of different cations and anions on carrier diffusion lengths and formation of a junction in high bandgap halide perovskite (HaP) film-based solar cells are studied in detail. HaP cells are of interest as high bandgap ones in solar spectrum splitting for boosting solar to electrical energy conversion efficiency/area by adding them to c-Si photovoltaic cells and driving photo-electrochemical reactions for chemical energy storage. Resolving how the addition of cations and anions change the (unintentional) doping of the HaP is of great importance for understanding the film and device physics as well as for performance improvement. We study Pb-based, $APbX_3$, HaP films, where A can be a mixture of formamidinium, methylammonium and cesium and X a mixture of bromine and chlorine, using a combination of *Dark-conductivity, Photoconductivity* and *Steady-State Photocarrier-Grating* (SSPG) techniques [1]. This way we measure the effect of the different cations and anions compositions on the majority and minority carrier diffusion lengths. We also use Electron Beam Induced Current (EBIC), [2] to identify the formation of the junction and built-in voltage and to track the position and size of the space charge region width following the changes in the HaP composition. In some HaP structures, EBIC is needed to measure diffusion length when it is unmeasurable in SSPG. We find mixed-cation HaP form a *p-i-n* junction with relatively long and ambipolar carrier diffusion lengths, in contrast to the single cation based bromide HaPs, who form a *p-n* junction and shorter diffusion lengths.

**References**

[1] I. Levine, *et al., J. Phys. Chem. Lett.* **2016**, *7*, 5219.

[2] N. Kedem, M. Kulbak, *et al., Phys. Chem. Chem. Phys.* **2017**, *19*, 5753.

---



P-37

## WATER CONDENSATION PROCESSES OCCURRING ON METALLIC MICRO-SCALED SURFACES

**Iryna Lehchenkova**[1], Anton Starostin[3], Viktor Valtsifer[3], Zahava Barkay[4], Viktor Danchuk[2], Edward Bormashenko[1]
[1]*Engineering Faculty, Chemical Engineering, Biotechnology and Materials Department, Ariel University, Ariel, Israel*
[2]*Exact Sciences Faculty, Physics Department, Ariel University, Ariel, Israel*
[3]*Institute of Technical Chemistry, UB RAS, Perm, Russia*
[4]*Wolfson Applied Materials Research Center, Tel Aviv University, Tel Aviv, Israel*

Environmental scanning electron microscopy of water condensation on superhydrophobic and fluorinated superoleophobic micro-rough aluminum surfaces is reported. We observed film-wise condensation on superhydrophobic surfaces and pronounced drop-wise condensation on the superoleophobic surfaces, possessing the similar topography.

Nano- and micro-scaled surfaces are of much industrial interest in a view of their numerous applications as water-repellent (self-cleaning) [1], superoleophobic [2] and ice-phobic surfaces [3]. This paper is focused on water condensation on micro-scaled aluminum surfaces. Water condensation could be generally classified as drop-wise and film-wise. In our investigation, we focus on the possibility of fine tuning of surface properties of aluminum micro-rough surfaces enabling switching from film-wise to drop-wise pathway of water condensation and on the kinetics of growth of droplets. Water condensation was studied on

superhydrophobic and superoleophobic micro-rough aluminum surfaces of the same topography. The difference in the pathways of condensation was attributed to the various energy barriers separating the Cassie and Wenzel wetting states on the investigated surfaces. The higher barriers inherent for superoleophobic surfaces promoted the drop-wise condensation.

The structures were studied in the Quanta 200FEG ESEM (Environmental Scanning Electron Microscope) while imaging the sample surface using the gaseous secondary electron detector. In-situ imaging of water condensation was performed within the ESEM at wet-mode using water vapor from a built-in distilled water reservoir. ESEM study shows the very different pathways of condensation processes on the micro-scaled chemically modified superhydrophobic and superoleophobic surfaces.

1. Nosonovsky, B. Bhushan, Superhydrophobic surfaces and emerging applications: Non-adhesion, energy, green engineering, Curr. Opin. Colloid Interface Sci. 14 (2009) 270-280.

2. Tuteja, W. Choi, M. Ma, J.M. Mabry, S.A. Mazzella, G. Rutledge, G.H. McKinley, R.E. Cohen, Designing superoleophobic surfaces, Science 318 (2007) 1618-1622.

3. Hejazi, K. Sobolev, M. Nosonovsky, From superhydrophobicity to icephobicity: forces and interaction analysis, Sci Rep. 3 (2013) 2194.

---

POSTER SESSION – Materials Science

P-38

## Halide Exchange in Macro-Sized Halide Perovskite Single Crystals

**Aya Osherov**, Gary Hodes, David Cahen
*Materials and Interface, Weizmann Institute of Science, Rehovot, Israel*

Halide Perovskites, rising star materials in photovoltaics, with the general formula $ABX_3$, where A=methylammonium (MA), formamidinium (FA) or Cs, B=Pb and X=halide have remarkable electronic and optical characteristics. Still, much remains unknown regarding the connection between their physical and chemical properties. The identity of the X component influences greatly the band gap of the material, and mixed halide compositions have been used for band gap-tuning. Halide exchange was previously reported in thin-films and in micron-sized single crystals.

We demonstrate halide exchange in mm-sized $MAPbX_3$ single crystals, achieved by diffusion. In these macro-sized crystals, the effect of surface and defects is significantly smaller than in the microcrystals and polycrystalline thin films studied previously. Therefore, they are better suited to examine the fundamental exchange process(es), unencumbered by possible grain boundary and surface diffusion effects. Initially, the halide exchange creates normal concentration gradients of the out-going and in-coming halides, on a scale of a few microns to a few hundred microns. The depth (from the surface) of the substituted area depends on the halide pair and the role of each halide (which one is being exchanged and which one is exchanging). As expected the concentration gradient of the in-coming halides decreases from the surface of the crystal towards its inner core and *vice versa* for the out-going halides. While these gradients do cause a lattice parameter change and may cause a symmetry change, we show that if the interchanged halide pair is such that their sizes are relatively similar (e.g., $Br^-$ and $Cl^-$, $Br^-$ and $I^-$, not $Cl^-$ and $I^-$) the product crystal remains surprisingly single crystalline. This finding is valid, no matter which one of the two halides is being exchanged. Our results suggest that for these similar-sized halide pairs, this exchange occurs through a solid-state chemical reaction such that the resulting crystal orientation is determined by that of the initial crystal (a topotactic reaction). This is demonstrated by scanning microscope images, electron dispersive spectroscopy and X-ray diffraction measurements. This phenomenon is crucial when one wishes to achieve a specific composition of halide perovskite crystals/crystallites, using multi-synthesis steps without compromising the degree of crystallinity and orientation.

---

P-39

## NOVEL AUTOMATION FOR SEM & DUALBEAM WITH PYTHON SCRIPTING

**Daniel Phifer**
*Materials Science, Thermo Fisher Scientific, Eindhoven, The Netherlands*

Repetitive electron microscopy tasks that could be automated are often not due to the microscope/instrument manufacturer not allowing control of these systems. Manufacturers chose the most commercially viable routines to sell as dedicated software such as "Auto Slice and View" or "Auto TEM" and these applications are quite successful for high volume applications. Unfortunately, many applications that are routine and repetitive are extremely specific to real research needs and there is a real desire for control and automation solution for SEM and DualBeam™ systems to meet this need. Python appears to be the premier open source scripting language for scientific research so Thermo Fisher Scientific has developed a Python interface library, "AutoScript", to interfaces the SEM and DualBeam platforms with modern operating systems to enable simple automation routines to be constructed which can do a variety of routine tasks..

The AutoScript API allows automation routines to be constructed which can do a variety of non-routine tasks as well and decision trees can be integrated for unattended operation. Combining control of most all microscope functions including setting and reading values, calling auto functions, saving images and storing values with other existing open source Python scripts can be supplemented with image matching, data graphing, automated response and feedback loops to create novel performance. Many nice examples of custom scripts have already been created that adjust settings with a feedback loop, extract and graph *in situ* data, and perform image capture automatically at specified positions. The availability of so many Python based routines in the open source environment allows various components to be integrated/combined for specific purposes. With the ability to control both the SEM and FIB columns, GIS, Manipulator, and other accessories, the AutoScript interface allows writing advanced automation for most tasks. Python libraries exist for image matching, data display and data export that complete the suite of capabilities needed for custom automation of systems on Windows 7 and higher.

---



P-40

## ON THE TENSION–COMPRESSION YIELD ASYMMETRY IN AN EXTRUDED MG–ZM21 ALLOY

**Shmuel Samuha**[1], Adi Ben Artzy[1,2], Arie Bussiba[1], Shahaf Baron[3], Lior Snarski[3]
[1]*Materials Engineering, NRCN, Beer-Sheva, Israel*
[2]*IAEC, Israel Atomic Energy Commission, Tel-Aviv, Israel*
[3]*Materials Engineering, Ben-Gurion University of the Negev, Beer-Sheva, Israel*

Due to their high strength-to-weight ratio, magnesium alloys (Mg) offer a favored alternative to steels and aluminum alloys for engineering components in the transportation industry. The application potentials are, however, impeded by poor room temperature formability and strong directional anisotropy. At room temperature, an insufficient number of slip systems are activated, thus plastic deformation is also accommodated by twinning. Due to its' polar characteristic, the type of the nucleate twin, {10-12} extension or the {10-11} contraction type-twin, depends on the texture with respect to the loading direction. In turn, twinning was found as the key role for the tension–compression yield asymmetry, where Tensile yield strength (TYS) diff ers significantly from the Compressive yield strength (CYS) along the same direction. This asymmetry restricts the structural application of magnesium alloy, especially for beams subjected to tension and compression simultaneously.

Current research deals with the yield response of hot-extruded Mg-ZM21 alloy at a temperature of 190, 220 or 350℃with a constant extrusion ratio. This is carried out through a comparative study consist of uniaxial

tension and compression experiments. The inter-connection between asymmetry ratio (CYS/TYS) to microstructure phenomena and texture modification is carried out through the characterization at different extruded conditions. The microstructural and micro-textural investigations is carried out by means of Electron Back-Scattered Diffraction (EBSD) technique. Macro-texture analysis is carried out using X-Ray diffractometer, applying the Schultz reflection method. The MTEX package, a freely available MATLAB toolbox, is employed for the post-processing and the visualization of EBSD data. Qualitative intra-grain strain analysis and recrystallization fraction at different thermo-mechanical states are performed based on the local misorientation approach using kernel-average misorientation (KAM) maps and the grain-orientation spread (GOS) plots.

---

POSTER SESSION – Materials Science

P-41

## MICROSTRUCTURE DETERMINATION OF OXIDE PARTICLES IN THE 14%Cr OXIDE DISPERSION STRENGTHEND STEEL

**Yael Templeman**[1], Denis Sornin[2], Malki Pinkas[3], Louisa Meshi[1]
[1]*Department of Materials Engineering, Ben Gurion University of the Negev, Beer Sheva, Israel*
[2]*CEA, DEN, SRMA,, LTMEx, 91191 Gif-sur-Yvette, France*
[3]*., Nuclear Research Center-Negev, Beer Sheva, Israel*

Oxide dispersion strengthened (ODS) steels offer superior strength and creep resistance at high temperatures due to the reinforcement of fine nanosized oxides dispersed throughout the matrix. These alloys have been applied in the aerospace, thermal processing and glass processing industries. Due to their exceptional strength and creep resistance at high temperatures, they became one of the most promising candidates for material components in the nuclear power plants. The addition of Ti to these alloys reduces the particle size, leading to higher dispersion of fine Y-Ti-oxide particles. These oxides block mobile dislocations, resulting in increased hardness and strength. The most common types of such oxides which were reported to exist in these steels are $Y_2Ti_2O_7$ and $Y_2TiO_5$. However, most common diffraction patterns shown in the literature for these structures can also be indexed in terms of $Y_2O_3$, and despite numerous studies focused on the characterization of these oxides, ambiguity regarding their composition and structures remains. Since structure and properties of materials are intimately linked, in depth characterization is crucial for understanding of physical properties. In the present study, detailed transmission electron microscopy (TEM) analysis, including high angular annular dark field (HAADF) and energy filtered TEM (EFTEM), was conducted in order to determine the distribution, composition and structure of oxide particles in a 14wt% Cr ODS alloy. It was found that oxides are composed mainly of Y, Ti and O. However, diffraction patterns obtained from several particles could not been indexed in terms of the $Y_2Ti_2O_7$ or $Y_2TiO_5$ structures. Electron diffraction tomography data set obtained from one particle was successfully indexed in terms of $YTiO_3$ (distorted perovskite derivative), which is rarely reported in the literature regarding these steels.

---

P-42

## IMAGING ORGANIC CRYSTALLIZATION IN AQUEOUS MEDIA

**Yael Tsarfati**, Haim Weissman, Shaked Rosenne, Boris Rybtchinski
*Organic Chemistry, Weizmann Institute of Science, Rehovot, Israel*

Organic crystals are of primary importance in pharmaceuticals, functional materials, and biological systems. Nevertheless, the understanding of organic crystallization mechanism is still limited. Understanding the transformation from “Non-classical” Prenucleation phases into crystals is a key challenge. In this study a Perylene Diimide (PDI) crystallization, within aqueous solution, is studied by optical spectroscopy and cryogenic electron microscopy, in order to address this challenge. Direct imaging of evolving prenucleation phase reveals a fascinating complexity of a nonclassical crystallization path, providing new insights into organic crystallization mechanism.

---



P-43

## USING MICROSCOPY AND SPECTROSCOPY TO DIAGNOSE TRANSFORMATION OF AMORPHOUS OPAL TO QUARTZ CHERT IN DEEP SEA SEDIMENTS

**Anastasia Yanchilina**, Ruth Yam, Aldo Shemesh
*Earth and Planetary Sciences, Weizmann Institute of Science, Rehovot, Israel*

The processes that control the evolution and maturation of amorphous opal (opal-A) to opal-CT to quartz chert in deep sea sediments are not yet fully constrainted. Specifically, to what extent do in situ lithologies and geothermal temperatures contribute to the transformation of silica to more stable thermodynamic states? We use sediments from two ODP cores 795 and 799 retrieved from the Sea of Japan where these mineralogical transitions are documented to have occurred. We isolated the silica phases with a robust cleaning and physical separation procedure. To analyze the mineral state of the silica (i.e., whether it is amorphous opal, opal-CT, or chert) we use XRD, SEM/EDS, XRF, XPS, and FTIR. Here we present images and intepret authigenic mineral overgrowths and substitutions in those sedimentary environments where the abundance of amorphous opal relative to clay is poor, suggesting that that silica is converted to clay rather than opal-CT or chert. In environments where the initial abundance of of opal-A is rich, we observe the amorphous opal matures to opal-CT and chert (this happens in these sediments of ages ~4 Myr and older).

---



P-44

## LIGHT-INDUCED EFFECTS ON OPTOELECTRONIC PROPERTIES OF HALIDE PEROVSKITES

**Arava Zohar**, Michael kulbak
*Material and Interfaces, Weizmann Institute for Science, Rehovot, Israel*

Halide Perovskites, HaPs, present high optoelectronic quality semiconductors, which is remarkable due to their low-temperature solution preparation. Evidence for significant densities of optoelectronically active defects, i.e., with levels in the band gap is contradictory and, especially for single crystals, very low densities have been deduced. These findings led us to propose the occurrence of self-repair of defects. Clarifying these

issues, is the defect density indeed unusually low, and is there self-repair, under solar cell working conditions is important both for fundamental understanding of the HaP materials and for guiding us in designing or identifying other materials with such behavior. Here we use high solar cell quality HaPs with systematically varying compositions, to address these questions. Highly specialized electron beam-induced current (EBIC) measurements with and without illumination, as function of bias and/or temperature allow to map and track changes in junction positions and diffusion/ drift lengths. We find that the EBIC profile shape changes and that the diffusion lengths increase as function of supra band gap illumination in the device configuration. The physical origin of the illumination effect is not simply the photogeneration of the carriers as we observed an increase of electron diffusion length with light intensity, which suggests structural electronic rearrangements to screen the increased generated carries. By adding studies of the mobility-lifetime product, photoconductivity, and work function, we arrive at a first description of these, beyond PV, photogenerated changes.

---

P-45

## BREAKING THE ICE

**Zohar Eyal**
*Structural Biology, Weizmann Institute of Science, Rehovot, Israel*

This image shows what is likely to be crystals of potassium uranyl acetate. The crystals were observed in a negative stain of *Staphylococcus aureus* ribosomes on a pre-coated carbon grid with 2% uranyl acetate. Image was taken with the T-12 electron microscope in the EM unit of the Weizmann Institute of Science. The features in this image resemble to glaciers` melting down as a result of global warming.

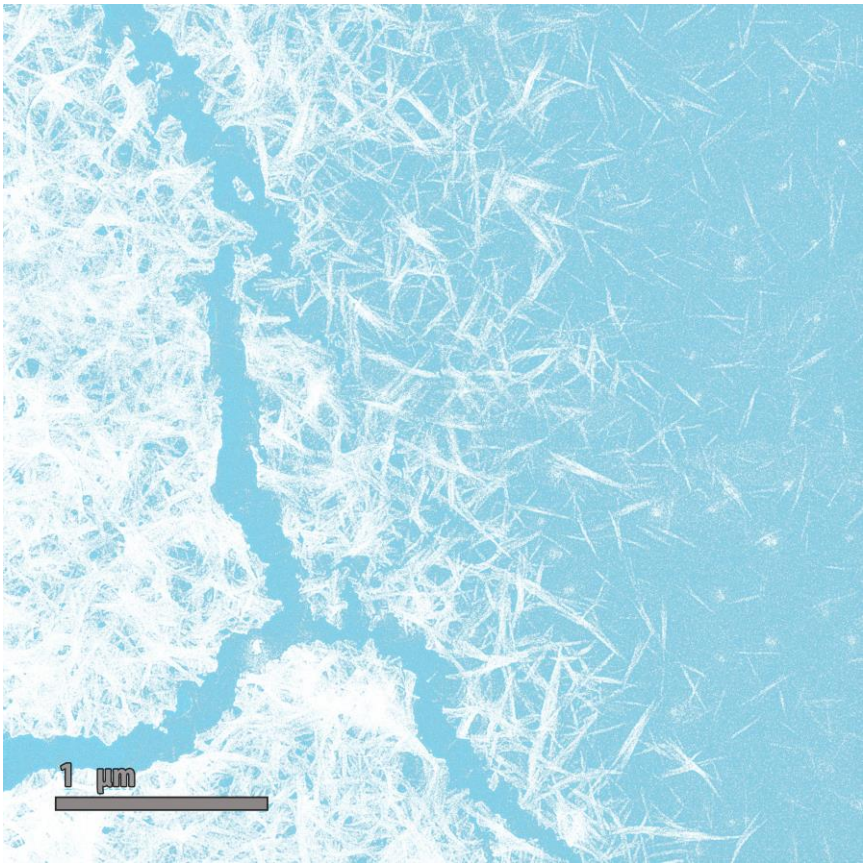


---



P-46

## FIND SANTA IN THE IMAGE

**Ilana Shtein**
*Department of Agriculture, Eastern Region R&D, Ariel, Israel*

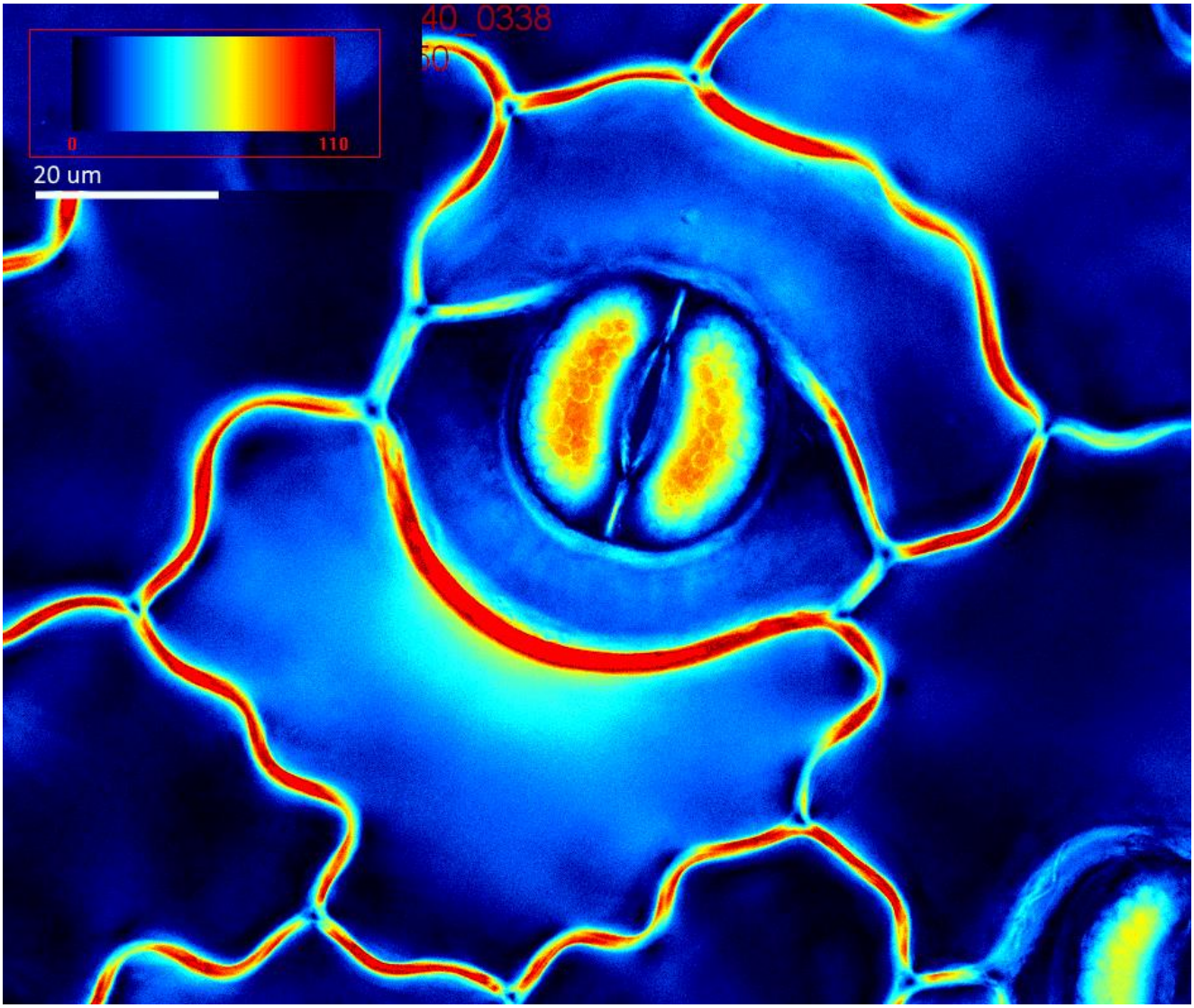


Stoma of the fern *Platycerium bifurcatum* under polarized light (LC-PolScope). The image shows the light retardance of the sample.

---

MICROGRAPHS COMPETITION

P-47

## VESICLES FLEEING MITOCHONDRIA

**Zipora Lansky**
*Structural Biology, Weizmann Institute of Science, Rehovot, Israel*

Segmentation of cryo-STEM tomogram coming out of a z-slice from the tomogram. Image shows a portion of a WI fibroblast cell containing mitochondria (red), membrane formations (blue), and intake vesicles (blue spheres) filled with gold-labeled collagen VI (red dots).

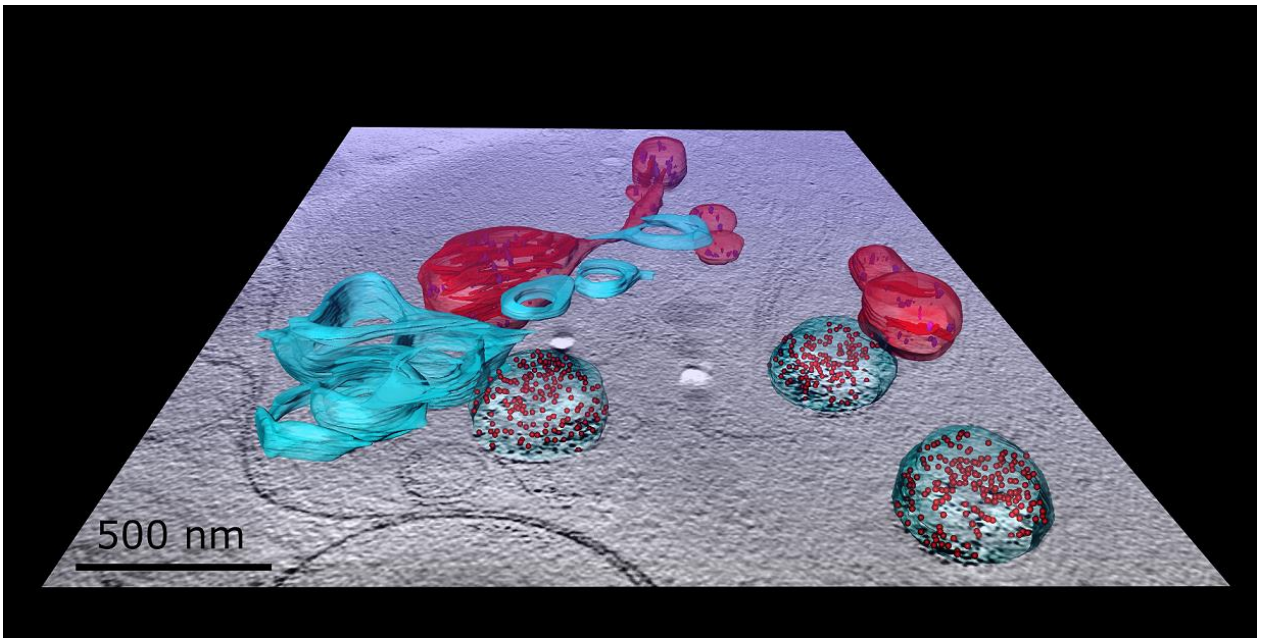


---

P-48

# IT`S COFFEE TIME !!!

Einat Zelinger, **Yulia Pollak**
*The CSI Center for Scientific Imaging, The Robert H. Smith Faculty of Agriculture, Food and Environment, The Hebrew University of Jerusalem, Rehovot, Israel*

**The "cookies" are pollen grains of the local plant of *Acacia saligna. Bar= 10 µm.***

***The image of the pollen was taken for the Israeli site: Wild Flowers of Israel**

*Acacia saligna*

---

P-49

# A THOUSAND SPLENDID SUNS

**Maya Barzilay**
*Department of Materials Science and Engineering & Solid State Institute,*
*Technion - Israel Institute of Technology*

This image shows  a CBED pattern taken from {100} zone axis in BaTiO3 nanoparticle with tetragonal structure. The image was taken with Titan Themis $G^2$ 300 (FEI / Thermo Fisher) in HR-STEM mode.